UNIVERSITÉ DE MONTRÉAL

EUMELANIN FILMS FOR ORGANIC BIOELECTRONICS: GROWTH, CHARGE TRANSPORT, AND INTERACTION WITH METAL ELECTRODES

JULIA WUENSCHE
DÉPARTEMENT DE GÉNIE PHYSIQUE
ÉCOLE POLYTECHNIQUE DE MONTRÉAL

THÈSE PRÉSENTÉE EN VUE DE L'OBTENTION
DU DIPLÔME DE PHILOSOPHIÆ DOCTOR
(GÉNIE PHYSIQUE)
JUIN 2014

UNIVERSITÉ DE MONTRÉAL

ÉCOLE POLYTECHNIQUE DE MONTRÉAL

Cette thèse intitulée :

EUMELANIN FILMS FOR ORGANIC BIOELECTRONICS:
GROWTH, CHARGE TRANSPORT, AND INTERACTION WITH METAL ELECTRODES

présentée par : WUENSCHE Julia
en vue de l'obtention du diplôme de : Philosophiæ Doctor
a été dûment acceptée par le jury d'examen constitué de :

M. YELON Arthur, Ph.D., président
Mme SANTATO Clara, Doct., membre et directrice de recherche
M. ROSEI Federico, Ph.D., membre et codirecteur de recherche
M. BUSCHMANN Michael, Ph.D., membre
M. BAUER Siegfried, Ph.D., membre

ACKNOWLEDGEMENTS

First, I would like to express my deepest thanks to my research director, Clara Santato, for guiding, supporting, and encouraging me during these last four years. Your passion for science, your personal involvement in each student's project, and your persistence are extraordinary and helped me to overcome the more difficult moments. You always have a sympathetic ear for the concerns of your students, professional and personal, which is remarkable. Thank you for putting so much confidence in me and for entrusting me with such a challenging project. I also very much appreciate that you gave me the chance to meet and discuss with so many great scientists.

I thank my codirector, Federico Rosei, for providing me with a "quick start" in Montreal by means of an internship at INRS, for encouraging me to apply for scholarship, and for his advice during my PhD. Furthermore, I am grateful to the jury members, Arthur Yelon, Michael D. Buschmann, and Siegfried Bauer, for their time and interest in my work.

Financial support from NSERC through a Vanier Canada Graduate Scholarship is gratefully acknowledged.

Many thanks to all the collaborators that have contributed to my research projects over the last years and who made my work more enjoyable and interesting. I would like to thank Alessandro Pezzella for sharing his invaluable knowledge on melanin chemistry. I am very grateful to Francesca Soavi and Marco Rolandi for the long and insightful discussions on the electrical and electrochemical properties of eumelanin. Special thanks to Fabio Cicoira for his continuous, pleasant support, and in particular for his advice on microfabrication. I very much thank Luis Cardenas for his support in the characterization of Au-eumelanin dendrites. I really enjoyed working with you. Many thanks to Yingxin Deng for the PdH measurements and her kind collaboration. I am very grateful to Suzie Poulin who took and analyzed many ToF-SIMS and XPS measurements for our project. I would like to thank Carlos F. O. Graeff for providing melanin samples and for his advice. I am also grateful to Reynald Gauvin for the SEM images taken in his lab. Many thanks to Alberto Salleo for GIXRD measurements by his group.

I have not yet thanked the collaborators who were also my colleagues at Polytechnique. Special thanks to Prajwal Kumar for the many CV measurements, which required perseverance and patience. A big thank you to Jonathan Sayago for the many times he helped me out in the lab and for being such a nice and generous colleague over all these years. Many thanks to Eduardo di Mauro for his enthusiastic start into this project and for proof-reading the first part of the thesis.

Of course, I would also like to thank my other colleagues, former and present, for their unlimited support in the lab, their advice, for making work pleasant, and for the interesting discussions about different cultures. Special thanks to Frédéric Venne for revising the French abstract.

I am very grateful to P. Moraille for her king support with AFM, to Alireza H.Mesgar for support in microfabrication to Josianne Lefebvre (XPS and ToF-SIMS), N. Brodusch (SEM), C. Chilian (NAA), and Samir Elouatik (Raman) for measurements.

Merci beaucoup à Joël Bouchard, Christophe Clément, Yves Drolet, Jean-Paul Lèvesque et Lucas Majeau pour leur support technique et les discussions dans le corridor. Je remercie aussi tous les étudiants qui ont contribué aux différents projets réliés à la mélanine dans le cadre des cours ou des stages d'été.

I am grateful to Patrick Desjardins, Antonella Badía, Richard Martel, Mihai Irimia-Vladu, Alon Gorodetsky, David Ordinario, Paul Meredith and the many other scientists I met for fruitful discussions.

I would also like to thank former collegues and collaborators that worked with me during the last years on research projects other than those presented in this thesis, in particular Simone Bertolazzi, Giuseppe Tarabella, Ivan A. Velasco Davalos, and Andreas Rüdiger.

Merci beaucoup à mes amis à la Polytechnique pour rendre les pauses de midi plus que agréables. Merci à toute mon équipe de volleyball qui m'a donné plein de distractions après le travail. Je remercie tous mes amis à Montréal pour les nombreux moments de plaisir, leur soutien et pour me recevoir si bien quand je suis arrivée. Ich danke auch meinen Freunden in Deutschland, die mich nach so vielen Jahren Abwesenheit immer noch gerne empfangen und die mich aus der Ferne unterstützt haben.

Ich möchte mich ganz herzlich bei meiner Familie, insbesondere meinen Eltern und meiner Schwester, bedanken. Vielen Dank für eure uneingeschränkte Unterstützung, auch als ich nach Montreal zog, und für eure Ermutigungen.

Finalement, je remercie de tout cœur Jean-Francois Desjardins pour son soutien, pour me faire venir à Montréal et pour la traduction du résumé. Merci beaucoup pour me faire profiter de la vie à tous les jours !

ABSTRACT

Organic semiconductors are mechanically soft materials and generally exhibit mixed ionic and electronic conduction. These properties are exploited in organic bioelectronics, a new field of research at the interface of electronics and biology that aims at providing knowledge and technology required for applications such as biosensing, drug delivery, and neuronal stimulation. In addition to well-characterized organic electronic materials already used in organic light-emitting diodes and solar cells, researchers in the field of organic bioelectronics are exploring the use of biomolecular electronic materials. The search for suitable biomolecular materials is motivated by potential benefits such as biocompatibility and biodegradability, for applications at the interface with living systems. On a more general level, biomolecular electronic materials are relevant because they could lead to more environmentally friendly electronics.

The biomolecular material eumelanin has been considered to be an amorphous semiconductor since the 1970's. Eumelanin is a pigment ubiquitous in flora and fauna and has many functions in the human body including UV-protection, free radical scavenging, metal ion chelation, and thermoregulation. Eumelanin has a π-conjugated backbone and is characterized by a high degree of energetic and structural disorder. Different types of eumelanin can be distinguished according to their (bio-)synthetic origin, resulting in different molecular and supramolecular structures. Pressed powder pellets of eumelanin show thermally activated conductivity and photoconductivity. However, in contrast to typical organic semiconductors, the conductivity of eumelanin pellets strongly increases with hydration. Although there are reports about mobile ions in eumelanin, the amorphous semiconductor model prevailed and was used to interpret the electrical properties of eumelanin during the last four decades. During the work for this thesis, a new study on eumelanin pellets was published showing that this model cannot correctly describe the hydration-dependent conductivity of eumelanin. Instead, the work suggests that eumelanin is a mixed ionic-electronic conductor. This report underlines the need to reinvestigate the electrical properties of eumelanin and reinforces the recent interest in eumelanin as a material for organic bioelectronics. The integration of eumelanin in device structures has been facilitated by the recent progress in the preparation of eumelanin thin films. Indeed, first attempts to employ eumelanin in chemical sensors and batteries have been reported. However, the properties of eumelanin thin films are far from being fully characterized. In particular, the electrical properties of hydrated films are largely unexplored.

In this thesis, the structural and the electrical properties of eumelanin films are inves-

tigated in view of possible applications in bioelectronics. The first focus of this work is to identify a suitable procedure for the solution-processing of eumelanin films to achieve homogeneous and smooth films, a non-trivial task due to the insolubility of eumelanin in common solvents. Several combinations of different synthesis routes and processing solvents are compared in terms of the morphology and the chemical composition of the films prepared, using atomic force microscopy (AFM) and x-ray photoelectron spectroscopy (XPS). It is shown that the use of ammonia solution, suggested in the literature, severely affects the chemical composition of eumelanin. The use of dimethyl sulfoxide (DMSO) as processing solvent in combination with commercial synthetic eumelanin yields homogeneous films with sub-nanometer surface roughness, good adhesion on hydrophilic substrates, and without significantly changing the elemental composition of the films. Based on the comparison of eumelanins of different origins and a more detailed XPS study, it is argued that there is a trade-off between the solution-processibility of a eumelanin-derived material and its chemical resemblance to natural eumelanin. Furthermore, the growth of eumelanin films deposited from DMSO is investigated by AFM. This investigation reveals that the films are composed of nanoaggregates and assemble in a quasi layer-by-layer fashion. The observation of nanoaggregates supports the stacked-oligomer model for the eumelanin samples investigated in this work, as opposed to the heteropolymer model.

The core of this thesis is devoted to a better understanding of the electrical response of hydrated eumelanin films and the charge carrier transport properties of eumelanin. Eumelanin is characterized in thin film form with coplanar metal electrodes under controlled humidity, using voltages $\leq$ 1 V. A surprisingly strong interaction of hydrated eumelanin thin films with Au electrodes under electrical bias is revealed. This interaction leads to the growth of Au-eumelanin dendrites between the electrodes paralleled by a sudden resistive change of the sample. The growth of the dendrites is investigated by AFM, scanning electron microscopy, and time-of-flight secondary ion mass spectroscopy. Samples of eumelanin of various sources are compared to gain insight into the role of molecular structure and impurities. Based on this study, a mechanism for the formation of the dendrites is proposed, involving the electrochemical oxidation of Au enabled by the presence of chloride traces and enhanced by the metal chelation properties of eumelanin. The phenomenon described herein is interpreted considering electrochemical metallization cells and suggests the possibility to conceive biocompatible eumelanin-Au based memory devices.

To investigate the intrinsic electrical properties of eumelanin, further experiments are conducted with Pt electrodes. Transient current measurements, current-voltage measurements, and electrochemical impedance spectroscopy (EIS) are employed to distinguish different contributions to the electrical current by their voltage and time/frequency-dependence. The

effect of sample hydration, film and electrode dimensions on the electrical current is investigated. The strong hydration dependence of the current, previously investigated for pellets, is confirmed for eumelanin thin films. It is shown that the electrical current is capacitive at voltages below 0.2 V (over 10 μm) and that electrochemical reactions dominate the non-capacitive currents at higher voltages. Current measurements with proton-transparent PdH_x electrodes reveal the strong contribution of protons to the current in hydrated eumelanin films. EIS provides a first estimate (10^{-4} S cm^{-1}) for the proton conductivity at 90% relative humidity. In contrast, the experimental results do not show clear evidence of electronic conduction. Based on the recent suggestion that the density of mobile electrons is governed by a pH-dependent comproportionation equilibrium, a qualitative model is developed for the electrical response of hydrated eumelanin films. The model suggests how the interplay of proton migration, the redox properties of eumelanin, and the comproportionation equilibrium could limit electron transport over micrometric distances. Subsequently, results of this thesis and from the literature are discussed in terms of protonic conduction and the possibility of electronic conduction in eumelanin.

In view of bioelectronic applications, the main contribution of this thesis is the first detailed investigation of the electrical properties of strongly hydrated eumelanin films. This investigation revealed the importance of electrochemical processes in the electrical response of hydrated eumelanin films. Such processes can yield interesting new phenomena such as the growth of Au-eumelanin dendrites. For the study of charge transport in eumelanin, it is important to consider the contribution of electrochemical processes to the electrical current. This thesis provides new insights into the charge carrier properties of eumelanin films. It demonstrates and quantifies protonic conduction in hydrated eumelanin films. In contrast, it places a question mark over the paradigm of electronic conduction in eumelanin. Furthermore, this work emphasizes the necessity to consider the specific chemical composition of the eumelanin under investigation and the effect of the processing solvent on this composition. In a wider context, this thesis promotes the awareness of the effects of water, impurities, and electrochemical processes on the electrical performance of organic bioelectronic devices.

RÉSUMÉ

Les semi-conducteurs organiques sont des matériaux souples à conduction ionique et électronique mixte. Ces propriétés sont exploitées dans la bioélectronique organique, un nouveau champ de recherche à l'interface de l'électronique et de la biologie qui vise à fournir les connaissances et la technologie pour des applications telles que les biocapteurs, la livraison de médicaments et la stimulation neuronale. Outre les matériaux électroniques organiques qui ont été bien caractérisés à des fins d'applications de diodes électroluminescentes organiques et de cellules solaires, les chercheurs dans le domaine de la bioélectronique organiques explorent l'utilisation des matériaux électroniques biomoléculaires. La recherche de matériaux biomoléculaires est motivée par ses bénéfices potentiels en biocompatibilité et en biodégradabilité, essentiels pour des applications à l'interface avec des systèmes vivants. Sur un plan plus général, les matériaux électroniques biomoléculaires pourraient éventuellement être utilisés pour la conception de systèmes électroniques plus écologiques.

L'eumélanine, un matériau biomoléculaire, a été considéré comme un semi-conducteur amorphe depuis les années 1970. L'eumélanine est un pigment omniprésent dans la flore et la faune. Il possède de nombreuses fonctions dans le corps humain: la protection UV, le piégeage des radicaux libres, la chélation des ions métalliques, et la thermorégulation. L'eumélanine a une structure électronique moléculaire de type pi-conjugué qui se caractérise par son haut degré de désordre énergétique et structurel. Il y a différents types d'eumélanine et ils se distinguent par leurs structures moléculaires et supramoléculaires, lesquelles dépendent des conditions de (bio-)synthèse. Par exemple, les pastilles de poudre pressée d'eumélanine possèdent une conductivité et photoconductivité activée thermiquement. Cependant, contrairement aux semi-conducteurs organiques typiques, la conductivité des pastilles d'eumélanine augmente drastiquement avec l'hydratation. Bien que la mobilité des ions dans l'eumélanine ait été rapportée, le modèle de semi-conducteur amorphe est le modèle prévalent dans la communauté scientifique depuis quatre décennies et il est encore utilisé pour interpréter les propriétés électriques de l'eumélanine. Pendant le travail qui a mené à cette thèse, une nouvelle étude sur les pastilles d'eumélanine a été publiée démontrant que ce modèle ne peut pas décrire correctement la conductivité de l'eumélanine en fonction de l'hydratation. Cette étude suggère plutôt que l'eumélanine est un conducteur ionique-électronique mixte. Cela souligne la nécessité de réexaminer les propriétés électriques de l'eumélanine et renforce l'intérêt d'utiliser l'eumélanine comme matériau de base dans la bioélectronique organique. L'intégration d'eumélanine dans des dispositifs est facilitée par les récents progrès dans la préparation de couches minces d'eumélanine. Récemment, des premiers essais à employer l'eumélanine

dans les capteurs chimiques et les piles ont été rapportés dans la littérature. Cependant, des propriétés des couches minces d'eumélanine restent à être caractérisées, particulièrement les propriétés électriques des couches hydratées qui demeurent inexplorées.

Dans cette thèse, l'étude des propriétés structurales et électriques des couches d'eumélanine est présentée dans l'optique d'une éventuelle application dans la bioélectronique. L'objectif premier est de mettre au point une procédure adéquate pour la préparation des couches d'eumélanine homogènes et lisses à partir de solutions. Cette tâche est un défi en raison de l'insolubilité de l'eumélanine dans les solvants usuels. Dans ce travail, des combinaisons de différentes voies de synthèse et de solvants de dépôt sont comparées en termes de la morphologie et de la composition chimique des couches obtenues. La caractérisation s'est faite à l'aide de la microscopie à force atomique (AFM) et la spectroscopie photoélectronique par rayons X (XPS). L'utilisation d'une solution d'ammoniaque comme solvant est rapportée dans la littérature. Pourtant, les résultats présentés dans cette thèse montrent que ce solvant affecte grandement la composition chimique de l'eumélanine. L'utilisation de diméthylsulfoxyde comme solvant de dépôt combinée à l'eumélanine synthétique commerciale permet la synthèse de couches homogènes dont la rugosité de surface est sub-nanométrique. Elles présentent une bonne adhérence sur des substrats hydrophiles, et ce, sans faire de modification significative dans la composition élémentaire des couches. S'appuyant sur une comparaison de différents types d'eumélanine et une étude XPS détaillée, il est suggéré qu'un compromis doit être fait entre la possibilité de préparer des couches lisses de l'eumélanine à partir des solutions et sa ressemblance à l'eumélanine naturelle. La caractérisation par AFM de la croissance de couches déposées à partir d'une solution d'eumélanine révèle que les couches sont composées de nanoagrégats et sont assemblées dans une mode quasi couche-par-couche. L'observation de nanoagrégats supporte le modèle d'oligomères empilés pour les échantillons d'eumélanine examinés dans cette thèse, par opposition au modèle d'hétéropolymère.

Le noyau de cette thèse est consacré à une meilleure compréhension de la réponse électrique de couches d'eumélanine hydratées et des propriétés de transport de charges dans l'eumélanine. L'eumélanine est caractérisée sous forme de couche mince en utilisant des électrodes coplanaires métalliques dans un environnement d'humidité contrôlée, sous des tensions ≤ 1 V. Sous tension électrique, une forte interaction des couches minces d'eumélanine hydratées avec les électrodes Au est remarquée. Cette interaction se traduit par une croissance de dendrites Au-eumélanine entre les électrodes, en parallèle avec un changement brusque de la résistance de l'échantillon. La croissance des dendrites est étudiée par AFM, par microscopie électronique à balayage et par spectrométrie de masse à ionisation secondaire à temps de vol. Les échantillons d'eumélanine provenant de diverses sources sont comparés afin de mieux comprendre le rôle de la structure moléculaire et des impuretés. À partir de cette étude,

un modèle est proposé pour le mécanisme de formation des dendrites, impliquant l'oxydation électrochimique de Au activée par la présence de traces de chlorure et renforcée par les propriétés de chélation de métal de l'eumélanine. Le phénomène décrit est interprété en considérant les cellules de métallisation électrochimiques et suggère la possibilité de concevoir des dispositifs de mémoire biocompatibles basés sur l'eumélanine et Au.

Pour étudier les propriétés électriques intrinsèques de l'eumélanine, des mesures électriques ont été menées avec des électrodes en Pt. Des mesures de courant en régime transitoire, de courant-tension et de spectroscopie d'impédance électrochimique (EIS) ont été effectuées pour distinguer les différentes contributions au courant électrique. L'effet de l'hydratation et des dimensions des couches et des électrodes sur le courant électrique a été étudié. Tel que démontré dans des études sur les pastilles d'eumélanine, la forte dépendance du courant électrique à l'hydratation de l'échantillon est confirmée pour les couches minces de l'eumélanine. Il est observé que le courant électrique est capacitif à des tensions inférieures à 0.2 V (distance d'électrodes 10 μ m) et que les réactions électrochimiques dominent les courants non-capacitifs à des tensions plus élevées. Les mesures de transport de charges avec électrodes en PdH_x transparent aux protons révèlent que les protons contribuent fortement au courant dans les couches d'eumélanine hydratées. Les mesures d'EIS fournissent une première estimation (10^{-4} S cm^{-1}) pour la conductivité protonique à 90 % d'humidité relative. En contraste, les résultats expérimentaux ne montrent pas de preuve claire sur la présence d'une conduction électronique. En considérant la récente suggestion que la densité des électrons mobiles est régie par un équilibre de médiamutation dépendant du pH, un modèle qualitatif est proposé pour décrire la réponse électrique de couches d'eumélanine hydratées. Le modèle suggère comment la migration de protons, les propriétés d'oxydoréduction de l'eumélanine et l'équilibre de médiamutation pourraient limiter le transport d'électrons sur des distances micrométriques. Subséquemment, les résultats de cette thèse et de la littérature sont discutés en termes de conduction protonique et de la possibilité de conduction électronique dans l'eumélanine.

En vue d'applications bio-électroniques, la contribution principale de cette thèse est la première étude détaillée des propriétés électriques des couches d'eumélanine fortement hydratées. Cette étude révèle l'importance des processus électrochimiques dans la réponse électrique des couches d'eumélanine hydratées. De tels processus peuvent mener à de nouveaux phénomènes intéressants, tels que la croissance des dendrites Au-eumélanine. Pour l'étude du transport de charges dans l'eumélanine, il est important de considérer la contribution des processus électrochimiques pour le courant électrique. Cette thèse fournit de nouvelles connaissances sur les propriétés des porteurs de charge dans les couches d'eumélanine. Elle démontre et quantifie la conduction protonique dans les couches d'eumélanine hydratées. En revanche, elle met un point d'interrogation sur le paradigme de la conduction électronique dans l'eumé-

lanine. En outre, ce travail met l'accent sur la nécessité de considérer la composition chimique spécifique à l'eumélanine étudiée et de comprendre l'effet des solvants utilisés lors des dépôts sur cette composition. Dans un contexte plus large, cette thèse contribue à sensibiliser aux effets de l'eau, des impuretés et des processus électrochimiques sur la performance électrique des dispositifs bioélectroniques organiques.

TABLE OF CONTENTS

LIST OF TABLES

LIST OF FIGURES

LIST OF APPENDICES

LIST OF ABBREVIATIONS

AFM	Atomic force microscopy
BMPyrr-TFSI	1-Butyl-1-methylpyrrolidinium bis(trifluoromethylsulfonyl)imide
BSE	Backscattered electron
CPE	Constant phase element
CV	Cyclic voltammetry
DDQ	2,3-Dichloro-5,6-dicyano-1,4-benzoquinone
DHI	5,6-Dihydroxyindole
DHICA	5,6-Dihydroxyindole-2-carboxylic acid
DMF	Dimethylformamide
DMSO	Dimethyl sulfoxide
DNA	Deoxyribonucleic acid
DTG	Differential thermogravimetric analysis
EDS	Energy-dispersive X-ray spectroscopy
EIS	Electrochemical impedance spectroscopy
ESR	Electron spin resonance
FET	Field-effect transistor
FT-IR	Fourier-transform infrared spectroscopy
GIXRD	Grazing incidence X-ray diffraction
H_2Q	Ortho-hydroquinone
HOMO	Highest occupied molecular orbital
IL	Ionic liquid
IPES	Inverse photoelectron spectroscopy
ITO	Indium tin oxide
LUMO	Lowest unoccupied molecular orbital
MAPLE	Matrix-assisted pulsed laser deposition
NA	Nano-aggregate
NAA	Nuclear activation analysis
OLED	Organic light-emitting diode
OTFT	Organic thin film transistor
Q	(Indole)quinone
QI	Quinone imine
RH	Relative humidity
RIE	Reactive ion etching

SCE	Saturated Calomel Electrode
SEM	Scanning electron microscopy
SQ	Semiquinone
TGA	Thermogravimetric analysis
ToF-SIMS	Time-of-flight secondary ion mass spectroscopy
TTF	Tetrathiafulvalene
UPS	Ultaviolet photoelectron spectroscopy
XPS	X-ray photoelectron spectroscopy
XRD	X-ray diffraction

LIST OF SYMBOLS

A	In-plane electrode area
C	Capacitance
C_{DL}	Double layer capacitance
d	Film thickness
D_{σ}	Proton conductivity diffusion coefficient
D_{H_2O}	Water self-diffusion
Δ_q	XRD peak width
E_F	Fermi level
E_g	Energy gap
E_{HOMO}	Energy of the highest occupied molecular orbital
E_{LUMO}	Energy of the lowest unoccupied molecular orbital
E°_{ox}	Standard oxidation potential
E°_{red}	Standard reduction potential
$\overrightarrow{F}$	Electric field
g	Paracrystalline parameter
Δ G	Change in Gibbs free energy
G_0	Quantum of conductance
H	Hydration
I	Current
k_b	Boltzmann constant
k_{el}	Electron transfer rate
κ	Dielectric constant
L	Interelectrode distance
λ	Reorganization energy
μ	Charge carrier mobility
μ_h	Hole mobility
μ_e	Electron mobility
n	Charge carrier density
p	Pressure
pK_a	Acid dissociation constant
q	Charge
q_z	XRD scattering vector
r	Screening length of electric charge

R	Resistance
R_{CT}	Charge-transfer resistance
R_q	Root mean square surface roughness
σ	Conductivity
t	Time
T	Temperature
$\overrightarrow{v}$	Carrier velocity
V	Voltage
W	Electrode width

CHAPTER 1

INTRODUCTION

Since the discovery of the first conductive polymers four to five decades ago [1–3], research on organic electronics has made substantial progress. Displays based on organic light-emitting diodes (OLEDs) are now commercially available on a large scale and other organic electronic devices such as white OLEDs for lighting and organic solar cells might follow soon [4]. Organic electronic devices make use of thin films of π-conjugated small molecules or polymers with semiconducting or conducting properties. The structural, optical, and electrical properties of these materials can be tuned by chemical synthesis to meet the requirements of a wide range of applications. Organic thin film devices can be produced under low energy consumption by printing or low-temperature evaporation. They are light-weight and conform to flexible substrates. The goal of organic electronics is not to exceed the performance of Si-based devices but rather to reduce the cost and the environmental impact of electronics, as well as to enable new fields of applications such as semitransparent and flexible electronics [5, 6]. Thousands of peer-reviewed publications per year indicate both that the potential of organic electronics has not yet been fully exploited and that some challenges have not yet been met. These challenges include understanding the effect of microstructure on charge transport [7], the optimization of charge separation in organic solar cells [8], printable electrode and semiconductor materials [9], stable and efficient n-type materials and blue emitters [10, 11], and large scale processing [12].

Starting about ten years ago, another property of organic electronic materials has gained much attention. While inorganic (semi-)conductors usually conduct only electronic charge carriers, their organic counterparts often support both electronic and ionic/protonic currents. This property allows for ion-to-electron transduction and opens new possibilities for the interaction of electronic and biological systems, now explored in the field termed *Organic Bioelectronics* [13]. Potential applications include bio-sensing for health and environmental monitoring, drug delivery, and neuronal signal recording and stimulation [13–16]. Naturally, biocompatibility is an important requirement for such applications. Indeed, biocompatibility and biodegradability, in addition to low power consumption during production and operation, is a desirable feature for any electronic device in the effort to reduce its environmental footprint. The vision of sustainable electronics and the potential benefits from coupling electronic and biological systems has recently encouraged several research groups to search for biomolecular and bio-inspired materials suitable as components of electronic and ionic de-

vices [17–20]. While the list of biomolecular materials that have been successfully employed as substrate or dielectric layer in transistors is long [17], the identification of biomolecules that are semiconducting or conducting in thin film form is much more challenging. Remarkably, during the work for this thesis, hydrogen-bonded pigments emerged as a new class of organic semiconductors, also including well-known natural pigments such as indigo [20]. Proton conductors such as maleic chitosane fibers have been employed in bio-protonic transistors [21]. In addition to the properties mentioned above, biomolecules often have remarkable mechanical, chemical, or optical properties related to their biological function.

Organic bioelectronics, a multidisciplinary field of research, is still in its infancy. The systems investigated are generally characterized by a high degree of structural and energetic disorder, the simultaneous conduction of ions and electrons, and a complex environment, possibly including water and redox-active species. Understanding the effect of all these factors on device performance requires models and characterization methods beyond inorganic solid state physics [18]. There is thus an urgent need for further studies contributing to a better understanding of charge carrier transport, structure-property relationships, and the interaction of organic and biomolecular materials with their environment and other device components.

1.1 Eumelanin - a natural pigment and a potential material for bioelectronics

The biomolecular pigment melanin, more precisely eumelanin, was reported to have semiconducting properties already in the 1960's and 70's [22–25]. Melanins are bio-macromolecules ubiquitous in flora and fauna that hold important functions in the human body including photo-protection, coloration of skin, hair and eyes, free radical scavenging, metal ion chelation, thermo-regulation, and might also be involved in neuronal signal transmission [26–28]. Furthermore, melanins play a role in diseases such as melanoma skin cancer and Parkinson's disease [29–31]. Eumelanin is the predominant form of melanin in the human body. Properties of eumelanin that caught the attention of material scientists and physicists include a persistent electron spin resonance signal, indicating stable free radicals [32], strong optical absorption with a featureless spectrum [33], and the hydration-dependent (photo-)conductivity of eumelanin pellets [34, 35]. These properties were mostly explained within the framework of the amorphous semiconductor model, building on the discovery of reversible threshold switching of eumelanin pellets by McGinness in 1974 [25]. Most recent works referring to the electrical properties of eumelanin still consider eumelanin as an amorphous semiconductor [19, 36–40]. However, there have also been reports about mobile ions, in particular protons, in eumelanin [41–44]. In 2012, Mostert *et al.* resumed the debate on the

origin of the electrical conductivity of eumelanin [42]. Their work on eumelanin pellets seems to disprove the amorphous semiconductor model and suggests that both electrons and protons are mobile in eumelanin pellets. Definitive proof of electron and proton transport over device-relevant distances, insights into the relative contribution of electrons and protons to the electrical current at different sample hydration states, and a new model for the charge carrier transport mechanism in eumelanin are still missing to date. In particular, reports on the electrical properties of hydrated eumelanin films are very sparse.

The characterization of eumelanin is complicated by its high degree of chemical and structural disorder and its insolubility in common solvents [45]. Furthermore, many properties of eumelanin are strongly affected by hydration [46]. It is now accepted that eumelanin does not have a well-defined chemical structure but is rather a mixture of different oligomers and polymers of 5,6-dihydroxyindole (DHI), 5,6-dihydroxyindole-2-carboxylic acid (DHICA) and their various redox forms. The stucture of eumelanin depends on (bio-)synthetic conditions and precursors [45, 47]. Chemical and structural disorder also implies energetic disorder and makes any structure-property correlation challenging. The insoluble nature of eumelanin defies many conventional techniques for the characterization of organic molecules and it is furthermore an obstacle for the preparation of eumelanin thin films. Indeed, strategies for the solution processing of eumelanin films have been suggested only recently [48, 49]. Thin films enable the use of a wider range of characterization techniques and facilitate the integration in device architectures. The next step in this line of research is to optimize film processing, characterize film structure and functional properties, and to investigate the interaction of eumelanin thin films with other device components.

The development of organic bioelectronics revived the interest in eumelanin as a functional material [17, 18, 50, 51]. The electrical and chemical properties of eumelanin in combination with its intrinsic biocompatibility have encouraged researchers to explore the use of eumelanin in tissue engineering [39], biocompatible batteries [52], memory devices [53], and sensors [37, 54]. The possibility of mixed ionic-electronic conduction makes eumelanin an interesting candidate for ion-to-electron transduction [42]. A glance at the vast literature on polydopamine, a synthetic eumelanin-like polymer, reveals further potential applications, including biosensing, drug delivery, and membranes for fuel cells [40, 55]. However, the electrical properties of polydopamine films are largely unexplored.

1.2 Objectives and organization of the work

The primary objective of this thesis is to investigate the structural and electrical properties of eumelanin thin films for potential applications in organic bioelectronics. The rich

biofunctionality of eumelanin in combination with its hydration-dependent electrical conductivity, possibly based on mixed ionic-electronic conduction, opens diverse possibilities for its use at the interface of electronics and biological systems. A better understanding of the fundamental properties of eumelanin is also of great fundamental interest considering its role in biology and medicine.

For device integration, it is advantageous to use eumelanin in the form of thin films. Furthermore, thin films offer a better control over sample morphology and dimensions, and enable the use of a wider range of characterization techniques such as scanning probe microscopy. Therefore, the first objective of this work is:

(1) The identification of a procedure for the solution-processing of eumelanin films that yields homogeneous, smooth films with good adhesion to the substrate and has little effect on the chemical composition of the eumelanin film.

Since the electrical properties of thin films strongly depend on film morphology and structure, the second objective is

(2) The investigation of the growth and morphology of eumelanin thin films.

Finally, the main focus of this thesis is

(3) The characterization of the electrical response of hydrated eumelanin thin films and to shed light on the charge carrier transport properties of eumelanin.

The thesis starts with a literature review of the thin film processing and the physical and chemical properties of eumelanin (Chapter 2). Special attention is paid to the charge carrier transport properties of eumelanin. Chapter 2 also contains a brief introduction to the processing, the growth, and the electron and proton transport properties of organic thin films. Subsequently, Chapter 3 to 5 are reprints of three articles resulting from the work for this thesis:

- Article 1: Eumelanin thin films: solution-processing, growth, and charge transport properties
- Article 2: In situ formation of dendrites in eumelanin thin films between gold electrodes
- Article 3: Proton conduction and transient nature of electronic currents in hydrated eumelanin thin films.

In the following, it is explained how these articles contribute to the objectives of the

thesis. In Article 1, published in the Journal of Materials Chemistry B, different synthesis routes and processing solvents for eumelanin suggested in literature are compared in terms of the morphology and the chemical composition of spin-coated thin films. The combination of the synthetic eumelanin and the processing solvent that was found to yield the best films with respect to the objective defined above is used in all subsequent studies of this thesis. Article 1 also addresses the second objective. Studying the growth of eumelanin films gave insight into the supramolecular organization of eumelanin in the form of nanoaggregates and the 3D film morphology of the films, suggesting that the processing technique employed is suitable to obtain continuous eumelanin films.

The first electrical characterizations in this project were carried out with Au electrodes, often employed in organic electronics for their chemical inertness and also in several previous studies on eumelanin. In Article 2, published in Advanced Functional Materials, an unexpected interaction between hydrated eumelanin films and Au electrodes, the growth of Au-eumelanin dendrites, is reported. The dendrites completely dominate the electrical properties of the sample and suggest interesting new applications of eumelanin. These results point to the importance of the electrode material and the consideration of electrochemical reactions in the electrical response of hydrated eumelanin films.

Further electrical measurements on eumelanin were conducted with Pt and Pd electrodes. In Article 1 the strong hydration dependence of the conductivity of eumelanin thin films is confirmed and the time-dependence of the current is investigated. The current transients suggest several contributions to the current. In Article 3, which has recently been submitted, these contributions are disentangled for strongly hydrated eumelanin films using a combination of electrical and electrochemical characterization techniques. The eumelanin films are shown to be proton conductive over micrometric distances and the proton conductivity is estimated. Furthermore, the results of Article 3 indicate that electrochemical processes play an important role in the electrical response of hydrated eumelanin films. In contrast, the results of Article 3 show no clear evidence of electronic conduction. A qualitative model is developed describing how the interplay of proton migration, the redox properties of eumelanin, and the comproportionation equilibrium, determining the density of mobile electrons, could limit electron transport in eumelanin thin films.

Following these three articles, supplementary methods and results that have been obtained during the work for this thesis are presented (6). These include details on the film processing, strategies for the patterning of eumelanin films, and attempts to enhance the conductivity of eumelanin films.

In Chapter 7, the results of this thesis are discussed as a whole, supported by the literature review in Chapter 2. Finally, conclusions are drawn and perspectives on future work are given

(Chapter 8).

CHAPTER 2

LITERATURE REVIEW

Eumelanin can be found in many plants and animals and has various functions in the human body. In addition, some of its intriguing solid-state properties have already been discovered in the 1970's. Nevertheless and despite considerable progress during the last years, many fundamental properties of eumelanin are still a matter of debate. This is partly due to the high chemical heterogeneity and the insolubility of eumelanin, making characterization challenging. This chapter starts with an overview of the current knowledge about the molecular and supramolecular structure of eumelanin (Sec. 2.1), followed by a brief description of the physical and chemical properties of eumelanin (Sec. 2.2). Following this, the processing, growth (Sec. 2.3), and charge carrier transport properties of eumelanin (Sec. 2.4) are reviewed in more detail. The latter two sections also include a brief introduction to general concepts of organic thin film growth, electron transport in organic semiconductors, and proton transport in hydrated polymers.

2.1 Synthesis, molecular and supramolecular structure of eumelanin

The terms *melanin* and *eumelanin* are used ambiguously in literature. In 2013, leading chemists in melanin research made a new attempt in establishing a common nomenclature [47]:

> "Melanins: Pigments of diverse structure and origin derived by the oxidation and polymerization of tyrosine in animals or phenolic compounds in lower organisms. Eumelanins: Black-to-brown insoluble subgroup of melanin pigments derived at least in part from the oxidative polymerization of L-dopa via 5,6-dihydroxyindole (DHI) intermediates."

Accordingly, eumelanins are defined via their oxidative formation pathway, which can lead to different macromolecular structures depending on precursors and oxidation conditions. The biosynthetic formation of eumelanin from tyrosine is described by the Raper-Mason scheme shown in Fig. 2.1 [56]. The last step of the formation is the oxidative polymerization of DHI and 5,6-dihydroxyindole-2-carboxylic acid (DHICA). In eumelanin, different oxidation states of these monomer units coexist, the ortho-hydroquinone (H_2Q), -semiquinone (SQ), and -(indole)quinone (Q) form (Fig. 2.2). Furthermore, the tautomer of Q, quinone imine (QI) is often found [46, 57, 58]. Eumelanin thus contains phenolic hydroxyl, amine, and

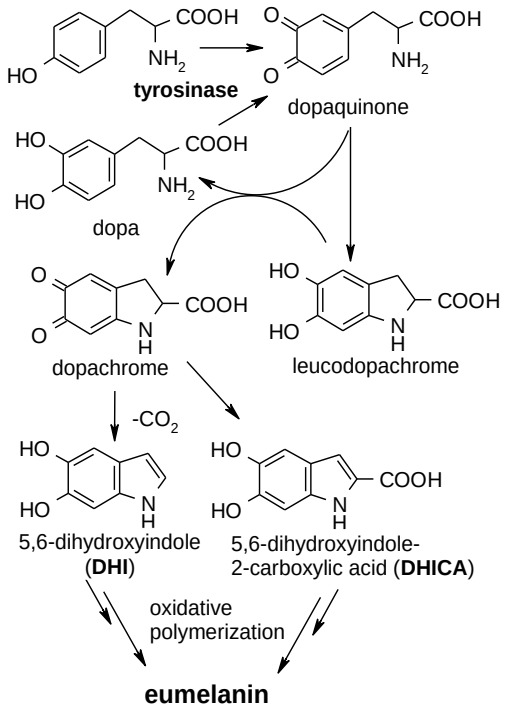

Figure 2.1 Raper-Mason scheme for the biosynthesis of eumelanin. Reprinted from Ref. [50].

carboxyl groups, which can act as proton donors or acceptors depending on their degree of protonation. The ratio of oxidized and reduced forms as well as of monomers with and without carboxyl groups strongly depend on the biological origin of eumelanin or, in the case of synthetic eumelanins, on precursors and reaction conditions. Due to difficulties in the extraction and purification of natural eumelanin, synthetic forms of eumelanin are used in most chemical and physical studies. A list of the different synthetic procedures reported in literature can be found in Ref. [50]. Apart from the monomer units shown in Fig. 2.2, eumelanin can contain uncyclized units (residues of precursors or intermediates) and pyrroles (eumelanin degradation products) [47, 59]. The variety of monomers that can be present in eumelanins is a source of both significant chemical diversity between eumelanins of different origin and the chemical heterogeneity of a certain eumelanin.

Considerable variety and disorder is furthermore present on the macromolecular and supramolecular level of the eumelanin structure. Coupling between monomers can occur at the 2, 3, 4, and 7 position as indicated in Fig. 2.2 leading to the formation of mainly planar oligomers of different structure and size [45]. The presence of a carboxyl group at the 2 position in DHICA reduces the number of potential coupling sites and results in the formation of more linear structures.

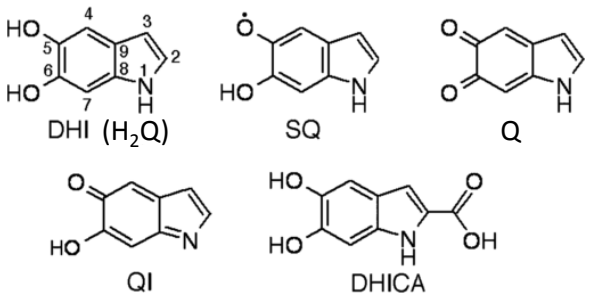

Figure 2.2 Constituent monomers of eumelanin: : 5,6-dihydroxyindole (DHI) and 5,6-dihydroxyindole-2-carboxylic acid (DHICA). The various redox forms that coexist in the eumelanin macromolecule are shown for DHI: H_2Q, SQ, and Q. QI is the tautomeric form of Q. Reprinted with permission from Ref. [46] (Copyright © 2006, John Wiley and Sons).

For a long time, it was commonly believed that eumelanin is a high-molecular-weight heteropolymer [23]. Evidence for polymeric structures of DHI of more than 30 monomer units was also recently collected by mass spectroscopy [60]. A possible heteropolymeric structure for eumelanin formed by polymerization of DHI is shown in Fig. 2.3a. However, most experiments, including AFM, scanning tunneling microscopy, transmission electron microscopy, and X-ray diffraction (XRD), point to a model commonly referred to as the "stacked-oligomer model" (Fig. 2.4) [61–65]. This model predicts the formation of planar sheets composed of 4-8 monomers, which stack in graphite-like manner via $\pi-\pi$ interaction with a spacing of 3.3-4.0 Å. The so-called protomolecule is about 1.5-2 nm large and 1-2 nm high and self-assembles via non-covalent binding to larger structures. The structure of eumelanin oligomers has been extensively studied [45, 50, 66] and examples for suggested structures are reported in Fig. 2.3b, c and d. The discussion above reveals that eumelanin has a conjugated backbone, whose extension depends on the (bio-)synthetic origin of eumelanin.

A comment should be made on the use of the term *polydopamine* at this point. Polydopamine is the "black oxidation product of dopamine" [67] and is also commonly referred to as "the dopamine-derived synthetic eumelanin polymer" [40]. Since the discovery of polydopamine as a versatile platform for biofunctional coatings in 2007 [55], publications on its application in biomedicine and other domains have been numerous [67]. It is commonly believed that polydopamine is a polymer of DHI or uncyclized catecholamines. However, it has recently been demonstrated that polydopamine can also contain other units and should be regarded as a mixture of various macromolecules [67], in analogy to eumelanin. It is generally accepted that the polydopamine structure strongly depends on the synthetic conditions. A notable difference to eumelanin derived from L-dopa or tyrosine lies in the apparent absence of DHICA and its redox forms. However, carboxyl groups can be formed by oxidative

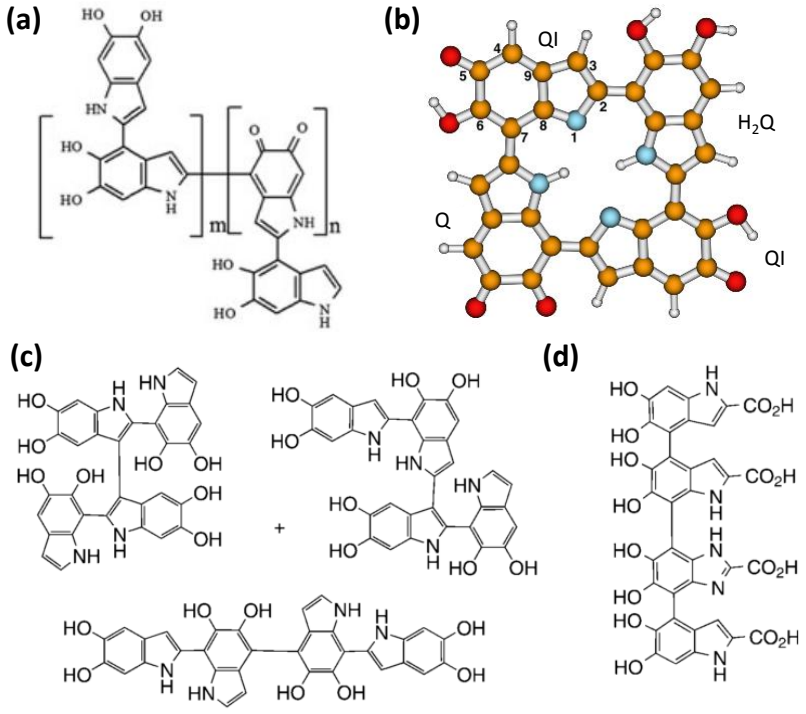

Figure 2.3 Examples for different macromolecular structures of eumelanin suggested in the literature: (a) polymer structure for eumelanin obtained from DHI, (b) and (c) tetramer structures for DHI, (d) tetramer structure for DHICA. In (b) the color orange refers to C, blue to N, and red to O atoms. Adapted with permission from (a) Ref. [60] (Copyright © 2012 John Wiley & Sons, Ltd), (b) Ref. [66] (copyright © 2006 by the American Physical Society) and (c) and (d) Ref. [45] (copyright © 2009 WILEY-VCH Verlag GmbH & Co. KGaA, Weinheim).

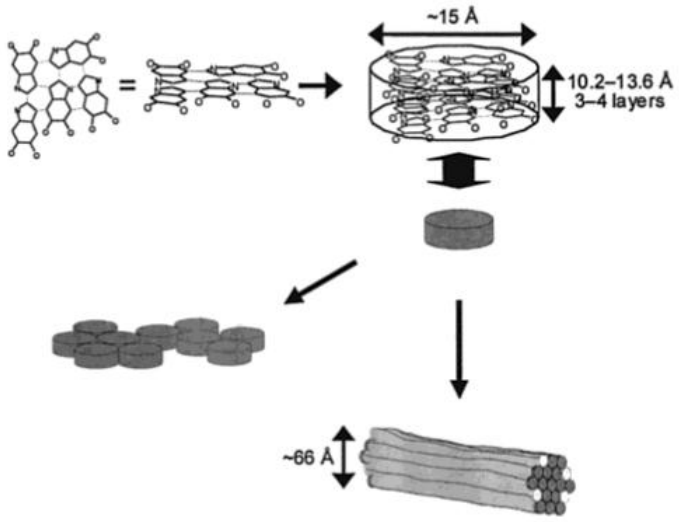

Figure 2.4 Stacked oligomer model according to Clancy *et al.* Reprinted with permission from Ref. [63] (copyright © 2001, American Chemical Society).

degradation of polydopamine [67]. To date, it is still unclear under which conditions the oxidation product of dopamine is similar in structure and properties to eumelanins derived from other precursors. Thus *polydopamine* and *eumelanin* should not be used as synonyms and, in general, the origin of eumelanin has to be considered when referring to literature. In this work, the precursor of the eumelanin investigated will often be included by referring to *dopa melanin*, *DHI melanin* etc. An exception is *DMSO melanin*, which is eumelanin derived from L-dopa by oxidation in dimethyl sulfoxide (DMSO) instead of aqueous suspension. Commercial synthetic eumelanin prepared by the oxidation of tyrosine with hydrogen peroxide (Sigma Aldrich) will be indicated as *Sigma melanin* and natural eumelanin from sepia officinalis (Sigma Aldrich) as *Sepia melanin*.

2.2 Physical and chemical properties of eumelanin

This section describes the physical and chemical properties of eumelanin that are of particular relevance for this work. The charge carrier transport properties of eumelanin are discussed separately and in more detail in Sec. 2.4.3.

2.2.1 Hydration

Eumelanin is hygroscopic and its properties are strongly dependent on hydration. Mostert *et al.* measured the absorption isotherms for water in eumelanin pellets [68]. The pellets contained about 11.5 wt% water at 50% RH and 16 wt% at 80% RH. Eumelanin is known

to contain at least two types of water, often referred to as weakly and strongly bound water [69,70]. Weakly bound water is easily removed by reducing the relative humidity in air or by gentle heating, while the sample has to be placed in vacuum or heated well above 100℃ to, at least partially, remove strongly bound water [36,71]. Recently, Bridelli *et al.* investigated the interaction of eumelanin and water by infrared spectroscopy [72]. The -OH stretching band revealed the presence of three different water species in synthetic *dopa melanin* and natural *Sepia melanin* drop cast from aqueous suspension: strongly bound water in the vapor-phase and two more weakly bound water species in the liquid phase, characterized by H-bonding. The presence of the different water species depend upon the pore size distribution of the sample investigated. For *dopa melanin*, only the liquid-phase water, which exist in larger pores, was found and hydration/dehydration was reversible. In contrast, in *Sepia melanin* vapor-phase water was also detected and dehydration was partly irreversible, i.e., the sample could reabsorb only a smaller amount of water after dehydration.

2.2.2 Optical properties

One of the characteristics of eumelanin is its strong broad-band absorption in the UV-visible, exponentially decreasing with wavelength. This was often considered an indication that eumelanin shows extended π-conjugation and can be described as an amorphous semiconductor (Section 2.4.3). However, it has been shown that the absorption spectrum can result from the superposition of the absorption of eumelanin oligomers of different size and structure [73]. Pezzella *et al.* furthermore reported that the coexistence of oxidized and reduced monomers contributes to the broad-band absorption [57].

In accordance with the role of eumelanin in photoprotection, the pigment efficiently transforms absorbed photon energy into heat via nonradiative relaxation pathways, which are still under investigation today [74–76]. It has been suggested that intramolecular proton transfer plays an important role in the dissipation process [74–76], as well as chemical and structural disorder [77].

Consequently, the fluorescence quantum yield of eumelanin is very low (about 10^{-4}) [78]. The fluorescence spectrum of eumelanin extends between 250 and 500 nm with the peak position and intensity depending on the excitation wavelength. The multi-exponential decay of the fluorescence is in agreement with the chemical disorder model [79].

2.2.3 Paramagnetic properties

Eumelanin shows a persistent electron spin resonance (ESR) signal, reflecting the presence of stable free radicals [32, 80]. The ESR is affected by pH, various metal ions, light, and

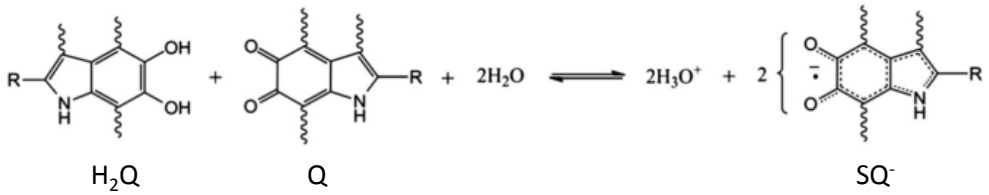

Figure 2.5 Comproportionation equilibrium between the different redox states of the eumelanin building blocks. Reprinted with permission from Ref. [42] (copyright © 2012 National Academy of Sciences).

hydration [41, 42, 80–84]. Two different types of unpaired spins can be distinguished in eumelanins, carbon-centered "intrinsic" spins and the "extrinsic" spins of the semiquinone radicals [42]. In aqueous suspension, the ESR signal at neutral and basic pH has been assigned to SQ radicals [85]. Numerous experiments have shown that the SQ radical population is controlled by the comproportionation equilibrium (Fig. 2.5) [80, 85]. The equilibrium strongly favors the reactants over the products resulting in only one SQ radical per 1000-1500 monomers in aqueous suspension at pH 7 [83,86]. The SQ population can be increased by increasing the pH [42,83,86] or by complexation of SQ with suitable metal ions [80,82].

The ESR signal of hydrated eumelanin pellets is more complex and was investigated only very recently [85]. The signal is dominated by carbon-centered radicals, resulting from the incomplete polymerization of the monomers, but also shows the response of SQ radicals as a minor component. An increase of hydration resulted in a decrease of the total signal intensity. The separation of the two components was difficult and no clear trend of the SQ population with hydration was observed. However, the relative contribution of SQ radicals to the ESR signal was stronger in basic pellets than in acidic or neutral pellets, in agreement with the comproportionation reaction [85]. A muon spin relaxation study by the same authors furthermore suggested the increase of the radical density with hydration [42].

2.2.4 Redox and proton-exchange properties

Eumelanin acts as a redox buffer in biological systems [87] and its redox ability is pH-dependent [88]. Eumelanin contains oxidized as well as reduced moieties [57]. Due to the insolubility and the aggregated structure of eumelanin, characterization of the redox activity of eumelanin in solution is difficult [58]. Serpentini *et al.* reported cyclic voltammetry (CV) measurements on *DOPA melanin* incorporated into a carbon paste electrode (0.1 M KCl aqueous solution, pH 5.6) [89]. Two irreversible oxidation peaks were observed at 460 and 550 mV (vs SCE), attributable to the oxidation of either a SQ or the amino group of an indole unit (QI) of eumelanin, and two reduction peaks at 20 and -355 mV. The absence of a

peak at +50 mV, where DHI (H_2Q) oxidation is usually located, was interpreted as the initial absence of DHI units at the surface of the eumelanin aggregates. The authors observed that only a small portion of the total number of monomers participated in the redox reactions and suggested that the eumelanin structure may be compact and have limited electronic conductivity.

Several CV studies have been reported on electropolymerized or electrodeposited eumelanin films. Films prepared by these means generally showed a higher electrochemical activity than solution-processed (drop cast or spin-coated) films [90]. Farmer *et al.* reported a spectroelectrochemical experiment on *DHI melanin* thin films, prepared by CV polymerization [58]. Partly reversible oxidation was observed at about 100 mV vs Ag/AgCl (0.1 M KCl pH 7.0), attributed to the two-electron oxidation of DHI (H_2Q) to Q state, followed by tautomerization to QI. This oxidation peak overlapped with an irreversible bleaching reaction. Only about one out of six monomers participated in the reversible oxidation process.

Eumelanin has several proton donating groups: a carboxyl group (pK_a 4.2-4.5) in DHICA, two phenolic hydroxyl groups (first pK_a 9-10 and second pK_a of about 13), and an amine group (pK_a >14) in DHI/DHICA [91,92]. The pK_a for the tautomer QI is 6.3 [86]. The pK_a of SQ has not been well established but, although a pK_a of 9-10 has been suggested [86], SQ is usually assumed to be deprotonated at neutral pH [42,80,93].

2.2.5 Metal ion chelation properties

In the following, the metal chelation properties of eumelanin are described due to their potential role in the interaction of eumelanin films with metal electrodes, presented in Article 2. Eumelanin strongly binds heavy metal ions such as Fe(III), Cu(II), and Pb(II), while the binding of lighter metal ions such as Ca(II), Na(I), and K(I) is weaker [91,94–96]. Binding sites have been investigated by ESR [80,83,97], FT-IR [95,98], and Raman spectroscopy [99] and were found to depend on the metal ion, its concentration, and pH. Fe(III) predominately binds to phenolic -OH groups [99], while Cu(II) binding sites vary with concentration and pH [83,98]. Ca(II), Na(I), and K(I) bind to -COOH groups [91,98]. Metal ions can bind to several eumelanin monomers simultaneously and various complexes of up to 5 monomers have been suggested [83,100,101]. Studies on the binding of Au, Pt, or Pd ions to eumelanin have not been reported. Recently, Kim *et al.* employed the binding of Na^+ by eumelanin in aqueous sodium-ion batteries with eumelanin as the anode material [52].

2.3 Thin film growth and processing

Thin films are the basis of state-of-the art organic (bio-)electronic devices and are also advantageous for the characterization of organic materials in the solid state. The physical properties of organic thin films, in particular their charge carrier transport properties, are strongly dependent on film morphology and crystalline structure. Thus, a good knowledge of the parameters governing film growth can help in tuning the film properties by processing. The preparation of continuous and smooth thin films of eumelanin is a challenge in itself due to the insolubility of eumelanin in common solvents [50] and its oligomeric/polymeric nature prohibiting thermal evaporation (see, for example, the investigation of thermal stability in Ref. [102] and Sec. 6.1). Therefore, most studies on solid-state eumelanin samples have been performed on pellets (compressed eumelanin powder). Recently, several strategies for the solution processing of eumelanin thin films have been suggested, as well as some alternative deposition techniques. This section first points out the particularities of organic thin film growth (Sec. 2.3.1) and discusses specific aspects of solution processing (Sec. 2.3.2). Subsequently, reports on eumelanin film processing and growth are reviewed (Sec. 2.3.3).

2.3.1 Characteristics of organic thin film growth

Thin film growth is determined by inter-adsorbate interaction and adsorbate-substrate interaction. The interactions depend upon the adsorbate properties but also on external parameters such as the deposition technique, deposition flux, and substrate temperature. Fundamental processes during film formation are: adsorption, desorption, surface diffusion, nucleation, and island growth [103]. In the following, the specific properties of organic thin film growth are described.

Since organic molecules are anisotropic, not only the positions of all molecules need to be known but also their orientation in space to fully describe the structure of an organic film [103]. Intermolecular and molecule-substrate interactions depend on the orientation of the molecule. Therefore, the structure of organic crystalline or polycrystalline films is difficult to predict [104]. This is further complicated by the fact that molecules are not rigid but can deform in contact with the substrate or the bulk [105]. Intermolecular interactions are dominated by van der Waals forces, which are much weaker than covalent bonds in inorganic films. This results in films that have a lower surface energy, are more tolerant to strain, and can be processed at low temperatures [103]. Since the footprint of organic molecules is large compared to atoms and the adhesion of organic molecules to the substrate is weak, organic film growth is usually incommensurate and non-epitaxial [103, 106]. The weak intermolecular and molecule-substrate interactions result in different crystalline structure

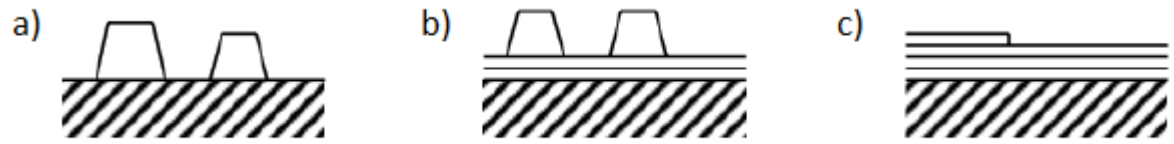

Figure 2.6 Illustration of island growth (a), layer-plus-island growth (b), and layer-by-layer growth (c) [109].

with similar energy. Therefore, different phases often coexist in organic films (polymorphism) [107, 108]. For these reasons, variations in the film processing parameters can have a huge impact on the film properties. This also means that film morphology and structure need to be characterized case-by-case.

The evolution of the surface topography with increasing film thickness substantially influence the final film morphology. One usually distinguishes between three growth modes: island growth (Vollmer-Weber), layer-plus-island growth (Stranski-Krastanov), and layer-by-layer growth (Frank-van der Merwe) [109]. Fig. 2.6 illustrates the different modes. In layer-by-layer growth, the second layer is only formed after the completion of the first layer and so on. In island growth, 3D-islands grow and even at higher film thickness, the substrate is still not completely covered. The Stranski-Krastanov mode refers to a mixed growth. After the formation of one or two wetting layers, the formation of 3D-islands becomes favorable. Organic thin film growth is said to follow a quasi-layer-by-layer mode if the growth of successive layers starts before the previous layers have been fully completed. The growth mode depends on both thermodynamics and kinetics. Important factors are the surface energies of the substrate and the film, the deposition flux, and the substrate temperature.

2.3.2 Solution processing

Techniques used for the solution processing of thin films include spin coating, drop casting, dip coating, stamping, and inkjet printing. The film growth and morphology is strongly dependent on the technique used and the processing conditions. Important parameters include the type of solvent, the concentration of the solution, the solvent evaporation rate, and the atmosphere during processing [110, 111]. Post-deposition treatments such as thermal annealing are common to increase molecular ordering and to remove solvent residues. As mentioned above, the substrate also plays a determining role in film growth.

Organic thin film devices commercialized so far are produced mainly by vacuum sublimation. Vacuum sublimation allows for the well-controlled deposition of small molecule

films of high purity and the straightforward fabrication of multilayer structures. Despite considerable progress, scalability and the potential for cost-reduction are limited in vacuum deposition [112]. The greatest potential for low-cost, large-area applications lies in solution-processing, compatible with roll-to-roll manufacturing processes [113]. However, solution-processed devices often show performances inferior to their vacuum-sublimed counterparts. This has several reasons. Polymers, which are most commonly used for solution-processing, are more difficult to purify than small molecules [114]. The solvent and the atmosphere during processing are further sources of impurities that can decrease device performance. Furthermore, the state-of-the-art of certain organic electronic devices such as organic light-emitting diodes is based on complex multilayer structures. It is difficult to obtain such structures by solution-processing, since solvents will generally affect previously deposited layers [114].

Many (semi-)conducting molecules are insoluble in common solvents. Different strategies have been developed to circumvent this problem. One of them is the addition of solubilizing side chains to the molecular structure. It is important to note that these side chains also affect other properties of the molecule and the molecular packing in the film [115]. The use of soluble precursors that convert to the final molecular structure after post-deposition treatment of the film has also been explored [116]. This and other synthetic approaches have yielded many solution-processable materials, which are now employed in high-performance organic electronic devices [117–120]. A further possibility to solubilize conducting polymers is blending with surfactants, which often simultaneously dope the polymer [121, 122].

The processing of (semi-)conducting biomolecular films has been explored only to a limited extent so far. This is because biomolecular materials only recently received more attention as potential components of electronic/ionic devices. Thin films of some natural pigments with high electron and hole mobilities, such as indigo and tyrian purple, have been fabricated by vacuum sublimation after thorough purification of the pigments [20, 123]. Proton-conducting nanofibres and amorphous films have been prepared by drop casting aqueous solutions of the polysaccharide-based biopolymers maleic chitosane and proline chitosane [124]. For the preparation of aligned and stretchable DNA films, DNA was mixed with a lipid and subsequently deposited by drop casting from organic solvents [125]. The processing of homogeneous and smooth films of biomacromolecules remains challenging because they are often insoluble, disordered on the macro- and supramolecular level, and/or self-assemble to larger structures [51].

2.3.3 Processing and growth of eumelanin thin films

First reports on eumelanin thin films were published in 2004 by the group of C. F. O. Graeff [48, 126]. The group developed a synthetic route for the formation of eumelanin from

L-dopa in the organic solvents dimethyl sulfoxide (DMSO) and dimethyl formamide (DMF). The synthesis product, referred to as *DMSO* or *DMF melanin*, showed UV-vis absorption, electron spin resonance (ESR), and infrared transmission (FT-IR) properties almost identical to eumelanin synthesized in aqueous solution according to one of the standard methods [80]. Thin films of *DMSO melanin* prepared by drop casting or spin-coating from DMSO or DMF solution on Si or glass showed micrometer-large terraces of 1-3 nm height and a root mean square surface roughness $R_q = 0.3$ nm, as well as round aggregates. The authors claimed that the synthesis of eumelanin in DMSO results in a more homogeneous product that facilitates solubilization and thin film deposition [48, 126]. AFM measurements showed that films of *DMSO* or *DMF melanin* deposited from DMSO or DMF solution were much smoother than films of water-based eumelanin dispersed in water [127]. From the analysis of the scaling of surface roughness with surface area, it was concluded that *DMSO melanin* films grow via diffusion-limited aggregation. Only in 2013, a structural characterization by the same research group revealed that the reason for the improved solubility and film forming properties of *DMSO melanin* are sulfonate (-SO_2-CH_3) groups that attach to the -OH groups of the eumelanin building blocks during synthesis [128].

"Device-quality" eumelanin thin films spin-coated from ammonia solution on glass and Si were reported by Bothma *et al.* in 2008 [49]. Eumelanin was prepared by a standard method by auto-oxidation of L-dopa in aqueous solution (*dopa melanin*) [80]. Eumelanin is known to be soluble in strongly alkaline aqueous solutions. Ammonia solution was chosen to avoid contamination of the film with cations (as possible in the case of NaOH amongst others), as verified by XPS. No further effort was made to investigate if the molecular structure of eumelanin was still intact after treatment with alkaline solution. The films were composed of spherical particles 20 nm in diameter and R_q was about 1 nm.

Bettinger *et al.* prepared films of commercial synthetic eumelanin (*Sigma melanin*) by spin-coating from aqueous NaOH and DMSO solution [39]. Films prepared from NaOH solution showed large dendritic stuctures, whereas films prepared from DMSO solution were very smooth ($R_q = 0.3$ nm). Elemental composition and presence of chemical groups were investigated by XPS and FT-IR, respectively, but no distinction between the two processing solvents was made.

Films of *Sigma melanin* were also deposited by spray coating on a heated glass substrate using a solvent mixture of DMSO:methanol (1:20) [36]. These films were smooth ($R_q =$ 0.3 nm) on a submicrometer-scale but showed larger agglomerates and discontinuities. The uniformity of the films was improved in a second study using electrospray deposition but film roughness remained rather high on a micrometer length scale (around 10 nm) [129]. The chemical composition of the films was studied by XPS and Raman spectroscopy, which

indicated the presence of all functional groups typical for eumelanin. However, the ratio of C, N, and O atoms was far from the ratio expected for eumelanin. This was not further discussed by the authors. It suggests that the molecular structure of eumelanin was affected by the film deposition procedure and/or that the eumelanin films contained large amounts of other organic species.

Some alternative film deposition techniques have been explored for eumelanin. Thin films of eumelanin have been prepared by matrix-assisted pulsed laser deposition (MAPLE) from frozen aqueous suspensions of *DHI melanin* [130, 131]. The advantage of this technique is that alkaline or organic solvents that might affect the molecular structure of eumelanin are avoided. However, the surface roughness of these films was very high ($R_q \approx 100$ nm) and could not be reduced by raising the substrate temperature [131]. For device applications, such high surface roughness can cause problems such as short circuits or hinder efficient charge transport.

Another approach is the electrodeposition/electropolymerization of eumelanin on conductive substrates. Díaz *et al.* deposited films from a *Sigma melanin*-containing 0.1 M NaOH solution on a Au electrode biased at -1 V vs SCE [90]. The authors suggested that the film growth is initiated by the electroreduction of Q to H_2Q. Borghetti *et al.* investigated the effect of potassium on the aggregate size in electro- and solution-deposited eumelanin films [132]. Free-standing eumelanin films were obtained by Subianto *et al.* by electropolymerization of L-dopa in aqueous suspension (pH 9) on indium tin oxide on glass [133]. Micrometer thick films were grown over several days under galvanostatic conditions (0.5 mA/cm^2).

Interestingly, film-forming properties of polydopamine are distinctively superior to those of eumelanin. Polydopamine films are readily prepared by simple dip-coating of a substrate in aqueous dopamine solution [55], which is one of the reasons for the great success of polydopamine coatings in biomedical research. This indicates that there are important differences in the molecular and/or supramolecular structure of polydopamine and eumelanins.

2.4 Charge carrier transport

A recent review chapter on the charge carrier transport properties of eumelanin stresses that "the highly conjugated sp^2 backbone, planar secondary structure and presence of multiple stable redox states all point to an intriguing possibility - the question of whether melanins could be naturally occurring organic semiconductors" [51]. Indeed, eumelanin in the solid state conducts electric charge, shows weak photoconductivity, switches between high and low resistive states under certain conditions, and can store electric charge or polarization. All these properties are strongly hydration-dependent and have intrigued biologists, chemists,

and physicists since the 1960's. Most studies have been conducted on pellets of eumelanin powder.

As a basis for the discussion of the charge carrier transport properties of eumelanin, this section starts with an introduction to electron (Sec. 2.4.1) and proton transport (Sec. 2.4.2) in organic materials. In the third part (Sec. 2.4.3), studies on the charge carrier transport properties of eumelanin pellets and thin films are reviewed.

2.4.1 Fundamentals of electron transport in organic semiconductors

Thin films of π-conjugated small molecules and polymers can have electrical properties similar to inorganic amorphous semiconductors. In this section, the origin of electron transport in organic solids and parameters affecting the electronic conductivity are briefly reviewed. Due to the presence of hydrogen-bonds in the supramolecular structure of eumelanin, recent results on the electron transport in hydrogen-bonded molecules are presented. At the end of this section, the peculiar property of certain organic semiconductors to transport both electrons and ions, is briefly discussed.

π-Conjugation

The electronic configuration of a single carbon atoms is $1s^2\ 2s^2\ 2p^2$. In organic semiconductors, the 2s- and 2p-orbitals hybridize to form three sp^2 orbitals, which lie in the same plane, leaving one p-orbital (p_z) perpendicular to the plane. The overlap of sp^2 orbitals in the plane of carbon atoms leads to the formation of σ-bonds, while the overlap of p_z-orbitals creates π-bonds. The formation of molecular orbitals is illustrated in Fig. 2.7 for the molecule benzene. When p_z-orbitals overlap along a chain or a ring, an extended π-electron system forms, in which electrons are delocalized. This phenomenon is called conjugation and is a common property of all organic semiconductors [134, 135]. Conjugation is often represented by alternating single and double bonds, where the double bond is made of a σ and a π-bond.

The smaller overlap of p_z orbitals compared to sp^2 orbitals results in a smaller energetic splitting of the bonding π and anti-bonding π^* orbital. Due to spin-orbit coupling, the π-states split further into substates. As illustrated in Fig. 2.7, the highest occupied molecular orbital (HOMO) is the π-orbital with the highest energy and the lowest unoccupied molecular orbital (LUMO) is the π^* orbital with the lowest energy. Thus, the energetically lowest excitations are $\pi - \pi^*$ transitions [137]. The energetic distance of the HOMO and LUMO from the vacuum level roughly correspond to the ionization potential I and the electron affinity A of the molecule, respectively. This approximation neglects any rearrangement of the electrons in the molecule cation or anion [134].

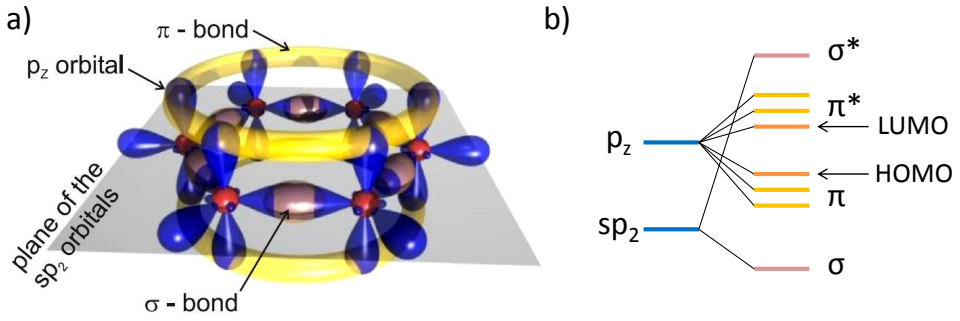

Figure 2.7 Illustration (a, reprinted from Ref. [136]) and electron energy level diagram (b) of the formation of molecular σ and π orbitals from atomic orbitals in benzene.

Electronic properties of disordered organic thin films

Due to the weak intermolecular interaction in organic solids, electron energy levels are largely determined by the energy levels of single molecules [138]. The transition from a single molecule to an organic solid is illustrated in Fig. 2.8. In the case of relatively strong intermolecular interaction and high order (e.g. in single crystals), narrow valence and conduction bands can form from the overlap of HOMO and LUMO levels, respectively. These allow for a delocalization of electrons and holes (missing electrons in the valence band) over many molecules. If the intermolecular interaction is weaker, HOMO and LUMO states remain localized on individual molecules separated by energy barriers. This is typically the case for less ordered organic solids. The width of the energy bands is so small that HOMO and LUMO are usually represented by a line. The HOMO (LUMO) of the solid is shifted towards higher (lower) energies with respect to a single molecule due to the polarization of the surrounding molecules [138]. This also results in the decrease of the band gap energy between HOMO and LUMO. Three types of polarization can be distinguished: the electronic polarization, intramolecular geometrical polarization (structural reorganization of the molecule), and intermolecular geometrical polarization [138]. Due to structural disorder, HOMO and LUMO energies vary from molecule to molecule and are often assumed to follow a Gaussian distribution.

Adding an electron to the LUMO of a molecule is equivalent to the reduction of the molecule, while removing an electron from the HOMO corresponds to the oxidation of the molecule. Therefore, HOMO and LUMO levels of organic thin films are related to oxidation and reduction energies as derived from solution-based cyclic voltammetry (CV) measurements [139]. However, this relationship is complex, because oxidation and reduction energies determined for solvated molecules are affected by solvent, electrolyte, and electrodes. Furthermore, the bulk polarization energy shifting the HOMO and LUMO is not accessible by

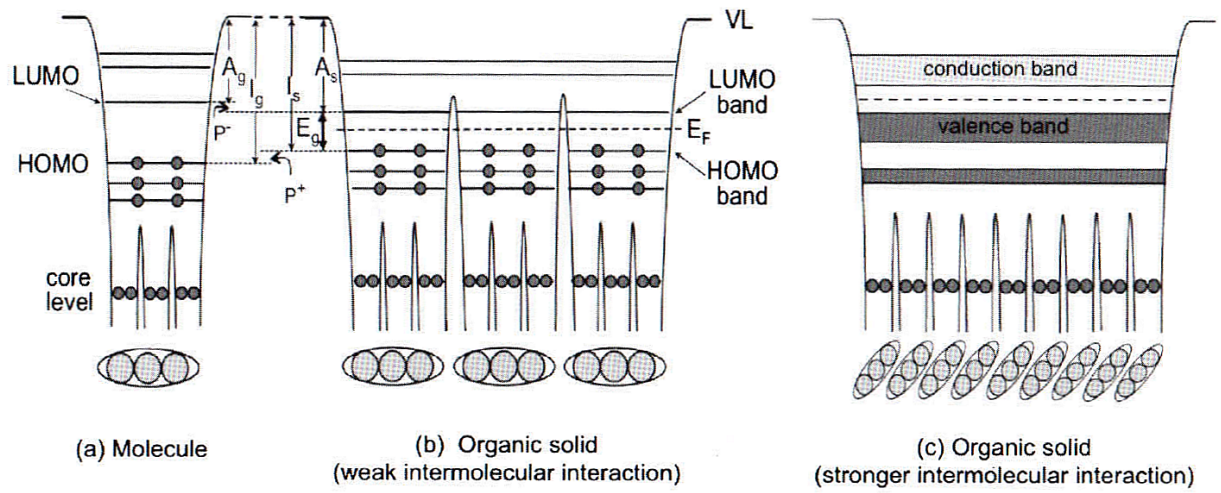

Figure 2.8 Energy level diagram for (a) a single molecule, (b) a solid with weak intermolecular interaction, and (c) a solid with strong interaction. The electron affinity A and the ionization potential I are indicated for the solid (s) and gas (g) phase. P is the polarization energy, E_g the energy gap, and E_F the Fermi level. VL is the vacuum level. Reprinted with permission from Ref. [138] (Copyright © 2012 Wiley-VCH Verlag GmbH & Co. KGaA).

CV.

Electron transport in disordered organic thin films

As illustrated in Fig. 2.8, electrons and holes are localized on individual molecules in disordered films of organic semiconductors. Charge carrier localization and the geometrical polarization of the environment reflect the strong electron/hole-phonon coupling [138]. To describe the transport of electrons/holes accompanied by the induced polarization, the quasi-particle *polaron* was introduced. Fig. 2.8 illustrates that electrons and holes have to overcome energy barriers to move from one molecule to the next. At low temperatures, electronic charge carriers can move by coherent tunneling. At room temperature, charge transport mostly takes place by thermally activated (phonon-assisted) charge carrier hopping [138].

The charge carrier mobility μ is defined by

$$\overrightarrow{v} = \mu \overrightarrow{F}, \tag{2.1}$$

where $\overrightarrow{v}$ is the charge carrier velocity and $\overrightarrow{F}$ is the electric field. The Einstein relation states that the mobility is proportional to the electron transfer rate k_{el},

$$\mu = \frac{eD}{k_b T} k_{el}. \tag{2.2}$$

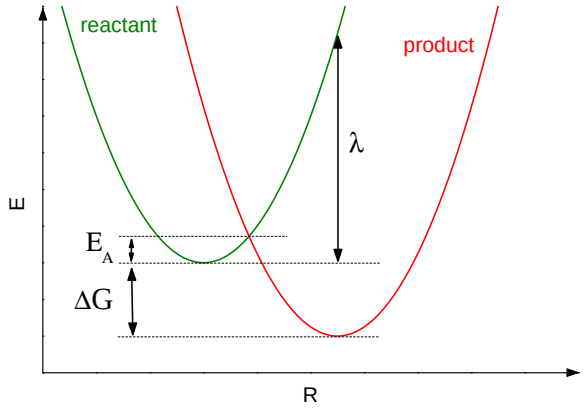

Figure 2.9 Energy diagram for the electron transfer according to Marcus theory. The configurational coordinate R describes the configuration of all nuclei of the molecule simplified to one dimension. The activation energy E_A equals $\frac{(\lambda+\Delta G)^2}{4\lambda}$. Reprinted from Ref. [140].

The electron transfer rate depends on the electronic coupling between two molecules, described by the intermolecular transfer integral t, and the reorganization energy of the molecules λ associated with charge transfer. For strongly localized charge carriers, Marcus theory predicts the temperature-dependence of k_{el} from the change in the Gibbs free energy ΔG due to the charge transfer and λ [138, 141]:

$$\mu \propto k_{el} \propto t^2 \frac{1}{\sqrt{4\pi\lambda k_b T}} \exp\left(-\frac{(\lambda+\Delta G)^2}{4\lambda k_b T}\right), \tag{2.3}$$

where k_b is the Boltzmann constant. Fig. 2.9 shows a schematic energy diagram for the electron transfer according to Marcus theory.

At high electric fields ($10^4 - 10^6$ V/cm), the mobility shows a field-dependence which is usually described with the Poole-Frenkel model [142]:

$$\mu \propto \exp\left(\gamma\sqrt{F}\right), \tag{2.4}$$

where γ is temperature-dependent. The charge carrier mobility is strongly affected by the molecular packing and the morphology of the film [143]. The correlation between film structure and electronic charge transport is also investigated in the article Wünsche *et al.*, *J. Mater. Chem. C*, vol. 1, no. 5, p. 967, 2013 for vacuum-sublimed tetracene films.

The conductivity σ of a material is not only determined by the carrier mobility μ but also by the charge carrier density n:

$$\sigma = nq\mu, \tag{2.5}$$

where q is the charge of one charge carrier. The occupancy of electron energy levels in the organic solid is given by the Fermi-Dirac distribution. The Fermi energy E_F lies approximately in the center of the energy gap between HOMO and LUMO if impurities can be neglected and the effective masses of holes and electrons are similar [138]. Since the energy gap in organic semiconductors is typically a few eV large, the density of thermally generated charge carriers at room temperature is very low. However, unintentional doping by impurities often leads to higher charge carrier densities.

There are several possibilities to further increase the electron and hole density. Amongst others, the film can be doped with suitable electron donor (reducing agent) or acceptor molecules (oxidizing agent) [4]. Charge carriers can be generated by photoexcitation (photoconductivity) or injected from the electrodes. Charge carriers injected from the electrodes can be accumulated in the organic film in thin film transistor structures via electrostatic or electrochemical doping [14, 144–146]. Many polymers with extended conjugation can achieve "metallic" conductivity when sufficiently doped [1].

It should be mentioned here that the electrical properties of an organic thin film sample depend not only on the properties of the film itself but also on the choice of electrodes and on the atmosphere during film processing and characterization. The position of the electrode work function with respect to HOMO and LUMO of the organic film largely determines the injection barrier for holes and electrons, respectively. Furthermore, charge injection is affected by surface reactions, trap states at the interface, and the formation of double layers [134, 147]. Water and oxygen from the atmosphere can introduce trap states that hinder electron transport [148, 149].

Hydrogen-bonded molecules

In the most general definition, a hydrogen bond is a directional bond between a proton donor and a proton acceptor via a hydrogen atom and is the result of the sum of various types of interactions [150]. At the most typical bond lengths, electrostatic interactions (including dipole-dipole) dominate but there is also a contribution from charge transfer. H-bonds play an important role in the supramolecular assembly of many biomolecules, e.g., DNA and proteins [151], and enable proton conduction via the Grotthuss mechanism, as will be discussed in Section 2.4.2.

The carbonyl and amine groups often present in H-bonded molecules are often considered to interrupt π-conjugation [151]. Recently, it has been demonstrated that a range of H-bonded small molecules can yield films with electron and hole mobilities comparable to benchmark organic semiconductors [20, 151–154]. For example, thin films of the natural pigment indigo were employed in organic field-effect transistors and showed electron and hole mobilities of

about 10^{-2} cm^2 V^{-1}s^{-1} and good air stability [20]. The strong H-bonding between indigo molecules induced high crystalline order with favorable molecular packing. The high degree of order and the reversible redox properties of indigo were identified as the main reasons for efficient electron/hole transport in the film. It should be noted that all materials cited above were purified and deposited by vacuum sublimation. These results indicate that molecules with limited intramolecular π-conjugation can show high electron and hole mobilities if the molecular packing is favorable. Such packing can be achieved by self-assembly induced by H-bonding [152]. In contrast, electronic conduction in H-bonded biomacromolecules such as DNA and eumelanin is still controversial [42, 155].

Mixed ionic-electronic conduction

In the previous sections, only the transport of *electronic* charge carriers was discussed. However, organic semiconductors are generally mixed conductors that transport both electronic and ionic charge carriers. The soft nature of organic thin films facilitates ion diffusion via interstices. The presence of mobile ions causes different device physics as compared to conventional semiconductor devices. For example, the presence of mobile ions opens the possibility to electrochemical reactions in organic solids. As discussed in Section 2.4.1, the injection of an electron (hole) is equivalent to the reduction (oxidation) of the acceptor/donor molecule in disordered organic solids. The difference between the electronic and the electrochemical perspective is the availability of ions to compensate the space charge created by carrier injection [156]. In organic electronic devices inspired by inorganic semiconductor devices, such as light-emitting diodes, solar cells, and field-effect transistors, electrochemical reactions are usually undesirable. Ions, solvents, water, and air can cause hysteresis in the device characteristics, introduce trap states, and reduce the device stability [156]. Therefore, their presence is avoided by material purification, processing, and encapsulation of the device under vacuum or inert atmosphere.

Recently, devices making use of ion migration and electrochemical reactions gained more attention, also due to potential applications at the interface of electronics and biology [15,157]. Ion migration can be employed in various ways. Mechanical actuators employ the swelling of the organic film [158]. Oxidation or reduction of the film upon insertion of ions can change the optical absorption properties of the film (used in electrochromic displays [159]) and its conductivity (used, for example, for sensing with electrochemical transistors [160]). Accumulation of ions at the electrodes can facilitate electron and hole injection, which enables low-voltage light-emitting electrochemical cells [161]. Furthermore, electrophoretic ion pumps have been realized with conducting polymers [162]. These examples illustrate the diverse applications enabled by the simultaneous conduction of ions and electrons/holes.

Despite its technological importance, ion transport in organic semiconductors is largely unexplored [163]. Many approaches have been suggested to distinguish and investigate simultaneous electron and ion conduction. These include impedance spectroscopy [164, 165], the measurement of polarization currents [166], coulometric measurements [43], the use of ion-blocking vs non-blocking electrodes [167], and the tracking of moving doping fronts [163,168]. However, most techniques do not yield unambiguous results when used on their own or can be applied only to certain classes of materials.

2.4.2 Fundamentals of proton transport

Proton transfer plays an important role in many biological processes, for example, in photosynthesis [169] and proton-activated bioluminescence [170]. Furthermore, many technologies rely on proton conduction, including fuel cells [171], and certain batteries and electrochemical transistors [172]. Recently, there has been considerable process in employing proton conduction in biocompatible materials for the development of sensing or stimulating devices that can interface with biological systems [124]. Thus, it is a common interest of various disciplines to understand and control proton transport in a wide range of systems. This section briefly introduces the basics of proton conduction (Section 2.4.2), focusing in the second and third part on hydrated acidic polymers (2.4.2) and analogies to electron and hole conduction in amorphous semiconductors (2.4.2).

Mechanisms of proton transport

Two limiting mechanisms for proton conduction can be distinguished, the vehicle mechanism and the Grotthuss mechanism, also referred to as structure diffusion mechanism [172]. In the vehicle mechanism, the proton is carried by larger species such as H_3O^+, which move at a rate corresponding to the molecular diffusion coefficient of the vehicle. The self-diffusion coefficient of liquid water at room temperature (D_{H_2O}) is $2 \cdot 10^{-5}\text{cm}^2\ \text{s}^{-1}$. The vehicle mechanism contributes about 22% to the conductivity of water under standard conditions [171].

In structure diffusion, the environment of the proton has no translational motion but its local dynamics are an inherent part of proton conduction [171]. Hydrogen interacts with up to two electronegative species (usually O, N, or F) in its close environment forming a hydrogen bond. The proton migrates along this H-bond network. The H-bond is usually asymmetric (O–H$\cdots$O), the shorter, stronger bond belonging to the proton donor and the longer, weaker bond to the proton acceptor [172]. To transfer from donor to acceptor, the proton has to overcome an energy barrier, which is smaller for stronger hydrogen bonds. For the case of a proton transfer from one O atom to another, the H-bond becomes symmetric

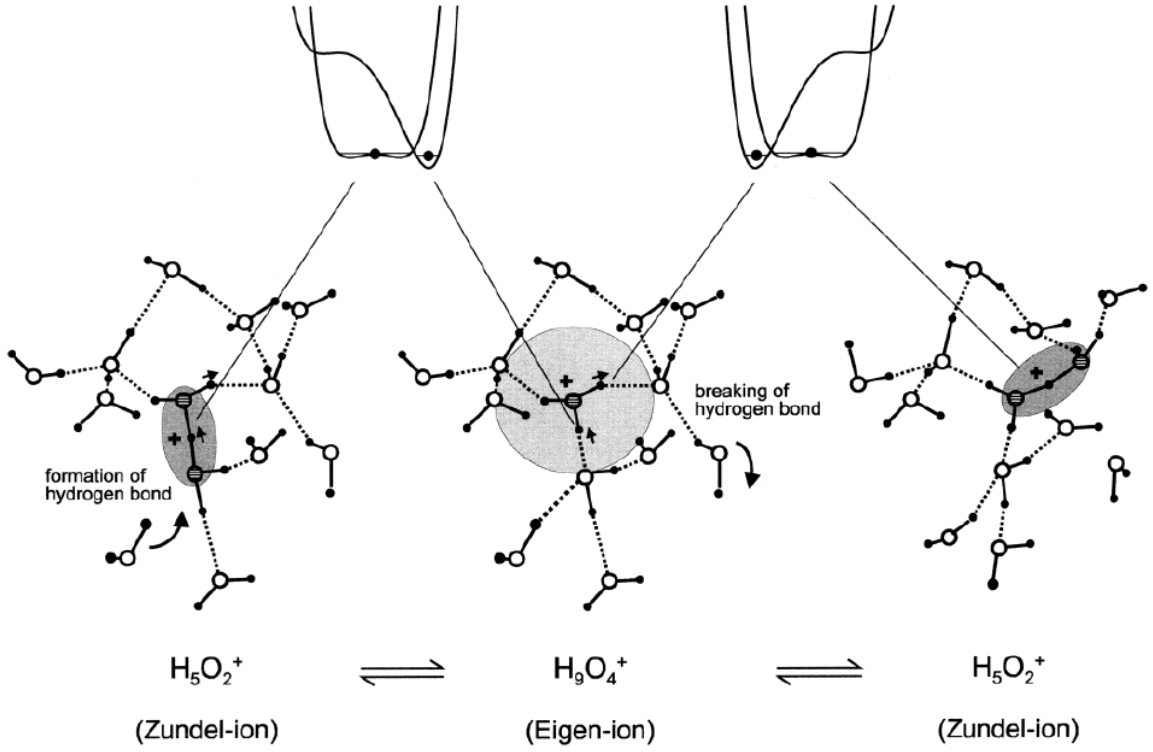

Figure 2.10 Illustration of proton conduction by structure diffusion in bulk water. The plots at the top of the figure schematically represent the potential seen by the proton in the various configurations. Reprinted with permission from Ref. [171] (Copyright © 2004 American Chemical Society).

and thus strongest (about 0.2 eV) at an O-O separation of about 240 pm [172]. However, proton conduction also requires the continuous breaking and reformation of H-bonds and the structural reorganization of the H-bond pattern. The proton conductivity depends on both the rate of proton transfer and the rate of reorganization of the environment. Indeed, compounds with weak or medium H-bond interaction (characterized by a proton donor-acceptor separation >260 pm) typically have the highest proton conductivities [172]. Fig. 2.10 illustrates the structure diffusion mechanism for proton conduction in water. The excess proton follows the diffusion of the center of symmetry of the H-bond network. During this process the proton can be considered part of either a Zundel ion ($H_5O_2^+$) or an Eigen ion ($H_9O_4^+$) as the limiting cases [171]. The transport of protons along H-bond chains in bulk water should not be imagined as the concerted transfer of many protons as suggested by early descriptions of the Grotthuss mechanism but rather as a step-wise local phenomenon. The character of proton conduction in low-dimensional water structures can be partly concerted. The transport of defect protons (OH^{-1}) can be described in a similar way as the transport of H^+. However, the coordination of the hydroxide ion to its environment is somewhat different

and still a matter of debate [171].

Hydrated acidic polymers

Hydrated acidic polymers play an important role as separator materials in low-temperature fuel cells [171]. Their nanostructure is characterized by hydrophobic domains (the polymer backbone) and hydrated hydrophilic domains, where proton conduction takes place. The hydration water creates mobile protons by dissociation from the acidic groups of the polymer and facilitates proton transport. For efficient proton conduction via structure diffusion, the H-bond network in the hydrophilic domains needs to provide continuous transport paths between the two electrodes. The formation of continuous pathways can be described by the percolation theory [171], which predicts a power law increase of the conductivity (σ) with hydration (H) beyond a certain critical value (H_c) [173, 174],

$$\sigma(H) \propto (H - H_c)^{\mu}\,, \tag{2.6}$$

where μ is an exponent depending only on the dimensionality of the system in an ideal case. The percolation threshold and in general the proton transport properties strongly depend on the morphology of the hydrated polymer [175]. For Nafion®, the archetype proton-exchange membrane material, good percolation is found at low hydration levels of few water molecules per sulfonic acid group [171]. However, the higher concentration of excess protons in water domains at low hydration suppresses protons transfer (reflected by a lower proton conductivity diffusion coefficient, D_σ (Fig. 2.11)). Therefore, the vehicle mechanism, determined by the water self-diffusion is dominant at low hydration [171]. Apart from proton concentration, important parameters that determine the contribution of vehicle mechanism and structure diffusion to the protonic current are temperature T and pressure p.

Analogies to electron and hole transport in amorphous semiconductors

Proton conduction is a thermally activated process, as can also be seen in Fig. 2.11. The temperature dependence of the conductivity is often described by the following formula [176]:

$$\sigma(T) \propto \frac{1}{T} \exp\left(\frac{E_A}{RT}\right), \tag{2.7}$$

where E_A is the activation energy and R the universal gas constant. Already in 1958, it was recognized by Eigen and de Maeyer that proton conduction along H-bond networks shows analogies to electron and hole transport in semiconductors [177]. Recently, this idea gained new popularity for the explanation of the working principle of protonic field-effect transistors

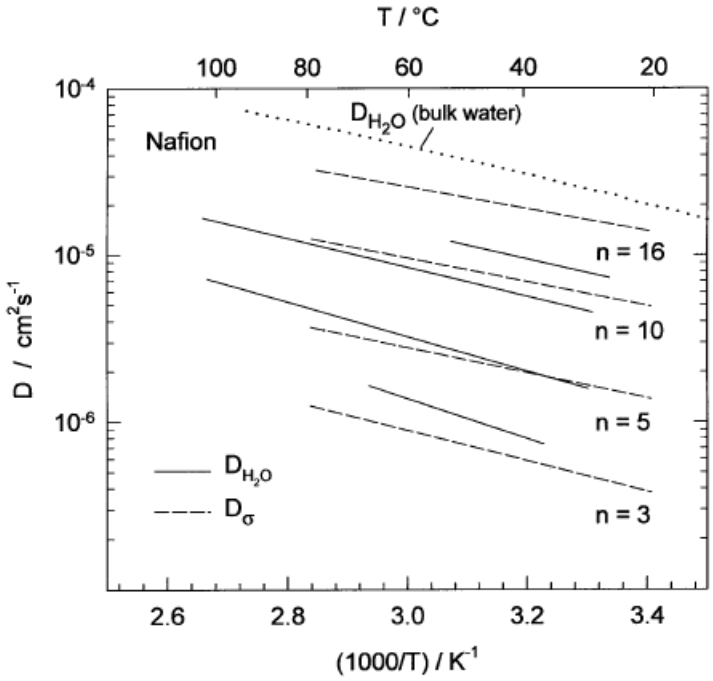

Figure 2.11 Temperature and hydration dependence of the proton conductivity diffusion coefficient, D_σ, and the water self-diffusion coefficient, D_{H_2O}, for Nafion®, representing proton conduction by structure diffusion and vehicle mechanism, respectively. n is the number of water molecules per sulfonic acid group. Reprinted with permission from Ref. [171] (Copyright © 2004 American Chemical Society).

(FETs) and p-n type junctions [21, 124]. Rolandi *et al.* modified chitin with acidic and basic groups so that the majority charge carriers are either H^+ or OH^-, the latter being treated as "proton hole". In this picture, the energy level of the neutral H-bond network corresponds to the valence band and the energy level of migrating excess protons to the conduction band. Valence and conduction band are separated by an energy gap, which was derived from the dissociation constant of water. Acidic and basic groups introduce donor and acceptor levels in the energy gap, respectively. This concept is schematically illustrated in Fig. 2.12. The authors support this model by the demonstration of p- and n-type protonic FETs, as well as of a rectifying junction. The protonic devices showed characteristics qualitatively similar to their electronic counterparts, with two exceptions: a true off-state was not achieved in the protonic FETs (this was attributed to the "doped" nature of the chitin derivatives used) and a slow increase of the current in the p-n junction was also observed under reverse bias (tentatively assigned to water splitting). By modeling the FET characteristics, the authors derived a proton mobility of about $5 \cdot 10^{-3}$ cm^2 V^{-1} s^{-1} [124]. The devices described above were realized with palladium hydride (PdH_x) electrodes, which are able to inject and extract

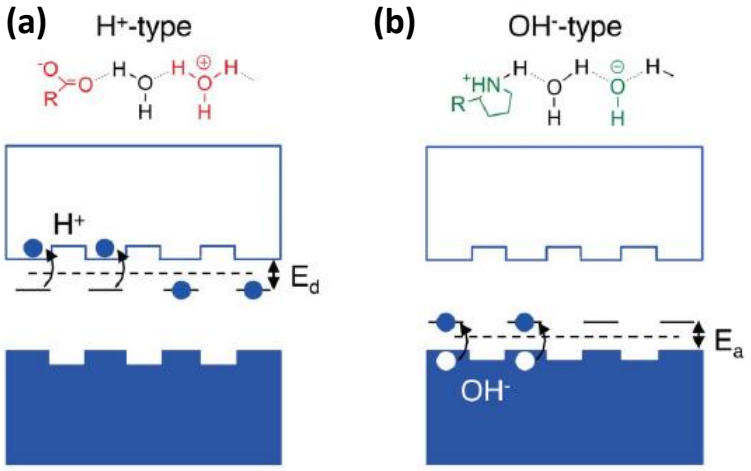

Figure 2.12 Energy diagram for proton conduction in H^+- and OH^--type chitin derivatives according to a semiconductor model. The diagram shows valence and conduction band for protons with hopping barriers. The "doping" effect of acidic and basic groups is also illustrated. Reprinted from Ref. [124] (Creative Commons license, Copyright © 2013, Rights Managed by Nature Publishing Group).

protons under electrical bias [176, 178].

2.4.3 Charge carrier transport properties of eumelanin

The first part of this section (2.4.3) summarizes important results on the electrical properties of eumelanin pellets. For the most part, these results have contributed to the paradigma that eumelanin is an amorphous semiconductor. A recent study, which seems to disprove the amorphous semiconductor model for eumelanin, is disscussed in more detail [42]. Section 2.4.3 is devoted to recent works on eumelanin thin films.

Eumelanin pellets

Several biomolecular materials are electrically conductive. Typically, the conductivity is higher in the hydrated than in the dry state [179]. The nature of the charge carrier and the mechanism of conduction in biomolecular materials has been a matter of intense debate since the discovery of their electrical properties [42, 180, 181]. Apart from eumelanin, a prominent example is DNA [155].

In 1960, Longuet-Higgins suggested that the free-radical properties and the broad optical absorption spectrum of eumelanin could be understood if eumelanin was assumed to be a one-dimensional semiconductor [22]. Shortly after, Pullman *et al.* proposed a band model for eumelanin [23]. At the end of the 60's, a wide range of biological substances,

including synthetic eumelanin, were considered to be semiconductive [43, 179]. *Semiconductivity* was defined by an Arrhenius temperature dependence of the conductivity. Rosenberg *et al.* stressed that the term does not imply any specific conduction mechanism or type of charge carrier, i.e., electrons or ions [179]. On the basis of solid-state electrolysis, Powell and Rosenberg suggested, that 65% of the current is protonic and 35% electronic in eumelanin pellets [43]. Surprisingly, they did not observe any change between 10 wt% and 35 wt% of hydration. It should be noted that coulometric measurements can be ambiguous [176]. To explain the strong hydration dependence of the conductivity σ, the phenomenological *modified dielectric theory* was developed [179]. According to this theory, water increases the effective dielectric constant of the hydrated material ($\kappa_h yd$), in turn decreasing the activation energy for charge carrier separation:

$$\sigma(T, \kappa_{hyd}) = \sigma_0 \exp\left(\frac{-E_{A,dry}}{2k_bT}\right) \exp\left[\frac{e^2}{2k_bTr}\left(\frac{1}{\kappa_{dry}} - \frac{1}{\kappa_{hyd}}\right)\right], \tag{2.8}$$

where κ_{dry} and $-E_{A,dry}$ are the dielectric constant and the activation energy for charge carrier separation in the dry state, respectively, T is the temperature, k_b the Boltzmann constant, and r the screening length of the electric charge.

In 1972, McGinness argued that the optical and electrical properties of eumelanin can be best understood within the framework of the amorphous semiconductor model, recently developed by Mott [24, 182]. His discussion is based on the featureless monotonic optical absorption spectrum of eumelanin, its photoconductivity [34], and field-dependent carrier mobility (derived from non-linear current-voltage characteristics) amongst others. Two years later, the same author reported reversible switching of eumelanin pellets from a high to a low resistive state beyond a certain threshold voltage [25]. Threshold switching was previously reported for inorganic amorphous semiconductors. The eumelanin pellets (thickness 0.1-10 mm) were sandwiched between carbon, copper, and Al electrodes and voltages up to 350 V were applied. Switching was observed only for hydrated samples, with on/off-ratios of 100-1000. By estimating the amount of water in the eumelanin pellet, McGinness *et al.* argued that the protonic contribution to the current in the on-state must be negligible.

In the following decades, electrical studies on eumelanin were mostly interpreted within the amorphous semiconductor model. Further band models were suggested based on temperature-dependent conductivity, optical absorption, and photoconductivity measurements [33, 183]. The optical band gaps determined varied from 1.4 to 3.4 eV. Important contributions came from Jastrzebska *et al.* [35, 71, 184–186]. They reported the thermoelectric effect for eumelanin suggesting p-type conduction and that eumelanin is able to retain its polarization state [184]. In a later study, they reported the hydration dependence of the conductivity

of eumelanin pellets ranging from 10^{-13} S cm^{-1} under vacuum to 10^{-5} S cm^{-1} at a fully hydrated state [71]. From the temperature dependence of the conductivity, they deduced an activation energy of 0.5-0.8 eV, which is in contrast to the values determined from their thermoelectric measurements, 0.2-0.3 eV. It has to be noted that the temperature was varied only over 50 K and that it is challenging to control temperature and sample hydration at the same time. This is reflected in the difference of heating and cooling curves even under vacuum conditions. Jastrzebska *et al.* also characterized dried eumelanin pellets by dielectric spectroscopy [185, 186]. Polaron hopping was deduced as the main conduction mechanism from the low-frequency dielectric response. Hopping distances of 1.5 and 3.6 nm were determined, which increased after further drying of the pellets by heating. Activation energies for pellets of *Sigma melanin* and *Sepia melanin* under vacuum were also reported by Ligonzo *et al.* [38]. Values between 0.4 and 0.9 eV were determined for *Sigma melanin* depending on the temperature range and previous heat treatment, as well as an optical band gap of 1.4 eV.

Bridelli *et al.* investigated the polarization properties of eumelanin pellets under N_2 [70]. They attributed the thermally stimulated depolarization currents to the re-orientation of water molecules. For a quantitative agreement, they had to assume an unusually high water content of 16 water molecules per monomer of eumelanin. As alternative interpretation, they suggested the hopping of protons from water dissociation to neighbouring water molecules.

While most works since the 1970's focused on electronic charge transport in eumelanin, Gonçalves *et al.* reconsidered the role of protons in the electrical properties of eumelanin in 2006 [41]. Temperature-dependent conductivity measurements on eumelanin pellets under vacuum showed the typical hysteresis due to water loss (Fig. 2.13). Infrared spectroscopy showed an increase of the -COOH signal upon heating, which the authors interpreted as a trapping of mobile interlayer protons by -COO$^-$ groups. At the same time the ESR signal increased, which was explained by the comproportionation equilibrium (Fig. 2.5) and an increase of the effective pH. Gonçalves *et al.* discussed the possibility of protons being the dominant type of charge carrier based on the strong decrease of conductivity during dehydration. However, they considered it more likely that protons modulate the density of mobile electrons on the polymer backbone, analogous to the pH-dependent electron conduction of polyaniline [121], since they did not observe any dependence of the DC current on time.

Important new insights came from a study published in 2012 by Mostert *et al.* based on hydration-dependent conductivity, ESR, and muon spin relaxation measurements [42, 187]. Mostert *et al.* showed that the use of a sandwich configuration, encountered in most experiments on eumelanin pellets, can lead to erroneous results in hydration-dependent conductivity measurements due to incomplete sample hydration. Their results, obtained with coplanar electrodes in van der Pauw configuration, are incompatible with the amorphous semiconduc-

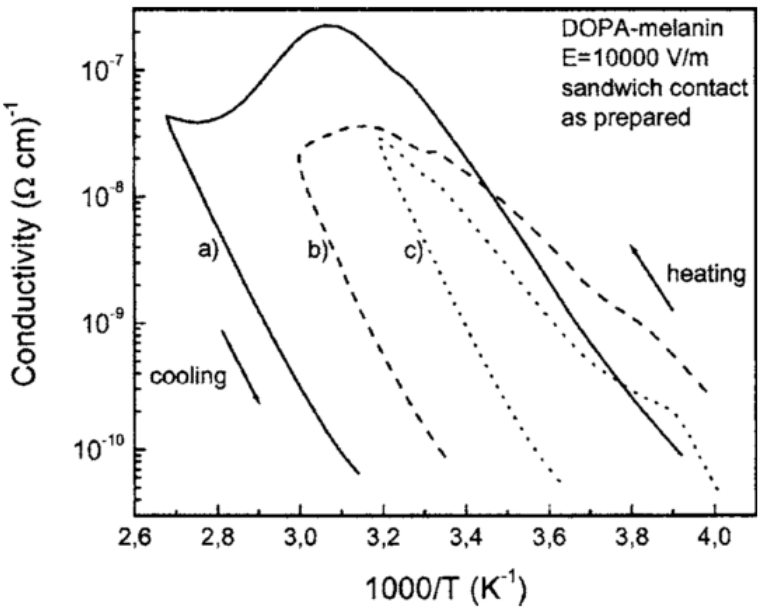

Figure 2.13 Temperature-dependence of the conductivity of synthetic eumelanin pellets under vacuum using different maximum temperatures: 373 K (a), 333 K (b), and 313 K (c). An activation energy of about 0.5 eV was deduced from the cooling curve. Reprinted with permission from Ref. [41] (copyright © 2006 American Institute of Physics).

tor model with modified dielectric constant (equation 2.8) using the Lorentz-Lorentz relation for $\kappa_h yd$ (Fig. 2.14a). The authors could furthermore show that the electron spin density as deduced from the relaxation rate of paramagnetic muons increases with hydration in a similar way as the conductivity (Fig. 2.14b). While the intrinsic carbon-centered spin density decreased with hydration, pH-dependent ESR measurement indirectly suggested that the semiquinone free radicals should increase with hydration according to the comproportionation equilibrium (Fig. 2.5). Thus, the authors concluded that semiquinone radicals are the electronic charge carriers in eumelanin. This contradicts the assumption of Gonçalves *et al.* that the increase of ESR signal during dehydration can be understood through the comproportionation equilibrium [41]. The muon hopping rate deduced from muon spin relaxation measurements can serve as an indication for proton mobility and was found to be constant over the hydration range studied. This was interpreted by the authors as a further indication that the comproportionation equilibrium governs both the density of mobile protons and electrons. They termed this phenomenon "water-induced self-doping" and suggested that it is responsible for the hydration dependence of the conductivity. A more detailed recent ESR study on hydrated eumelanin pellets by the same authors could only weakly support this hypothesis (discussed in Section 2.2.3) [85]. Mostert *et al.* also reported a photoconductiv-

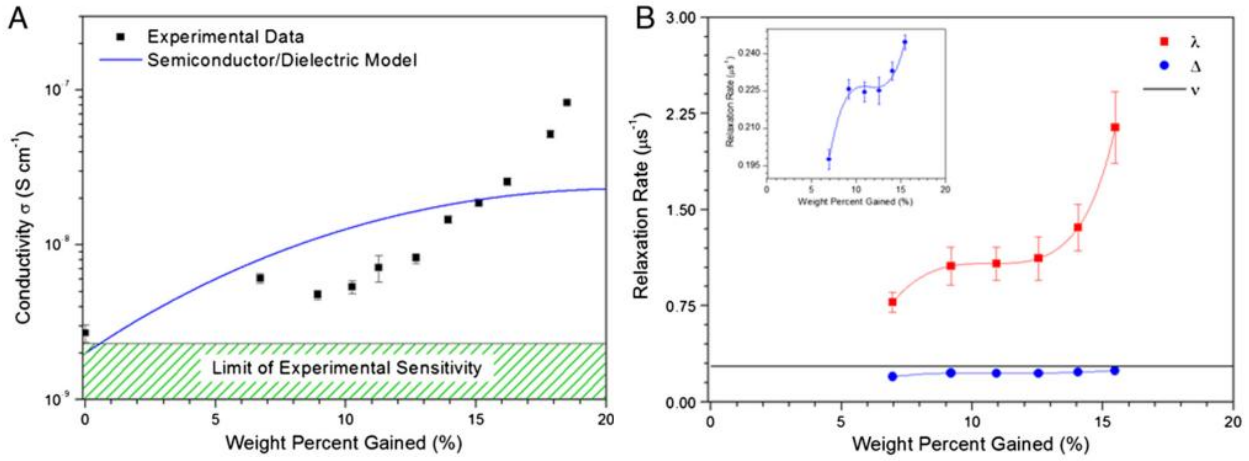

Figure 2.14 (a) Hydration dependence of the conductivity of eumelanin pellets with electrodes in van der Pauw configuration and best fit according the modified dielectric theory (equation 2.8). (b) Results from the muon spin relaxation experiments. λ is the relaxation rate for paramagnetic muons (a measure for the unpaired spin density), Δ is the relaxation rate for diamagnetic muons (a measure for the local field experienced by free protons), and ν is the muon hopping rate (a measure for the proton mobility). The inset shows Δ vs hydration on a different scale. Both measurements in (a) and (b) were conducted at room temperature. Reprinted with permission from Ref. [42] (copyright © 2012 National Academy of Sciences).

ity measurement of a partly hydrated pellet that shows no correlation to the intrinsic spin signal and demonstrates the long RC time often observed in electrical measurements of eumelanin [42]. The overall conclusion of their work is that eumelanin is a mixed ionic-electronic conductor and that the amorphous semiconductor model cannot be applied to eumelanin [51]. It should be noted that the spectroscopic techniques used by the authors only give qualitative insight on locally mobile carriers. It is not clear to which extent electrons and protons contribute to charge conduction over several micrometers or 1 mm (typical size of pellet samples).

Eumelanin thin films

Studies on eumelanin thin films have been reported only recently, due to the challenges in film processing. Dezidério *et al.* reported the temperature dependence of the in-plane current of *DMF melanin* films under vacuum. A voltage of 100 V was applied with Ag electrodes. Results indicated an activation energy of 0.9 eV and no effect of HCl treatment on the conductivity. Abbas *et al.* also investigated the temperature dependence of the in-plane resistance of eumelanin films (*Sigma melanin* electrospray deposited from methanol-DMSO suspension) under vacuum and N_2 [36, 129]. They observed hysteresis in the heating-

cooling curves of the electrical resistance above 375 K due to the removal of strongly bound water. The photoconductivity was found to be very small (10-15% increase of pA currents) under rigorous temperature control. To reach a steady-state, the samples were pre-biased at 50 V for 20 min before the actual measurement [36]. In a subsequent study, the authors derived two activation energies, 0.8 and 1.3 eV, from a temperature-dependent measurement over 180 K [129]. Current-voltage (I-V) characteristics at room temperature showed strong hysteresis, while hysteresis was absent at 480 K. The authors suggested electron transport through delocalized π-states and hopping between shallow trap states to explain their results at high and low temperature, respectively. In the works mentioned above, information on the sample geometry is missing, so that a comparison of conductivities is not possible.

In-plane conductivities have been reported for eumelanin films in fully hydrated state: $2.5 \cdot 10^{-5}$ S cm^{-1} for *dopa melanin* deposited from ammonia solution [49] and $7 \cdot 10^{-5}$ S cm^{-1} for *Sigma melanin* films from DMSO solution [39]. Ohmic behavior was reported in the former work, without specifying over which voltage range. In the latter work, which uses thermally evaporated Au top electrodes, it was suggested that the contact resistance was zero (channel length variation between 50 and 200 μm). Voltages up to 10 V were applied. Ohmic behavior was also reported by Bloisi *et al.* for MAPLE-deposited eumelanin films with uncontrolled partial hydration ($V \leq 50$ V). It is important to note that at such high voltages the electrical response of the samples might be dominated by water electrolysis if the samples are sufficiently hydrated and protons are mobile.

A series of electrical measurements on vertical structures with eumelanin (*Sigma melanin* spin-coated from ammonia solution) sandwiched between Au and indium tin oxide (ITO) or doped Si has been reported by Ambrico *et al.* between 2010 and 2014 [44, 53, 188, 189]. Measurements were conducted under vacuum or ambient air (40-50% relative humidity) and aimed at investigating the charge storage/memory characteristics of eumelanin thin films. Cyclic I-V measurements between -1 V and 1 V on ITO/eumelanin/Au structures showed symmetrical hysteresis in vacuum but asymmetric hysteresis and superlinear increase of the current in air [53]. The loop area increased with the sweep rate and the maximum voltage. Charge trapping was suggested as the cause of hysteresis under vacuum and electron or hole accumulation at one of the interfaces for the hysteresis in air. Also the transient nature of the photocurrent under vacuum was explained by charge storage. In contrast, light had no measurable effect on the current in air. It was shown that samples switched to a low resistive state beyond -3 to -4 V both in air and under vacuum. No "erasing" voltage was found to reset the sample to its initial high resistive state.

For doped Si/eumelanin/Au structures, Ambrico *et al.* reported capacitance-voltage measurements that show hysteresis with a different loop direction in air and under vacuum [44].

The eumelanin film was modeled by a parallel RC circuit. The authors claim that water bridges and H-bonds form a percolation path for hole and electron conduction between the eumelanin molecules and that weakly bound water acts as a hole and electron trapping site at the same time, when measurements are done in air. Under vacuum, both the continuous path for electrons and holes and the water-induced trapping sites were considered absent. In apparent contradiction, the authors argue that the drift of H^+ and OH^- ions from residual water causes the observed hysteresis. It has to be noted that this interpretation is based on capacitance-voltage measurements alone and seems to be in contradiction with what the authors suggested in their previous study on ITO/eumelanin/Au samples. The memory behavior of p-Si/eumelanin/Au was investigated by further capacitance-voltage measurements before and after the application of a writing voltage in air [188]. The capacitance-voltage curves shifted towards negative voltage after biasing at -2.5 V (Au electrode negative). The authors assigned this behavior to hole injection from p-Si and subsequent trapping in the eumelanin film. This state was retained for several days and the initial state was re-established after more than one week. To explain the behavior under positive and negative voltages as well as the absence of an erasing voltage, Ambrico *et al.* suggested that in addition to hole injection, the drift of H^+ and OH^- induces a "persistent electrical polarization".

In 2014, Ambrico *et al.* reported EIS measurements on planar and nanostructured p-Si/eumelanin/Au as well as ITO/eumelanin/Au samples, measured in air (50% RH) [189]. Different equivalent circuits were used to fit the Nyquist plots of each structure (Fig. 2.15). For the planar devices, a low-frequency capacitance C_{ad} and a Warburg element W for carrier diffusion were assigned to the melanin layer. In series to these components, the authors used parallel RC and R-CPE (CPE-constant phase element) circuits to describe the Si or eumelanin film high-frequency impedance and charge carrier trapping at the Au/eumelanin interface. For the nanostructured devices, a CPE-R_{CT} element parallel to a double-layer capacitance C_{DL} was introduced. Such a circuit is characteristic for Au/polyelectrolyte interfaces and suggests the presence of redox processes at the Au/eumelanin interface. R_{CT} is the corresponding charge-transfer resistance. C_{DL} was found to be two orders of magnitude lower than in typical Au/polyelectrolyte interfaces (0.1 μF/cm^2). The application of a +15 V pulse to the Si side of the nanostructured device resulted in a decrease of the contribution of the CPE element, assigned to detrapping of charge carriers at the Au/eumelanin interface and the removal of the double layer capacitance. The initial value of the CPE element was partially restored after 1 h, explained by slow re-trapping of the charge carriers. The authors also mention the possibility of a redox cycling process. Similar behavior was found for nanostructured reference devices without eumelanin. It was shown that the charge-transfer resistance assigned to the Au/polyelectrolyte interface was reduced by the presence

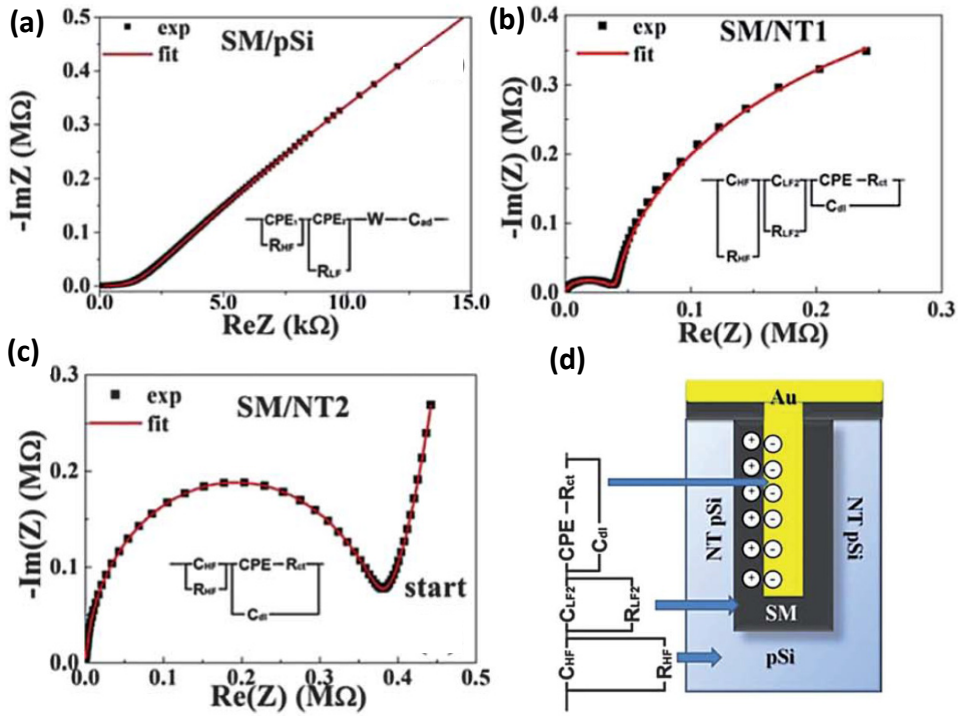

Figure 2.15 Nyquist plots of the impedance spectroscopy results for a planar p-Si/eumelanin/Au device (a) and for two devices with differently nanostructures p-Si/eumelanin interfaces, (b) and (c). (d) schematically illustrates the assignments of equivalent circuit elements used to fit the Nyquist plots. Reprinted with permission from Ref. [189] (copyright © 2013 The Royal Society of Chemistry).

of eumelanin.

In summary, it is no exaggeration to say that the charge carrier transport properties of eumelanin are poorly understood. Although charge transport in eumelanin has been studied since the late 1960's, the type of charge carrier (electronic vs. ionic, positive vs. negative) and the charge transport mechanism are unclear. Charge transport parameters such as energy gap and activation energy vary widely from one study to another and data interpretation is sometimes contradictory. This should be partly due to the often poor control of the sample hydration state and, in particular in the case of pellets, sample morphology. Furthermore, it should be noted that the sample geometry, size and the applied voltage strongly differ from one study to another. The charge carrier transport properties of strongly hydrated eumelanin films have not been systematically investigated. Nevertheless, several works from Mostert *et al.* [42, 187] and Ambrico *et al.* [188, 189] over the last two years contain important new information about the potential role of protons/ions in charge transport and the origin of the electronic charge carrier.

CHAPTER 3

ARTICLE 1: Eumelanin thin films: solution-processing, growth, and charge transport properties

This article has been published in the Journal of Materials Chemistry B as part of a themed issue on Carbon Bioelectronics in 2013 [1] and was submitted upon invitation. It reports a comparison of different procedures for the solution-processing of synthetic eumelanin thin films, an investigation of the growth and morphology of these films, and the hydration-dependent transient electrical properties of eumelanin films. The supporting information for this article is reprinted in Appendix A of this thesis.

3.1 Authors

Julia Wünsche,[a] Fabio Cicoira,[b] Carlos F. O. Graeff,[c] and Clara Santato[a]

[a] *Département de génie physique, École Polytechnique de Montréal,CP 6079, Succursale Centre-Ville, Montréal, Québec H3C 3A7 (Canada)*
[b] *Département de génie chimique, École Polytechnique de Montréal, CP 6079, Succursale Centre-Ville, Montréal, Québec H3C 3A7 (Canada)*
[c] *DF-FC, UNESP - Univ Estadual Paulista, Av. Eng. Luiz Edmundo Carrijo Coube 14-01, 17033-360 Bauru (Brazil)*

3.2 Abstract

Eumelanin pigments show hydration-dependent conductivity, broad-band UV-vis absorption, and chelation of metal ions. Solution-processing of synthetic eumelanins opens new possibilities for the characterization of eumelanin in thin film form and its integration into bio-electronic devices. We investigate the effect of different synthesis routes and processing solvents on the growth, the morphology, and the chemical composition of eumelanin thin films using atomic force microscopy and x-ray photoelectron spectroscopy. We further characterize the films by transient electrical current measurements obtained at 50%-90% relative humidity, relevant for bioelectronic applications. We show that the use of dimethyl sulfoxide is preferable over ammonia solution as processing solvent, yielding homogeneous films with

1. J. Wünsche, F. Cicoira, C. F. O. Graeff, and C. Santato, *Journal of Materials Chemistry B*, vol. 23, pp. 3836-3842, 2013

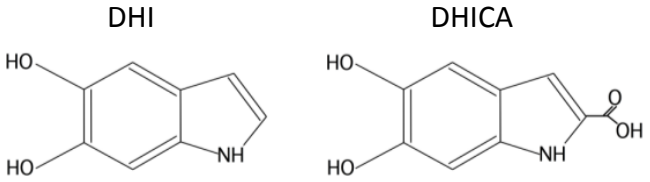

Figure 3.1 Main building blocks of eumelanins: 5,6-dihydroxyindole (DHI) and 5,6-dihydroxyindole-2-carboxylic acid (DHICA).

surface roughnesses below 0.5 nm and a chemical composition in agreement with the eumelanin molecular structure. These eumelanin films grow in a quasi layer-by-layer mode, each layer being composed of nanoaggregates, 1-2 nm high, 10-30 nm large. The transient electrical measurements using a planar two-electrode device suggest that there are two contributions to the current, electronic and ionic, the latter being increasingly dominant at higher hydration, and point to the importance of time-dependent electrical characterization of eumelanin films.

3.3 Introduction

Melanins are biomacromolecules responsible for the pigmentation of many plants and animals. The biological functions of melanins, also present in the inner ear and the substantia nigra of the human brain, go far beyond coloration and include photoprotection, anti-oxidant behavior, and metal chelation [27, 56]. Melanins are also intensively studied for their involvement in melanoma skin cancer and Parkinson desease [29, 31].

Eumelanins, macromolecules mainly composed of 5,6-dihydroxyindole (DHI) and 5,6-dihydroxyindole-2-carboxylic acid (DHICA) and their redox forms, are the most ubiquitous melanins in humans and the most studied by material scientists (Fig. 3.1) [46]. Back in the 1960-70s, eumelanin in form of pressed pellets was discovered to be conductive, photoconductive, and to show threshold switching [25, 33, 34]. These properties and the broadband UV-vis absorption of eumelanin were explained mostly within the amorphous semiconductor model [24, 71]. However, this interpretation has been challenged several times, especially considering the strong hydration dependence of the electrical properties of eumelanin [43, 187]. There is now growing evidence that protons play an important role in the charge carrier transport in eumelanin [41, 42, 44]. The potential for mixed ionic-electronic conduction combined with anti-oxidant, metal chelation properties, and the intrinsic biocompatibility of eumelanin make it an interesting candidate for organic bioelectronic applications.

Despite the recent research efforts, most fundamental properties of eumelanin such as its molecular structure and charge transport mechanism are still poorly understood [46]. In

particular, it is still a matter of debate whether eumelanin has an extended heteropolymeric structure or is composed of smaller oligomers, stacked in a graphite-like manner [45, 60]. Eumelanin should furthermore be regarded as a mixture of chemically similar macromolecules rather than a well-defined chemical entity [56, 77]. This chemical heterogeneity, the limited solubility of eumelanin and the amorphous character of materials based thereon make its characterization challenging [45].

Due to difficulties in the extraction and purification of natural eumelanin without alteration of its molecular structure, different synthesis routes have been developed to prepare model eumelanins [50]. Only recently, protocols for the solution processing of synthetic eumelanin thin films have been reported and the selection of potentially suitable solvents seems to be restricted to dimethyl sulfoxide (DMSO) [48], dimethyl formamide, [48] and ammonia solutions [49]. Therefore, there is an urgent need to investigate the effect of the synthesis route and processing conditions on the growth mechanism of eumelanin thin films and their final properties.

To explore the potential of eumelanin thin films for bioelectronics, which typically involves operation in aqueous environment, the charge transport properties of strongly hydrated eumelanin films need to be well characterized and understood. This effort would represent a first step towards the interfacing of eumelanin thin films with biologically relevant solutions. Studies of electrical properties of eumelanin thin films reported so far have been carried out in vacuum and ambient air (i.e. low film hydration) [36, 41, 44, 48, 130, 133] or are limited to the determination of the film conductivity at 100% relative humidity (RH) [39, 49]. Studies on (partly) hydrated eumelanin films were commonly performed at high voltages ($\leq$10 V) [39, 130, 133], which might result in undesired currents due to water electrolysis, for example. Furthermore, Au or Ag were typically used as electrode materials in melanin thin film devices [39, 41, 44, 49, 130]. However the use of these metals should be avoided, since they can electrochemically react with eumelanin, as we recently demonstrated (Article 2).

In this work, we investigate the morphology and chemical composition of solution-processed eumelanin thin films obtained with three different procedures: the auto-oxidation of L-dopa in aqueous suspension (*Dopa melanin*) [80], a standard method reported in 1978; the auto-oxidation of L-dopa in DMSO suspension (*DMSO melanin*) [48], which has been reported to yield a more homogeneous product with higher solubility; the oxidation of tyrosine with hydrogen peroxide, a product that is commercially available from Sigma Aldrich (*Sigma melanin*). Eumelanins films were spin-coated from DMSO and ammonia suspensions. Atomic force microscopy (AFM) and X-ray photoelectron spectroscopy (XPS) were employed to identify the most promising synthesis routes and processing solvents amongst those studied here, in terms of film morphology and chemical composition. AFM characterization of

eumelanin films of various thicknesses also permitted to identify the growth mode of the solution-processed eumelanin films giving a simple explanation for the low surface roughness obtained even at film thicknesses of several hundreds of nanometers and lending support for the stacked oligomer picture of the eumelanin structure. Furthermore, we performed transient current measurements of eumelanin thin films at controlled humidity, ranging from 50% to 90%, using Pt electrodes, upon application of electrical biases ≤ 1 V. Such measurements supply important information on mixed ionic-electronic transport in eumelanin thin films, where the presence of mobile ions/protons has been revealed by infrared, electron spin resonance, and muon spin relaxation measurements [41,42]. Our measurements, at short and long timescales support the hypothesis of mixed ionic-electronic conduction and give new insights into the contribution of these two types of charge carriers at different hydration states.

3.4 Experimental

3.4.1 Sample preparation

Dopa melanin was synthesized according to the standard method reported in Ref. [80]. *DMSO melanin* was synthesized as described in Ref. [48]. *DMSO melanin* has to be stored under inert atmosphere, since it is prone to a slow degradation in air, significantly reducing its solubility [128]. *Sigma melanin* and all other chemicals were purchased from Sigma Aldrich and used as received. The eumelanins were suspended in DMSO or ammonia solution (2:1 by volume, NH_3(aq) (28%) in deionized water), stirred for 30 minutes, and filtered. Concentrations of 0.3, 3, 15, and 30 mg ml^{-1} were used to obtain films about 8, 15, 30, and 50 nm thick by spin-coating. Film thicknesses were determined by AFM measurements on a scratch done on the film as well as by ellipsometry, the error associated to the measurement was of 25%. The suspensions were spin-coated at 1000 rpm for 2 minutes, followed by 4000 rpm for 30 s, on glass or thermally grown SiO_2 on Si substrates (SiO_2/Si). The substrates were pre-cleaned with isopropanol and acetone in an ultrasonic bath; SiO_2 substrates were also exposed to UV-ozone for 15 min after wet cleaning. For electrical measurements, Pt electrodes (30 nm thick, including a 5 nm Ti adhesion layer) were deposited onto Si/SiO_2 wafers by e-beam evaporation and patterned by photolithography (planar configuration, interelectrode distance $L = 10$ µm, electrode width $W = 7810$ µm [2]). Eumelanin films were deposited onto these patterned substrates using the same experimental conditions as described above.

2. This value misses a factor π. The correct W is 24.5 mm.

3.4.2 Sample characterization

AFM measurements were taken with a Dimension 3100 (Digital Instruments) with Si probes (tip radius <10 nm, spring constant 20-100 N/m) in tapping mode. Images were analysed with Nanoscope Analysis from Bruker. The root mean square roughness was averaged over 3 images of the same sample.

XPS measurements were taken with an ESCALAB 3 MKII from VG Scienta with a Mg Kα source. Measurements were taken on 30 nm thick films. The contribution of the SiO_2 substrate was subtracted.

Electrical measurements were performed in air, in a chamber with controlled relative humidity. The Pt electrodes were contacted with micromanipulated tungsten probes. A software-controlled source/measure unit (Agilent B2902A) was used to apply voltage pulses between 0.2 and 1 V to a 30 nm thick *Sigma melanin* film and to record the current-time characteristics. After each pulse the voltage was set to 0 V for 1000 s to allow the sample to equilibrate. For verification, the backward current was recorded during these phases. The first measurement was taken at 90% RH and the humidity was then decreased in steps of 10% for subsequent measurements. The sample was left for at least 24 h at constant humidity to equilibrate hydration before each measurement. A different device on the same substrate was used for each of the relative humidity states. Conductivity values were determined at an electrical bias $V = 0.6$ V by calculating $I(t)L/(VWd)$.

3.5 Results and discussion

3.5.1 Thin film processing

Figure 3.2 shows 10 µm × 10 µm AFM images of 30 nm thick films of *Dopa melanin*, *DMSO melanin*, and *Sigma melanin* spin-coated from DMSO and NH_3(aq) suspensions. The film root mean square roughness (Rq) was only 0.3-0.4 nm for films deposited from DMSO and 0.4-0.5 nm for films deposited from NH_3(aq), with the exception of *Dopa melanin*, which tended to yield films decorated with larger aggregates, especially when deposited from NH_3(aq). Except for the latter case, AFM images show that homogeneous and smooth films can be deposited using the eumelanin-solvent combinations studied here. The morphology is very similar for all these films, especially on a 1 µm × 1 µm scale (Fig. S1).

Interestingly, the similar film morphologies shown in Fig. 3.2 and S1, correspond to distinct chemical compositions, as revealed by XPS measurements (Tab. 3.1). While *Dopa* and *Sigma melanin* deposited from DMSO suspension have a C/N/O content approximately within the expected range for a macromolecule consisting of DHI and DHICA, *DMSO melanin* has a non-negligible concentration of S and higher C/N and O/N ratios than the other two

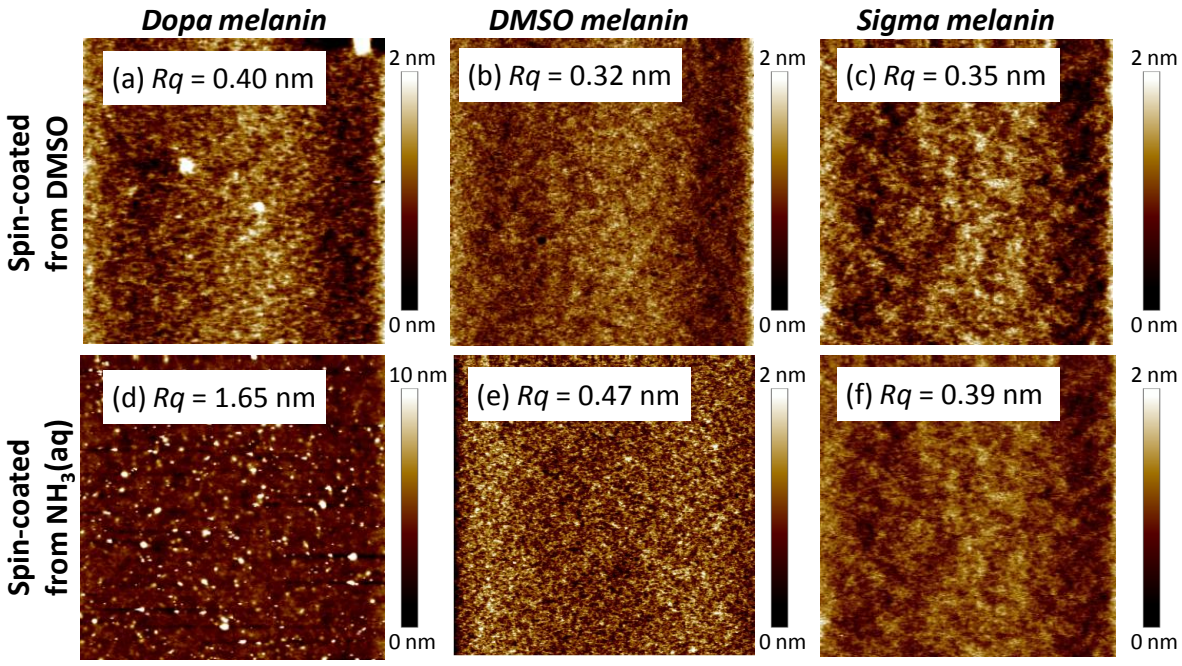

Figure 3.2 10 µm × 10 µm AFM images of 30 nm thick films of different eumelanins spin-coated from DMSO and NH_3(aq) suspensions as indicated. The root mean square roughness *Rq* is indicated for each film.

eumelanins. XPS data also reveal that processing eumelanin films in NH_3(aq) significantly increases the N content of the film and likely alters the molecular structure of eumelanin. The C/N and O/N ratios are more than a factor two lower for Sigma melanin films deposited from NH_3(aq) compared to films deposited from DMSO. The use of DMSO led to a slight increase in S content of less than 1 at%. The increase in S concentration is not necessarily related to a modification of the eumelanin molecular structure but might reflect residues of the low volatile solvent DMSO.

Although a complete structural picture of eumelanin synthesis products is usually obscured by the heterogeneous and insoluble character of these pigments, it is well known from numerous studies that different precursors and oxidation conditions during synthesis lead to eumelanins differing in macromolecular structure, DHI/DHICA ratio, and the presence of different monomers [50, 59]. For example, it has been recently reported that *DMSO melanin* contains $–SO_2CH_3$ groups bound to the phenolic hydroxyl groups, which is consistent with our results [128]. The effect of the processing solvent on the chemical composition of eumelanin films has been poorly investigated. Our results suggest that the use of *Dopa* and *Sigma melanin* deposited from DMSO suspensions yields preferentially films of a macromolecular

Table 3.1 XPS results on the chemical composition (in atomic %) of eumelanin films prepared according to different synthesis routes and deposited from DMSO and NH_3(aq) suspensions. The difference to 100% in sum is due to impurities not specified here. The atomic ratios of the three main elements most abundantly present in eumelanin apart from H (C/N, C/O, O/N) are also given. This permits to compare such ratios with those expected for eumelanin, which is composed of DHI and DHICA building blocks and their redox forms.

	Dopa melanin	*DMSO melanin*	*Sigma melanin*	*Dopa melanin*	*DMSO melanin*	*Sigma melanin*	Theoretical	
Solvent	DMSO	DMSO	DMSO	NH_3(aq)	NH_3(aq)	NH_3(aq)	DHI	DHICA
C1s	67.7	69.9	66.3	60.9	68.8	62.9	-	-
O1s	22.9	22.4	26.1	22.9	21	22.4	-	-
N1s	9.1	5.4	6.8	15.2	8.6	14.1	-	-
S2p	0.2	1.9	0.5	0.1	1.1	0.3	-	-
C/N	7.4	12.9	9.8	4.0	8.0	4.4	8	9
C/O	3.0	3.1	2.5	2.7	3.3	2.8	4	2.25
O/N	2.5	4.1	3.8	1.5	2.4	1.6	2	4

material resembling the eumelanin pigment. The use of *DMSO melanin* or NH_3(aq) can yield smooth films, at the expense of a modified chemical composition. Because of the chemical modifications produced by the use of NH_3(aq) as processing solvent, we will not consider films deposited from NH_3(aq) suspensions any further in this work.

3.5.2 Film growth

To shed light on the growth of eumelanin thin films deposited from DMSO, spin-coated and drop cast films of various thicknesses d were characterized by AFM. Spin-coated films with thicknesses of 30 and 50 nm consistently had smooth, homogeneous, and granular morphologies similar to those reported in Fig. 3.3 and S1. Besides that, most images on drop cast films ($d = 0.1 - 1$ µm) show comparably smooth surfaces (Fig. S2).

In contrast, films with a thickness of 15 nm thick and less, had a more complex surface topography featuring flat islands at different stages of coalescence. Figure 3.4a-c shows these islands for an 8 nm thick film of *Sigma melanin*. Similar morphologies were observed also for spin-coated *DMSO melanin* films ($d = 15$ nm, 8 nm, and less, Fig. S3) and for several drop-cast samples, including *DMSO melanin* (Fig. 3.4d-f) and *Dopa melanin* (Fig. S4). These flat islands observed at different film thicknesses indicate a quasi layer-by-layer growth mode and explain the low surface roughness observed for films with thicknesses of several hundreds of nanometers.

The height of the islands, typically 1-2 nm, is consistent with the height suggested for the fundamental nanoaggregate of eumelanin, composed of 3-6 stacked oligomers [45, 62]. High-

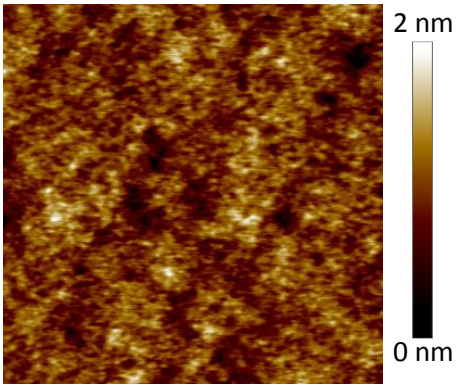

Figure 3.3 1 µm × 1 µm AFM image of a 30 nm thick film of *Sigma melanin* spincoated from DMSO.

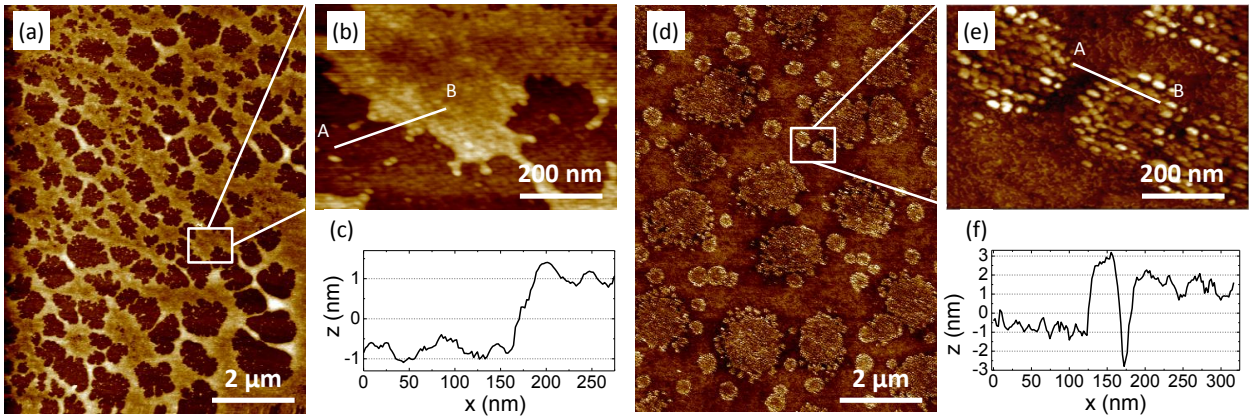

Figure 3.4 AFM images of an about 8 nm thick film of *Sigma melanin* spin-coated from DMSO suspension on SiO_2 ((a) and (b), z-scale 6 nm) and of drop-cast film of *DMSO melanin* on glass (thickness > 100 nm), also using DMSO as a solvent ((d) and (e), z-scale 8 nm). (c) and (f) are sections along the lines indicated in the images (b) and (e), respectively. Point A corresponds to $x = 0$, B to $x = 275$ nm and 325 nm, respectively.

resolution AFM images indicate that islands are made-up of disk-shaped nanoaggregates, with a lateral extension of 10-30 nm (Fig. 3.4b; occasionally larger as for the drop cast film, Fig. 3.4e). Nanoaggregates of such width have been observed before [49, 190] and indicate either an edge-to-edge aggregation of the eumelanin fundamental nanoaggregate (with a width of about 2 nm) [45, 62, 100] or oligomers with a relatively large lateral extension. The observation of these disk-shaped nanoaggregates for films of *Dopa*, *DMSO*, and *Sigma melanin* with different thicknesses suggest that they are very stable and likely already present in the DMSO suspension (for this reason we avoided the word 'solution' in this work). It is possible that covalent bonds are formed between the stacked oligomers as suggested by Meng et al. [100], which would explain their insoluble character.

Eumelanin is known to aggregate in a hierarchical way forming structures with height and width up to several hundreds of nanometers [45, 190]. Our results suggest that DMSO stabilizes nanoaggregates of a height of about 1-2 nm and a width of 10-30 nm, preventing their further aggregation, and that their deposition in a quasi layer-by-layer manner allows the growth of homogeneous films with roughness below 0.5 nm.

3.5.3 Charge transport properties

Figure 3.5a shows the electrical response of eumelanin films (*Sigma melanin* deposited from DMSO) to 0.2 V - 1 V pulses 3000 s long, in air, at different relative humidity values (RH). The first measurement was taken at high film hydration, at 90% RH and the humidity was decreased for subsequent measurements. This procedure ensures that only the content of the weakly bound water is varied in the film, since the strongly bound water can be removed only by heating [46]. It thus permits to disentangle the effect of the weakly bound water from the effect of the strongly bound water. The electrical current is dominated by a fast decreasing transient current within the first 100-500 s, depending on sample hydration. The fast decrease is followed by a much slower, nearly exponential decrease over several thousands of seconds [3]. Longer measurements performed at 90% RH showed that the current decreases more and more slowly without reaching a steady state (Fig. S5). This behavior points to several contributions to the electrical current. We attribute the initial decrease of the current to the presence of ionic currents that are blocked at the Pt electrodes and persist until the electrochemical potential of mobile ions is equal throughout the eumelanin film. This interpretation is based also on previous reports on mobile protons in solid state eumelanin [41–43]. The slowly decreasing current at longer time scales could be either due to a slower component of the ionic current as well as to electrochemical reactions or electronic

3. The temporary increase of current visible in some of the curves is due to external noise that could not be completely avoided.

current. The persistence of this current even after many hours of biasing and its presence at applied electrical biases as low as 0.2 V suggest that this current is of electronic type.

The well-known hydration dependence of eumelanin conductivity is clearly indicated in our current measurements. Both the ionic and electronic components of the current increase with the amount of weakly bound water. This is in agreement with the recent study of Mostert et al. [42], which describes an increase in both mobile proton and extrinsic (semiquinone) free radical contents with hydration. We calculated, from the electrical currents at $V = 0.6$ V at 0 s and after 3000 s, an apparent effective conductivity, plotted over the relative humidity to facilitate discussion and comparison with literature (Fig. 3.5b). The initial current at 90% RH is more than 400 times larger with respect to the initial current at 50% RH, while the current after 3000 s is only about 20 times larger at 90% RH with respect to 50% RH.

This suggests that the ionic contribution to the electrical current is more important with increasing sample hydration and that neglecting the time-dependence of the electrical current in eumelanin films interfaced with ion-blocking metal electrodes can easily lead to inconsistencies in DC conductivity. As a function of the time of biasing before reading the current, the conductivity might vary up to almost two orders of magnitudes. Conductivity values reported for spin-coated eumelanin films at 100% RH (2.5×10^{-5} and 7×10^{-5} S cm^{-1}) [39,49] lie between those that could be obtained at short and long timescales according to our results when extrapolated to 100% RH [4].

It should be noted here that ionic and electronic contributions to the electrical current cannot be considered as independent. The ionic current inevitably affects the electronic current. On one hand, the ion accumulation close to the electrodes can facilitate electron and hole injection from the metal electrodes in the eumelanin films [161]. On the other hand, the electric field created by these space charges is opposed to the external electric field and thus reduces the driving force for electronic transport within the eumelanin film. The local concentration of mobile protons and free radicals is furthermore coupled by the hydration-dependent comproportionation reaction [42]. However, not all radicals and protons are necessarily mobile. Due to this complexity, further efforts using complementary experimental techniques and theoretical modeling are required to quantify the relative contribution of ionic and electronic conduction to the charge transport properties of eumelanin and to unravel the interplay of these two types of charge carriers in eumelanin thin films.

4. The extracted conductivity might also be affected by a number of other factors such as electrochemical reactions at the electrode-eumelanin interface, the presence of ionic impurities, and film morphology.

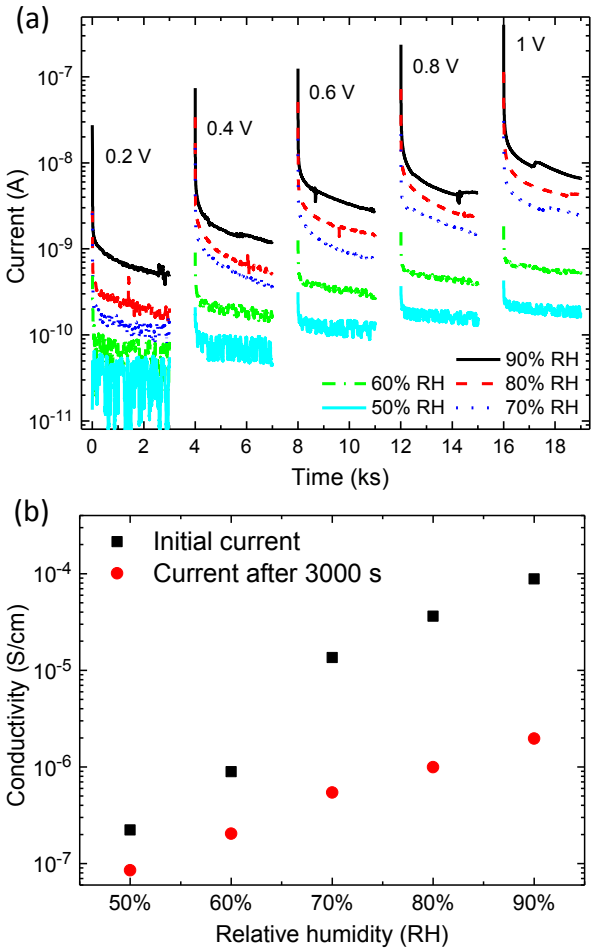

Figure 3.5 (a) Transient current measurement of *Sigma melanin* film for 3000 s long voltage pulses from 0.2 to 1 V at relative humidity (RH) varied between 90% and 50%. Zero voltage was applied during the 1000 s between subsequent voltage pulses. The curves have been smoothened to reduce spikes caused by external noise. (b) Effective conductivity derived from the electrical current at 0.6 V at 0 s and 3000 s as a function of relative humidity.

3.6 Conclusions

We investigated different combinations of synthesis routes and processing solvents for the fabrication of eumelanin thin films with respect to film growth, morphology, and chemical composition. We show that the use of *Dopa* or *Sigma melanin* deposited from DMSO is preferential for the fabrication of smooth eumelanin thin films with a chemical composition corresponding to eumelanin macromolecules. These nanoaggregates assemble in a quasi layer-by-layer growth mode, yielding films with surface roughness below 0.5 nm. This observation supports the stacked-oligomer model, according to which eumelanin is composed of aggregated stacks of small oligomers rather than being an extended heteropolymer. We also investigated the time- and hydration- dependence of electrical currents in eumelanin thin films interfaced with Pt electrodes. Our results suggest two contributions to the electrical current, both increasing with the weakly absorbed water content of the sample. These contributions can be interpreted as ionic and electronic currents in agreement with results observed in electron spin resonance and muon relaxation studies recently published [42]. The ionic current became increasingly dominant at higher sample hydration. Our results represent a contribution towards the discovery of the factors governing charge transport in eumelanin and indicate the need for time-dependent electrical measurements. Further efforts using a combination of different characterization techniques and modelling are ongoing to gain a deeper understanding of charge transport in eumelanin films.

3.7 Acknowledgments

The authors are grateful to P. Moraille, J.-P. Lévesque, J. Bouchard, and Y. Drolet for technical support, to J. Lefebvre and S. Poulin for XPS measurements, to Professors A. Pezzella and M. Rolandi for scientific advice. J.W. is grateful to H. Guerboukha, P. Léger, and G. Taillon for part of the AFM measurements. Part of this work was carried out at the Central Facilities of École Polytechnique / Université de Montréal. J.W. is grateful to NSERC for financial support through a Vanier Canada Graduate Scholarship. C.S. acknowledges financial support by FQRNT (Équipe) and by the Québec MDEIE-PSR-SIIRI. FC acknowledges financial support by NSERC (Discovery grant).

CHAPTER 4

ARTICLE 2: In situ formation of dendrites in eumelanin thin films between gold electrodes

This article has been published in Advanced Functional Materials in 2013 [1] and was featured on the cover of the corresponding issue. It reports the interaction of hydrated eumelanin films with Au electrodes leading to the growth of Au-eumelanin dendrites and the abrupt change of the electrical resistance of the sample. The supporting information for this article is reprinted in Appendix B of this thesis.

4.1 Authors

Julia Wünsche,[a] Luis Cardenas,[b] Federico Rosei,[b] Fabio Cicoira,[c] Reynald Gauvin,[d] Carlos F.O. Graeff,[e] Suzie Poulin,[a] Alessandro Pezzella,[f] and Clara Santato[a]

[a] *Département de génie physique, École Polytechnique de Montréal,CP 6079, Succursale Centre-Ville, Montréal, Québec H3C 3A7 (Canada)*

[b] *INRS-EMT, Université du Quebec, 1650 Boul. Lionel Boulet, Varennes, Québec J3X 1S2 (Canada)*

[c] *Département de génie chimique, École Polytechnique de Montréal, CP 6079, Succursale Centre-Ville, Montréal, Québec H3C 3A7 (Canada)*

[d] *Department of Mining and Materials Engineering, McGill University, 3610 rue University, Montreal, Quebec H3A 0C5 (Canada)*

[e] *DF-FC, UNESP - Univ Estadual Paulista, Av. Eng. Luiz Edmundo Carrijo Coube 14-01, 17033-360 Bauru (Brazil)*

[f] *Department of Chemical Sciences, Univ. of Naples Federico II, Via Cintia 4, 80126 Napoli (Italy)*

4.2 Abstract

Eumelanin is a ubiquitous pigment in the human body, animals, and plants, with potential for bioelectronic applications because of its unique set of physical and chemical properties,

1. J. Wünsche, L. Cardenas, F. Rosei, F. Cicoira, R. Gauvin, C. F. O. Graeff, S. Poulin, A. Pezzella, and C. Santato, *Advanced Functional Materials*, vol. 23, no. 45, pp. 5591-5598, 2013

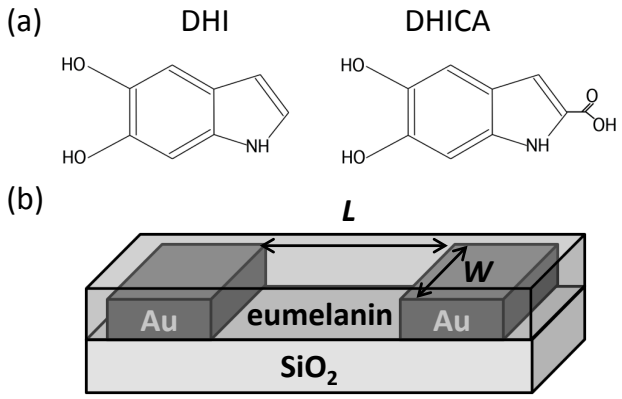

Figure 4.1 a) Main building blocks of the eumelanin macromolecule: 5,6-dihydroxyindole (DHI) and 5,6-dihydroxyindole-2-carboxylic acid (DHICA). b) Planar structure of Au electrodes and eumelanin film used in this work.

including strong UV-vis absorption, mixed ionic/electronic conduction, free radical scavenging and anti-oxidant properties. We report detailed investigations of eumelanin thin films grown on substrates patterned with gold electrodes as a model system for device integration, using electrical measurements, atomic force microscopy, scanning electron microscopy, fluorescence microscopy, and time-of-flight secondary ion mass spectroscopy. Under prolonged electrical biasing in humid air, we observed gold dissolution and formation of gold-eumelanin nanoaggregates, whose assembly led to the formation of dendrites forming conductive pathways between the electrodes. Based on results collected with eumelanins from different sources, we propose a mechanism for the formation of the nanoaggregates and dendrites, taking into account the metal binding properties of eumelanin. The surprising interaction between eumelanin and gold points to new opportunities for the fabrication of eumelanin-gold nanostructures and biocompatible memory devices and should be taken into account in the design of devices based on eumelanin thin films.

4.3 Introduction

Eumelanin has been the subject of intensive research in biology, biochemistry, and medicine due to its diverse functions in the human body and its involvement in diseases such as melanoma skin cancer and Parkinson's disease [27, 29, 56]. In the 1960's and 70's, after reports on the semiconductor-like behavior of eumelanin pellets, research on eumelanin extended to physics and materials science [22–25]. Nevertheless, the limited solubility and chemical heterogeneity of eumelanin macromolecules, based on 5,6-dihydroxyindole (DHI)

and 5,6-dihydroxyindole-2-carboxylic acid (DHICA, Fig. 4.1) building blocks, made its characterization challenging [45, 48, 59, 101]. Recent progress in eumelanin thin film processing has created new opportunities for the study of the fundamental and functional properties of eumelanin and its integration into thin film devices [36, 48, 49, 55, 130]. Eumelanin is of potential interest for organic bioelectronic applications due to their metal chelation properties [94], mixed ionic/electronic conduction [42], broad band UV-vis absorption [57], free radical scavenging properties [191], and their intrinsic biocompatibility [39].

A number of studies have been reported on the preparation and functionalization of coatings based on eumelanin for applications in catalysis, cell imaging, and nerve tissue engineering [39, 40, 55, 192, 193]. On the other side, only a few studies have been reported on the chemical and physical properties of eumelanin thin films in device structures relevant to bioelectronics. In particular, eumelanin-Au nanoparticle hybrid films have been prepared on electrode surfaces for biosensing [194, 195]. A piezoelectric sensor has been functionalized with eumelanin for metal ion sensing [196]. Ambrico et al. studied the memory-like behavior of eumelanin films sandwiched between Au and doped silicon/indium tin oxide [44, 53, 188]. To assess the potential of eumelanin for applications in bioelectronic devices, the properties of eumelanin thin films interfaced with device components, such as metal electrodes, in presence of water and ionic species need to be further explored.

Here we report on the interaction of hydrated eumelanin thin films with gold electrodes in a planar configuration. This geometry represents the first step towards transistor-based sensing devices [15,46]. We observed the in situ formation of Au-eumelanin dendrites, leading to a resistive change in the eumelanin film, and characterized their morphological, chemical, and electrical properties. Our results suggest an active role of eumelanin in Au dissolution and formation of dendrites, based on its metal-binding phenolic hydroxyl groups. The discovery of the interaction between eumelanin and Au in a thin film device structure opens new avenues for the fabrication of Au-eumelanin nanostructures and biocompatible memory devices [197] and emphasize how crucial is the choice of the electrode material in eumelanin-based electronic devices.

4.4 Results

4.4.1 Formation of Au-eumelanin nanoaggregates and dendrites: morphological and photoluminescent properties

Eumelanin films were deposited from dimethyl sulfoxide (DMSO) suspensions onto SiO_2 substrates pre-patterned with gold electrodes (Fig. 4.1). Upon application of 1 V bias between the metal electrodes in air with 90% relative humidity at room temperature, atomic force

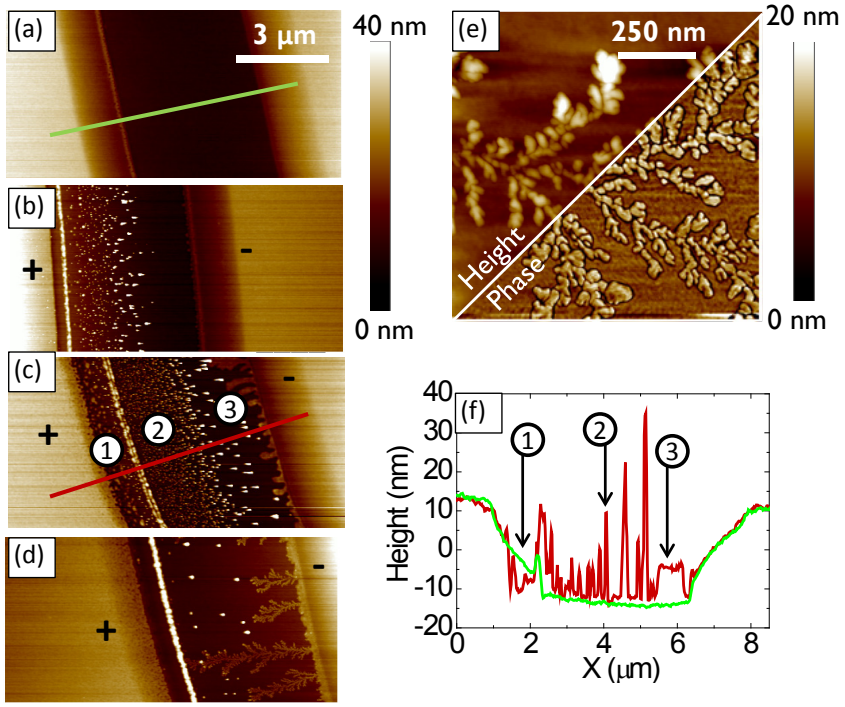

Figure 4.2 AFM images of eumelanin thin films between Au electrodes ($L = 6$ µm) a) before electrical biasing and b–d) after biasing at 1 V for increasing times. Numbers in (c) mark the distinct features of the growth of the nanostructures: (1) Decomposition of the positively biased Au electrode, (2) NAs moving towards the negatively biased electrode, and (3) dendrite growth. e) AFM height and phase image of dendrite structures. f) Height profile for the sections in (a) (green) and (c) (red).

microscopy (AFM) revealed the formation of nanostructures within the interelectrode region on the timescale of minutes to hours (Fig. 4.2a-f). Initially, nanoaggregates (NAs) formed in proximity of the positively biased electrode (Fig. 4.2b). These NAs are made up of Au and most likely also eumelanin, as will be shown below. Prolonged biasing, for a few more minutes, caused the NAs to move towards the negatively biased electrode (Fig. 4.2c). A comparison of the film cross section before (Fig. 4.2a) and after (Fig. 4.2c) biasing reveals a depression at the edge of the positive electrode (Fig. 4.2f). The bright line parallel to the positively biased electrode in Fig. 4.2c is likely an agglomeration of eumelanin and Au. Its position coincides with the initial position of the positive electrode edge. The depression beyond this line is due to the decomposition of the Au electrode (indicated with (1) in Fig. 4.2c). When the NAs reached the edge of the negative electrode, they nucleated and formed dendrite-like structures (indicated with (3) in Fig. 4.2c, see also Fig. 4.2e and S1), which are typical of diffusion-limited aggregation [198] The growth continues as long as the bias is applied, leading to dendrites extending over the interelectrode region (from the negative to the positive electrode) and beyond (Fig. 4.21). The profile in Fig. 4.2f reveals the typical heights for the newly formed structures: separate NAs (indicated with (2)) were up to several tens of nanometer-high, while dendrites (indicated with (3)) had a quite uniform height between the electrodes of a sample, typically only 5-10 nm. This height difference suggests that the NAs partially decomposed during dendrite formation.

Conductive AFM measurements showed that the dendrites are highly conductive and in electrical contact with the gold electrodes (Fig. 4.3). Charges were injected from the conductive AFM tip into the dendrites only above a certain threshold voltage, thus suggesting the presence of a poorly conductive material on top of the conductive structures, most likely eumelanin-based (Fig. S2). The height image in Fig. 4.3 further shows that the dendrites grow higher and larger once they reach the positive electrode since their extension in forward direction is blocked by the electrode.

High resolution scanning electron microscopy images (SEM) and energy-dispersive X-ray spectroscopy (EDS) measurements on the dendrites are shown in Fig. 4.4. The EDS spectra (Fig. 4.4e), taken at positions corresponding to those indicated in Fig. 4.4c, and the gold EDS mapping (Fig. 4.4d and S3) clearly indicate that the dendrites have a high gold content. The presence of carbon (originating from eumelanin and the environment), silicon (from the SiO_2 substrate), and oxygen (from substrate, eumelanin, and the environment) is also observable in the spectra (Fig. 4.4e).

In Fig. 4.4a, the horizontal bright line included in the upper circle corresponds to the edge of the positive electrode before electrical biasing. The dark regions beyond this line indicate that the nanostructures were formed under dissolution of gold at the electrode edge.

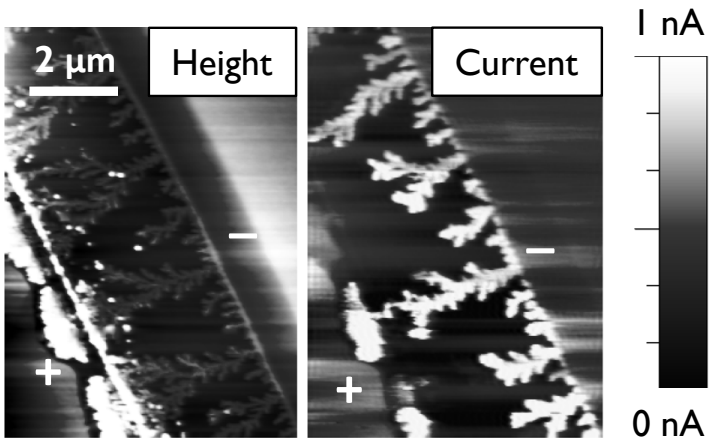

Figure 4.3 AFM and corresponding conductive AFM image of the dendrite-like structures extending from the negative to the positive electrode. The voltage applied to the AFM tip was -10 V.

The high-resolution images (Fig. 4.4b, c), corresponding to the regions marked with circles in Fig. 4.4, show that the dendrites initially had a porous fine structure (Fig. 4.4b) but became more and more compact during the growth (see the dendrite trunk in Fig. 4.4c). In the initial stage of dendrite growth, many gold-rich dendrite parts were not in direct contact with each other but appeared like equally spaced filaments and nanoparticles (Fig. 4.4b and S4). This suggests that the gold portion of the NAs is surrounded by eumelanin, which affects their assembly.

Fluorescence microscopy provided us with further insight on the nature of the nanostructures formed. In contrast to eumelanin, which has an extremely low fluorescence yield [199], and large Au particles, Au clusters can be fluorescent [200, 201]. A weak emission around 655 nm, attributable to Au clusters of about 25 atoms, was detected after biasing the eumelanin film (Fig. S5) [200, 202]. The fluorescence signal disappeared after removing eumelanin by exposing the sample to a 1 h-long UV-ozone treatment (Fig. S6). A possible interpretation of this result is that eumelanin stabilizes the Au clusters and that the clusters aggregate to form relatively large, non-fluorescent Au particles in the absence of eumelanin.

4.4.2 Resistive change in eumelanin films on Au electrodes

We carried out transient measurements of the electrical current between the Au electrodes during the formation of nanostructures (Fig. 4.5a). The rapidly decreasing current during the first few minutes was likely dominated by ionic currents (capacitive currents), in agreement with recent works suggesting the presence of mobile ions (such as H^+ and OH^-) in eumelanin

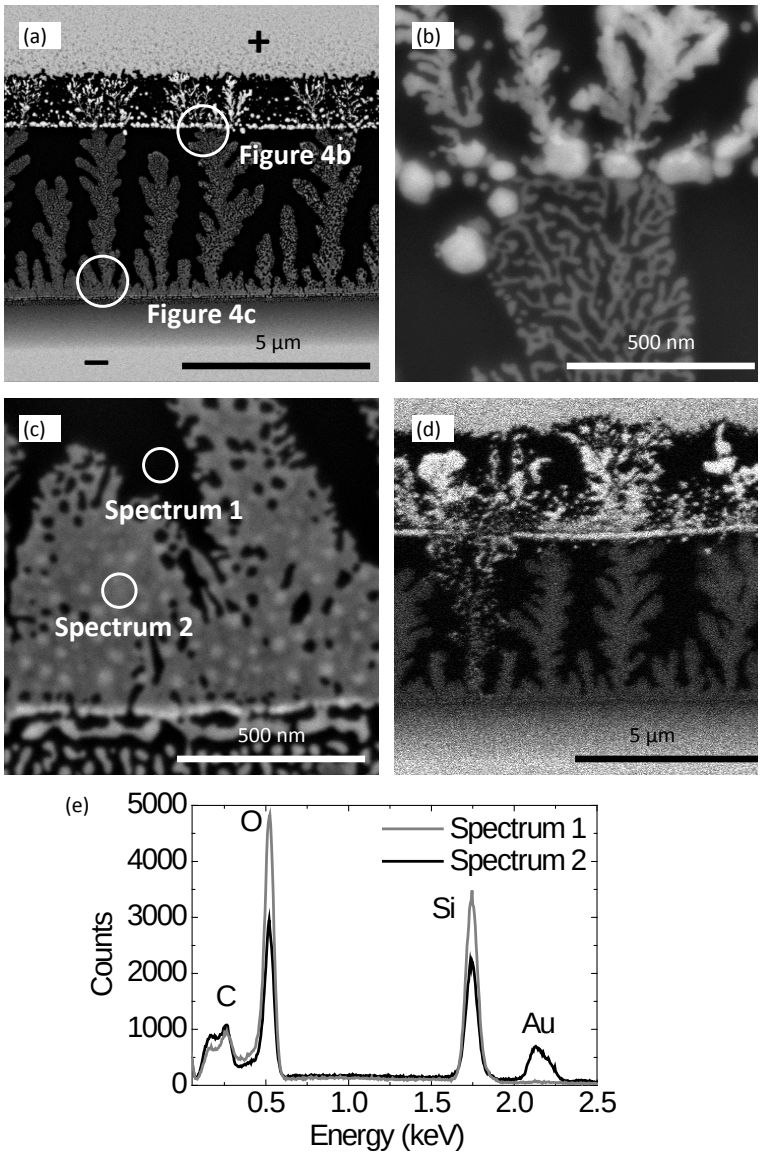

Figure 4.4 a) SEM images of the dendrites growing on the eumelanin film between the Au electrodes using the backscattered electron signal (BSE). b,c): High-resolution SEM-BSE images taken at positions similar to those marked in (a). d) Mapping of the gold distribution based on the EDS signal. e) EDS spectra taken at positions similar to those marked in (c).

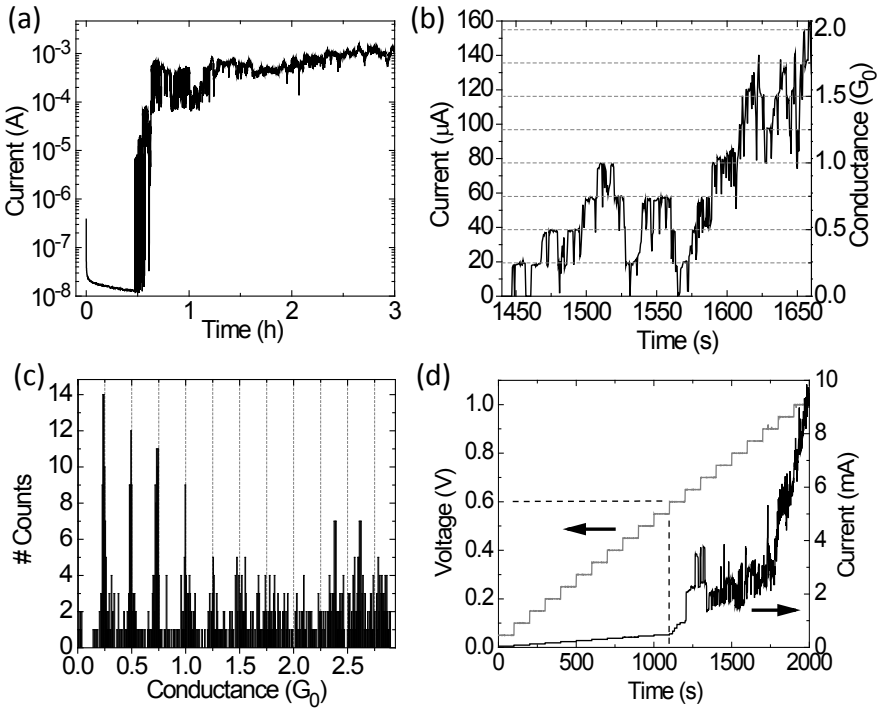

Figure 4.5 a) Transient current measurement for a eumelanin film between Au electrodes ($L = 10$ µm, $W = 2$ mm, applied voltage 1 V) at 90% relative humidity. The sample was left hydrating for 24 h before biasing. b) Example for the resistive change of eumelanin films with Au-eumelanin dendrites between states of discrete resistance ($L = 6$ µm, $W = 4$ mm, applied voltage 1 V). c) Conductance histogram corresponding to (b). d) Voltage-step measurement of an Au-eumelanin-Au structure ($L = 6$ µm, $W = 4$ mm). The sample was biased at 1 V beforehand to attain the highly conductive state. The dashed lines separate the region of linear $I - V$ characteristics from the region of electrochemical reactions.

films [42, 44]. It was followed by a slowly decreasing current including contributions from electrochemical reactions and, possibly, purely electronic charge transport. After several minutes to a few hours of biasing, a sudden increase of current over 3-6 orders of magnitude was observed. The onset of this increase corresponded to the first dendrite connecting the two electrodes, as indicated by AFM images (Fig. S7). The shape of the current transient after this first increase varied from sample to sample (Fig. S8). However, some features were typical: the current initially alternates between high and low values; the further increase occurred in discrete steps or under strong fluctuations, and the current saturated around 10^{-2} -10^{-3} mA (for an electrode geometry with $L = 6$ or 10 µm, $W = 2$ or 4 mm with a film thickness about 30 nm, Fig. 4.5a and b, Fig. S8).

The fluctuations in the electrical current are due to the growth of an increasing number of conductive dendrites between the electrodes and to the continuous evolution of the contact

between the dendrite and the positive electrode, including also a possible breaking of the contact. In some devices, the variation of the current between discrete values of conductance (Fig. 4.5b and c) reminds of the quantized conductance of atom-sized conductors, which is well studied for gold [203,204]. The conductance of the sample of Fig. 4.5b and c preferably varied between multiples of $G_0/4$, where $G_0 = 2e^2/h = 77.48$ µS, the quantum of conductance. This could be an indication of both the atom-size of the contact between the dendrite and the electrode and the organic-inorganic hybrid character of the eumelanin-Au dendrites (since conductance values smaller than G_0 were found) [204]. However, the current steps we observed varied from sample to sample and were not always well defined, which should be due to the hybrid character of the eumelanin-Au dendrites and their complex environment.

The highly conductive state was stable up to 0.55 V (Fig. 4.5d). At 0.60 V and above, current fluctuations occurred in the current vs time plot, caused by breaking and creating contacts between the dendrites and the electrode, likely due to electrochemical reactions (Fig. S4b). Within the stability window from -0.5 V to 0.5 V, the samples displayed highly linear I-V characteristics, even at a conductance below G_0 (Fig. S9).

4.4.3 Effect of electrical bias, sample hydration, and processing solvent on the formation of nanoaggregates and dendrites

We investigated the conditions that promote the formation of Au-eumelanin nanostructures between planar Au electrodes. NAs formed upon application of an electrical bias of 0.7 and 1 V, whereas 0.3 and 0.5 V were not sufficient (Fig. S10). This is in agreement with the voltage-step measurement reported in Fig. 4.5d and suggests that the electrochemical reactions leading to the formation of NAs set in for biases larger than 0.55 V.

The presence of water in the film was crucial for the formation of NAs. When eumelanin was deposited from anhydrous DMSO suspensions and sample processing and electrical characterization were conducted under dry nitrogen atmosphere (H_2O and O_2 content <0.1 ppm), no NA formation could be observed and the eumelanin film was not conductive enough to yield currents above noise level.

Another requirement for the formation of dendrites was the presence of traces of the low-volatility solvent DMSO that leaves the film in a gel-like state, enhancing the mobility of the NAs on the film surface. After solvent removal by heat treatment, NAs still formed under electrical bias but they were confined to a small region close to the positive electrode (Fig. S11). The dendrite growth and the highly conductive state were also reproduced with eumelanin films deposited from dimethyl formamide (DMF) suspensions indicating that the phenomenon is not specific to suspensions of eumelanin in DMSO (Fig. S12).

Table 4.1 Summary of results from electrical measurements, AFM/optical microscopy, and nuclear activation analysis of Cl^- concentration on eumelanins obtained from different sources.

Sample	Resistive change	Nanostructures	[Cl] (mg g^{-1})
Sigma melanin	Yes	Dendrites	7.0 ± 0.3
Sepia melanin	Yes	Difficult to image due to film inhomogeneity	64.1 ± 2.6
DHICA melanin	No	Strong accumulation at positive electrode	0.28 ± 0.02
DHICA monomer	Yes	Dendrites	0.20 ± 0.02
DMSO melanin	No	No	0.34 ± 0.02
NaOH-treated *DMSO melanin*	Yes	Dendrites	Not measured

4.4.4 Investigation of eumelanins from different sources

To investigate the mechanism of Au dissolution and dendrite formation, we tested eumelanins with different chemical compositions, obtained by different synthetic routes or as natural eumelanin [59, 128]. More precisely, we investigated: commercial eumelanin (Sigma Aldrich) obtained by the oxidation of tyrosine (from now on indicated as *Sigma melanin*), used for all experiments presented above; eumelanin obtained by the non-enzymatic polymerization of DHICA in aqueous solution (*DHICA melanin*); the *DHICA monomer* without further polymerization [205]; eumelanin obtained by the oxidation of 3,4-dihydroxy-L-phenylalanine (dopa) in DMSO solution (*DMSO melanin*);[11] *DMSO melanin* treated with NaOH; natural eumelanin extracted from Sepia officinalis (*Sepia melanin*) [128]. The results are summarized in Tab. 4.1 and described in detail in the Supplementary Information (Fig. S13-S17). In particular, we quantified the Cl^- concentration in the different eumelanins by nuclear activation analysis (NAA, Table 1), because halides, especially Cl^-, are known to enable the electrochemical oxidation and dissolution of Au [206–208]. Br^- and I^- concentrations were negligible compared to Cl^- and are therefore not listed.

Sigma melanin and *Sepia melanin* both led to sudden resistive change, although it was difficult to image the dendrites for *Sepia melanin*, due to a very inhomogeneous substrate coverage. *Sepia melanin* had the highest Cl^-, amongst the eumelanins investigated, followed by *Sigma melanin*, whereas all other eumelanins had much lower Cl^- concentrations.

DHICA melanin clearly interacted with the Au electrodes under electrical bias, as evident from the strong accumulation at the positive electrode (Fig. S14). However, no NAs or dendrites were formed, possibly related to a high degree of polymerization and limited substrate coverage. Therefore, we also prepared films directly from the *DHICA monomer*, which was easier to process. In this case, we observed dendrite formation and resistive change (Fig. S15).

Films of *DMSO melanin*, having a slightly higher Cl^- content than the *DHICA monomer* and *DHICA melanin*, did not seems to react with the Au electrodes or yield any other significant change under electrical bias (Fig. S16). As recently discovered, *DMSO melanin* differs in molecular structure from *Sigma* and *DHICA melanin* by the incorporation of sulfonate groups $–SO_2CH_3$, primarily binding to the phenolic hydroxyl groups [128]. The latter are known to be metal chelation sites of eumelanin [94, 209]. Only after removal of the sulfonate groups by treatment with NaOH [128], *DMSO melanin* also led to dendrite formation and resistive changes (Fig. S17). This result is a strong indication for the active participation of the eumelanin metal binding sites, particularly phenolic hydroxyl groups, in the process of Au dissolution and the subsequent formation of nanostructures.

To gain further insight into the chemical properties of the eumelanin-Au interface, Time-of-Flight Secondary Ion Mass Spectroscopy (ToF-SIMS) measurements were conducted on selected eumelanin-Au samples after electrical biasing. Dendrites could be located only if they were exceptionally large (about 100 nm in height and 1 µm in width) as in the sample of *Sigma melanin* in Fig. S18. In this case, ToF-SIMS indicated the presence of Cl^- in the dendrite region. A preliminary analysis of the high-mass region of the ToF-SIMS revealed the presence of a number of ionic complexes of the type $[(\text{M-H}_v)_x\text{-Au}_y\text{Cl}_z]^{--/-/+/++}$ (M=DHI monomer, $v = 0, 2, x = 1, 2, 3, y = 1, 2, z = 0, 1$). A chemometric analysis of the ToF-SIMS spectra is underway to get more insights into complex formation between eumelanin, Au, and Cl^-.

4.5 Discussion

AFM and SEM images show that the positively biased Au electrode in contact with the hydrated eumelanin film is partially dissolved upon application of an electrical bias above 0.55 V. Details of the Au dissolution and the role of Cl^-, present in all eumelanin samples, sometimes only in trace amounts, require further investigation. We hypothesize that the Au dissolution is due to the electrochemical oxidation of Au enabled by Cl^-[44] and that eumelanin with active phenolic hydroxyl groups, which act as metal binding sites, strongly enhances the Au dissolution. This hypothesis is supported by the results obtained on eumelanins with low Cl^- concentrations, having different molecular structures, namely *DHICA melanin*, *DHICA monomer* as well as untreated, and NaOH-treated *DMSO melanin*. The presence of a eumelanin with active phenolic hydroxyl groups was required to obtain dendrite growth and resistive changes at low Cl^- concentrations. The eumelanin analogue polydopamine and the eumelanin precursor dopa have been recognized as efficient binding and reducing agents for Au cations, which was ascribed to their phenolic hydroxyl groups [195, 210, 211]. Under-

standing the (electro-)chemical reactions leading to eumelanin-enhanced dissolution of Au is of significant interest. Nevertheless, at present, any conclusion supported by experimental evidence is challenged by the difficulties in locally probing the chemical compounds formed at the positive electrode and in predicting (electro-)chemical reactions in a hydrated solid-state environment with unknown local pH. Based on the process suggested for the halide-catalyzed dissolution of Au in acetonitrile [207], we suggest that Cl^- adsorbs on the surface of the positively biased Au electrode and enables the electrochemical oxidation of Au by the displacement of water and under formation of $AuCl_x$. Eumelanin binds and partly reduces Au_x+ ions from $AuCl_x$ complexes mainly through its phenolic hydroxyl groups. This leads to the release of Cl^-, which subsequently can facilitate the electrochemical oxidation of further Au atoms. Cl^- could thus have a purely catalytic role, when present at low concentrations.

Polydopamine and dopa have been exploited as reducing agents for the formation of Au nanoparticles in $HAuCl_4$ solution [195, 210, 211]. Along this line of thought, eumelanin can be expected to promote the formation of Au nanoparticles in our case. The NAs we observed are likely to contain Au cluster and/or nanoparticles, which is supported by fluorescence measurements .

The migration of NAs to the negative electrode indicates their residual positive charge. The drift and the residual charge of the NAs prevent their assembly to larger structures before arrival at the negative electrode. Once in contact with the negative electrode (directly or via dendrite), the NAs are electrochemically reduced, which is likely to break up some of the eumelanin-Au complexes. The NAs nucleate at the negative electrode and dendrites start to grow from the negative towards the positive electrode. This direction of growth is in agreement with the working principle of electrochemical metallization cells [197]. SEM images suggest that eumelanin is an integral part of the initial dendrite structure but that the Au parts of the dendrites become more and more connected as the growth continues. Eumelanin has been reported to chemisorb on negatively biased Au surfaces, permitting efficient charge transfer [90, 194], which favors the charge transport along the Au-eumelanin dendrites.

The conductive path created by the dendrites and their continuously evolving contact with the positive electrode lead to sudden changes in conductance, similar to resistive switching memory devices based on electrochemical metallization [197]. Such devices are composed of a solid electrolyte layer, as well as one electrochemically active, where faradic processes take place, and one inert metal counter electrode. By reversing the bias, the devices can be switched between the on- and off-state. Due to its chemical properties, Au is usually used as the inert electrode [197]. In this work, Au forms the electrochemically active and counter electrodes and eumelanin the solid electrolyte, playing an active role in the Au dissolution. We suggest that, in principle, biocompatible eumelanin-Au based memory devices could be

built by exchanging the counter Au electrode for a conductive material that is non-reactive with eumelanin.

Our findings on the interaction of Au, eumelanin, and Cl^- shed light on previously reported results about the electrical properties of eumelanin films in presence of Au electrodes. Ambrico et al. reported memory switching in vertical Au/eumelanin/p-Si and Au/eumelanin/indium tin oxide structures, claiming the absence of metallic nanoclusters in the eumelanin film without however reporting experimental evidence [44, 53, 188]. Au electrodes were also used in several other works to characterize the conductivity of hydrated eumelanins [39, 42, 187]. In particular, Bettinger et al. reported negligible contact resistance for hydrated films of Sigma melanin with Au electrodes [39]. Our results suggest that electrode materials alternative to Au, such as Pt, graphene, carbon nanotubes, or conductive polymers, should be considered to study the intrinsic properties of eumelanin.

4.6 Conclusions

We showed that hydrated eumelanin films between Au electrodes under electrical bias lead to the formation of Au-eumelanin NAs and dendrites in the interelectrode region. This phenomenon was observed with eumelanins from different sources, as long as they have active phenolic hydroxyl groups. We suggest that the dissolution of the Au electrode is enabled by low amounts of Cl^-, present in eumelanins, and that the reducing and metal binding ability of eumelanin is responsible for a strong enhancement of Au dissolution and the formation of NAs. The interaction between eumelanin and Au can potentially be exploited for the in situ formation of Au-eumelanin nanostructures and biocompatible resistive switching memory devices. Moreover, the interaction between Au and eumelanin has to be taken into account for the design of bioelectronic devices based on eumelanin thin films.

4.7 Experimental

4.7.1 Materials and sample preparation

Synthetic eumelanin (Sigma Aldrich, *Sigma melanin*) was dissolved in dimethyl sulfoxide (DMSO, Sigma Aldrich, purity >99.9%) to yield a 15 mg ml^{-1} suspension, unless otherwise stated. The suspension was stirred for 30 min and filtered. The substrates were silicon wafers with 200 nm thermal SiO_2 and 30-nm-thick Au electrodes on a 4-nm-thick adhesion layer of Cr, deposited by e-beam evaporation and patterned by photolithography. Before film deposition, substrates were cleaned in an ultrasonic bath with acetone, isopropanol, and de-ionized water, followed by 20 min UV-ozone treatment. Eumelanin suspension is spin-

coated onto the substrate at 1000 rpm for 2 min followed by 4000 rpm for 30 s. For a control experiment, dimethylformamide (Caledon Laboratories, purity >99.8%) was used instead of DMSO. DHICA was synthesized according to the procedure reported in Ref. [205]. For non-enzymatic polymerization, DHICA was dissolved in distilled water (12.5 mM). Oxygen was bubbled through the solution for 20 min, followed by exposure to ammonia vapors for further 20 min. Finally, the solution was kept under stirring for another 4 h in air. The DHICA polymer was extracted by lyophilization. *DMSO melanin* was synthesized and part of it was treated with NaOH according to the procedures described in Ref. [128]. *Sepia melanin* was purchased from Sigma Aldrich. The *DHICA monomer*, *DHICA melanin*, *Sepia*, and *DMSO melanin* were dissolved in DMSO (15 mg ml^{-1}) and spin-coated on the same substrates and with the same parameters as Sigma melanin. *DMSO melanin* treated with NaOH was deposited by drop casting due to its limited solubility in DMSO.

4.7.2 Sample characterization

Current transients and current-voltage curves were measured with a semiconductor parameter analyzer (Agilent B1500A) or software-controlled source/measure unit (Agilent B2902A). Measurements were taken in air with a controlled humidity of 90% after at least 1 h time to hydrate the eumelanin film, unless otherwise stated. W or Pt probes were used to contact the Au electrodes. AFM measurements were taken with a Dimension 3100 (Digital Instruments) with Si probes (tip radius <10 nm, spring constant 20-100 N m^{-1}) in Tapping mode. Images were analysed with Nanoscope Analysis from Bruker. For conductive AFM measurements, a Pt cantilever (constant force <6 nN) was used. A voltage of -10 V was applied between the tip and the Au electrodes on the sample.

SEM measurements were conducted with a Hitachi SU – 8000 cold field emission scanning electron microscope combined with a silicon drift detector provided by Oxford Instruments for EDS. Imaging was performed at 5 keV with a through the lens (TTL) backscattered electron (BSE) detector. Most images were taken in BSE mode, since the BSE signal is more sensitive to the chemical composition of the sample than the secondary electron signal. Photoluminescence spectra and images were obtained with a hyperspectral imaging system (PARISS, LightForm Inc), using the (550±10) nm emission of a X-Cite Series 120 short arc lamp. ToF-SIMS measurements were conducted with an ION-TOF SIMS IV using a Bi_1 source at 15 kV and 0.7 pA for spectral measurements and a Bi_3^++ source at 25 kV and 0.013 pA for imaging (both with 200 µs cycle time). The primary ion dose was limited to 1×10^{13} ions $cm^{-}2$. Spectra were recorded in Bunch mode using a 19.9 ns primary ion pulse to provide a mass resolution (m/δm) >8000 on ^{29}Si. Images were recorded in Burst mode, in which the lens magnification is set to zero to provide both high lateral resolution

of <300 nm and high mass resolution >5000 simultaneously. Nuclear activation analysis was performed with a SLOWPOKE nuclear reactor (Atomic Energy of Canada Limited) and a Ge semiconductor gamma-ray detector (Ortec, GEM55185). The samples were irradiated for 600 s at a thermal neutron flux of 5.4×10^{11} $cm^{-2}s^{-1}$. Gamma rays were detected after 120 s for 600 s at a distance of 35 mm.

4.8 Acknowledgments

The authors are grateful to P. Moraille, J.-P. Lévesque, K. Laaziri, J. Bouchard, and Y. Drolet for technical support, to N. Brodusch for SEM measurements, C. Chilian for NAA measurements, and to A. Badía and A. Rüdiger for scientific advice. Part of this work was carried out at the Central Facilities of École Polytechnique / Université de Montréal. J.W. is grateful to NSERC for financial support through a Vanier Canada Graduate Scholarship. L.C. acknowledges a personal fellowship from FRSQ (Quebec). F.R. is supported by NSERC (D.G.) and FRQNT (Équipe projects) and acknowledges partial salary support from the Canada Research Chairs program. C.S. acknowledges financial support by FQRNT (Équipe) and NSERC (D.G.). Supporting Information is available online from Wiley InterScience or from the author.

CHAPTER 5

ARTICLE 3: Proton conduction and transient nature of electronic currents in hydrated eumelanin thin films

This manuscript, which has recently been submitted, reports the investigation of the electrical response of hydrated eumelanin thin films, revealing the strong contribution of protonic currents and electrochemical processes. Furthermore, an investigation of the chemical composition of *Sigma melanin* is included. The supporting information for this article is reprinted in Appendix C of this thesis.

5.1 Authors

Julia Wünsche[a], Yingxin Deng[b†], Prajwal Kumar[c†], Eduardo Di Mauro[a], Jonathan Sayago[a], Fabio Cicoira[c], Marco Rolandi[b], Francesca Soavi[d], Alessandro Pezzella[e], and Clara Santato[a]

[a] *Département de Génie Physique, École Polytechnique de Montréal, C.P. 6079, Succ. Centre-ville, Montréal, Québec, Canada, H3C 3A7. E-mail : clara.santato@polymtl.ca*

[b] *Materials Science and Engineering Department, University of Washington, Seattle, Washington, 98105*

[c] *Département de Génie Chimique, École Polytechnique de Montréal, C.P. 6079, Succ. Centre-ville, Montréal, Québec, Canada, H3C 3A7*

[d] *Department of Chemistry "Giacomo Ciamician" Università di Bologna, Via Selmi, 2, Bologna, Italy, 40126*

[e] *Dipartimento di Scienze Chimiche, Via Cinthia, Complesso Monte Sant'Angelo, 21, Napoli, Italy, 80126*

[†] These authors contributed equally to the work.

5.2 Abstract

The electrical properties of eumelanin, a ubiquitous natural pigment, have fascinated scientists since the late 1960's. For several decades, the hydration-dependent electrical properties of eumelanin have mainly been interpreted within the amorphous semiconductor model. Recent works undermined this paradigma. Here we study protonic and electronic charge carrier transport in hydrated eumelanin in thin film form. Thin films are ideal candidates

for these studies since they are readily accessible to chemical and morphological characterization and potentially amenable to device applications. Current-voltage (I-V) measurements, transient current measurements with proton-transparent electrodes, and electrochemical impedance spectroscopy (EIS) measurements are reported and correlated with the results of the chemical characterization of the films, performed by X-ray photoelectron spectroscopy. We show that the electrical response of hydrated eumelanin films is dominated by proton conduction (10^{-4} S cm^{-1}) and electrochemical processes. To propose an explanation for the electrical response of hydrated eumelanin films as observed by EIS and I-V, we considered the interplay of proton migration, redox processes, ad electronic transport. These new insights improve the current understanding of the charge carrier transport properties of eumelanin opening the possibility to assess the potential of eumelanin for organic bioelectronic applications, e.g. protonic devices and implantable electrodes, and to advance the knowledge on the functions of eumelanin in biological systems.

5.3 Introduction

Eumelanin is the most common form of the pigment melanin in the human body, with diverse functions including photoprotection, anti-oxidant behavior, metal chelation, and free radical scavenging [27]. Melanin also plays a role in melanoma skin cancer and Parkinson's disease [29, 31]. Recently, biologically derived batteries and chemical sensors based on eumelanins have been reported [37, 52, 54]. Polydopamine, a melanin-like synthetic polymer, is a versatile platform for biofunctional coatings [55].

Eumelanin is a heterogeneous macromolecule arising in part from the polymerization of L-dopa via 5,6-dihydroxyindole (DHI) [47]. It is composed of oligomeric and/or polymeric species of DHI, 5,6-dihydroxyindole-2-carboxylic acid (DHICA), and their various redox forms, namely the *ortho*-hydroquinone (H_2Q), semiquinone (SQ), and (indole)quinone (Q) forms, as well as the tautomer of Q, quinone imine (QI) (Fig. 5.1) [47, 57, 58]. From the structural point of view, eumelanins feature significant similarities with polyindole conducting polymers [212, 213]. Macro- and supra-molecular structures of eumelanin depend on the (bio)-synthetic conditions [50]. Several studies indicate the formation of planar oligomer sheets, which stack via $\pi - \pi$ interaction and form disk-like aggregates [63, 214].

The electrical properties of eumelanin, characterized by a thermally activated, strongly hydration-dependent conductivity and weak photoconductivity, have fascinated scientists since the late 1960's [34, 43, 179]. Electronic band structures in analogy to inorganic semiconductors were suggested based on the strong broad-band UV-vis absorption and the π-conjugated molecular structure [23, 183]. After the observation of a reversible resistive switch-

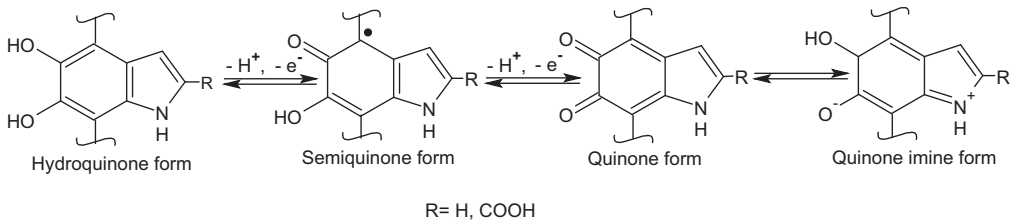

Figure 5.1 Redox forms of the final monomer precursors of eumelanin (5,6-dihydroxyindole (DHI) and 5,6-dihydroxyindole-2-carboxylic acid (DHICA)). Hydroquinone (H_2Q), semiquinone (SQ), and quinone (Q) forms. The quinone imine form (QI) is the tautomer of Q [58, 90]. Reversibility of the redox processes is indicated assuming that no other reactions occur after oxidation/reduction.

ing in eumelanin pellets reported by McGinness *et al.* in 1974 [25], electrical measurements on pellets [38, 41, 186] and thin films [36, 44] have been interpreted within the amorphous semiconductor model. Within this model, the strong hydration dependence of the conductivity [71] has been explained by the increase of the dielectric constant in presence of water, in turn decreasing the activation energy for charge carrier hopping [179]. Several reports on eumelanin pellets or thin films also show evidence of mobile protons [41, 43, 44, 70]. However, apart from the early work of Powell and Rosenberg based on a coulometric measurement [43], none of these reports assigned a dominant role to protons in charge transport. Recently, Mostert *et al.* demonstrated that the amorphous semiconductor model cannot properly describe the hydration-dependent conductivity of eumelanin pellets [187]. The same authors probed the presence of locally mobile protons and extrinsic free radicals by muon spin relaxation and electron spin resonance measurements and concluded that eumelanin is a hybrid ionic-electronic conductor [42].

It is now of paramount importance to establish to which extent protons and electrons contribute to the electrical response of hydrated eumelanin in view of possible applications of eumelanin in bioelectronics, e.g., protonic devices and implantable electrodes. Thin films are ideal candidates for these investigations since they are readily accessible to chemical and morphological characterization and potentially amenable to device applications. We recently investigated the growth and the hydration-dependent conductivity of eumelanin thin films [215], and the their interaction with Au electrodes [216].

In this work, we study ionic and electronic transport in strongly hydrated eumelanin thin films. Current-voltage (I-V) measurements, transient current measurements with proton-transparent electrodes, and electrochemical impedance spectroscopy (EIS) are reported and correlated with the chemical composition of the eumelanin thin films, investigated by X-ray

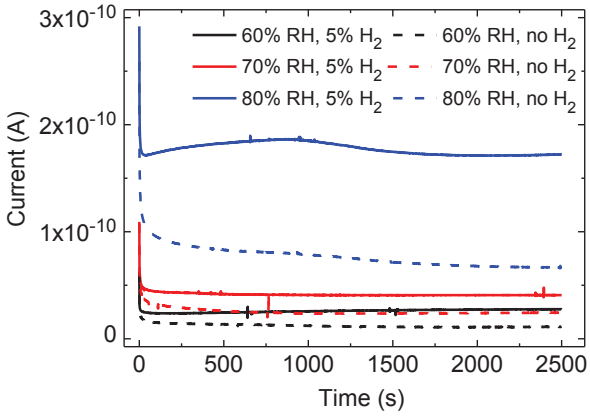

Figure 5.2 Transient current measurements of a eumelanin film ($d = 50$ nm) with Pd electrodes ($L = 9$ μm, $W = 20$ μm) at 60, 70, and 80 % RH, under proton- and electron-injecting (with H_2) vs electron-injecting (no H_2) conditions. The applied bias is 0.5 V.

photoelectron spectroscopy (XPS).

5.4 Results and discussion

5.4.1 Measurement of proton current using PdH_x electrodes

To establish to which extent protons contribute to the electrical current in hydrated eumelanin thin films, we investigated proton transport by transient current measurements with Pd electrodes in a planar two-electrode configuration at 60-80% RH (Fig. 5.2). In the pristine state, Pd injects only electrons. When exposed to H_2, Pd forms PdH_x, which can also inject and extract protons, into and from the material under investigation [21, 124, 178]. For every proton injected in the material, an electron is collected by the leads that complete the circuit. Therefore, PdH_x contacts are able to measure both the electronic and protonic contribution to the current in eumelanin films. The steady-state current in eumelanin films is higher with PdH_x contacts. The largest difference is found at 80% RH, indicating that the protonic component of the current increases with sample hydration, [1] as expected for most proton-conducting biomolecular materials [21, 124]. The transient component also contains contributions from dielectric polarization and possibly double layer charging by ions other than protons (Fig. S1).

1. Thicker films of eumelanin show an enhancement of the steady-state current of up to a factor of 10 with PdH_x contacts and a very pronounced hydration dependence (Fig. S1)

5.4.2 Chemical characterization by XPS: Proton donor sites

To gain insight into the molecular structure and the nature of proton donor sites of our eumelanin samples, we performed a XPS survey. The chemical composition of eumelanin depends on its (bio-) synthetic origin and can also be affected by thin film processing [47,215]. The commercial synthetic eumelanin (*Sigma melanin*) used in this study is synthesized by oxidation of tyrosine. The standard oxidative path leads via L-dopa to DHI and DHICA, which subsequently polymerize to eumelanin (Fig. S2). Pyrrolic acids can form due to oxidative degradation. We analyzed the elemental composition and the C1s, N1s, and O1s peaks regarding the relative contribution of the various precursor units to the eumelanin macromolecule (Fig. S3 and Tab. S1-S3). The N1s peak suggests that a rather large portion of the units, 37%, is uncyclized. The elemental ratio [C]/[N]=8.8 and the portion of C bound in -COOH moieties (8.5%), indicate a low content of pyrrolic acids. Indeed, combining these three numbers yields a composition of 22% DHI units, 41% DHICA units (both can be present in H_2Q, SQ, or Q form), 37% of L-dopa or tyrosine, and the absence of pyrrolic acids. Several impurities (F, Fe, S, Cl) were also detected in the wide scan survey. Although XPS alone does not permit to draw a complete picture of the chemical composition of *Sigma melanin*, it reveals the presence of about 0.8 -COOH moieties per monomer unit and a relatively high content of uncyclized units in the eumelanin films. Based on the XPS results, the -COOH group (pK_a 4.2 [92]) should be the dominant source of protons in the eumelanin films. Further proton donors in eumelanin include the amine group of the tautomer QI (pK_a 6.3 [86]) and the hydroxyl group of SQ. However, only about one out of 1500 indole units is in SQ form at neutral pH [86]. [2]

5.4.3 Exploring electronic transport by EIS and I-V measurements

EIS was performed on eumelanin thin films at 90% RH with Pt electrodes in two electrode configuration (Fig. 5.3). At zero bias, the Nyquist plot, showing the impedance Z of the sample on the complex plane, consists of a semicircle at high frequencies (Fig. 5.3a) and a low-frequency tail indicating ion and electron blocking electrodes (Fig. 5.3b). This behavior is typical of electrolytes sandwiched between metal electrodes with the semicircle usually assigned to the ionic resistance in parallel to the geometric capacitance [164]. [3] From the diameter of the semicircle, we extracted an ionic conductivity in the range of $2 \cdot 10^{-5}$ to

2. It should be noted that the pK_a given above have been determined in aqueous suspensions. In solid state, both pK_a and pH are unknown. Therefore, an estimation of the proton concentration from pK_a values is impossible at this stage [42]

3. The deviation from a vertical line at low frequencies is a general observation for solid electrolyte/electrode interfaces and reflects the non-ideal properties of the blocking interface, associated with interface roughness and ion diffusion, among others [217]

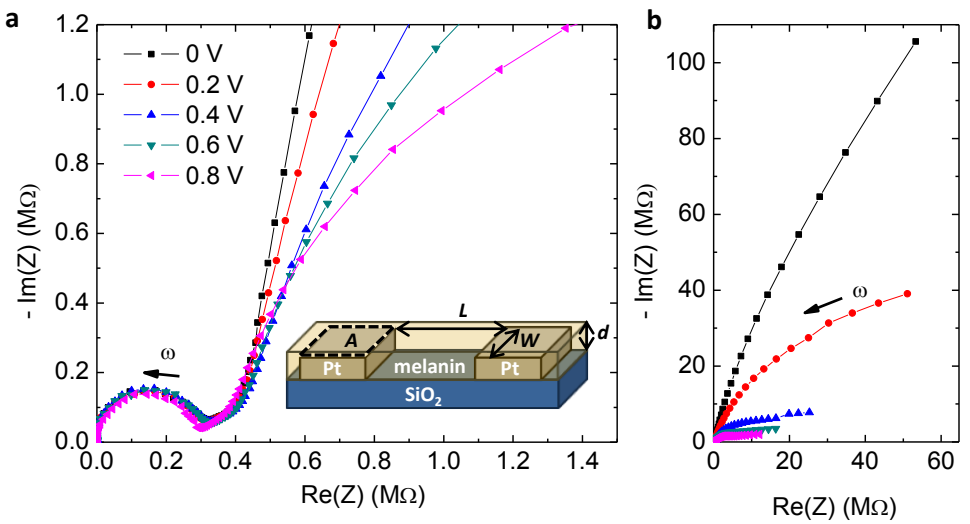

Figure 5.3 Nyquist plots of the EIS measurement on a eumelanin film at 90% RH, applying a bias between 0 and 0.8 V ($L = 10$ μm, $W = 24.5$ mm, $d = 50$ nm). (a) High-frequency range. The inset illustrates the sample geometry. (b) Entire frequency range ($10^{-2} - 10^{6}$ Hz).

$6 \cdot 10^{-4}$ S cm^{-1}. XPS measurements showed the presence of impurities, including some that might be present in the films in the form of mobile ions. These ions could contribute to ionic currents and the capacitive response of the eumelanin films at $|V| < 0.2$ V. However, due to the high diffusion coefficient of protons in hydrated systems as compared to other ions and the high density of potential proton donor sites, we expect that protons dominate the ionic currents in hydrated eumelanin films. Hence, the ionic conductivity as determined by EIS is a good estimate of the proton conductivity at 90% RH. The values are slightly higher than the DC conductivity (not attributed to a specific charge carrier) of strongly hydrated eumelanin films reported in literature [39, 49]. The blocking behavior of the electrodes dominates up to a bias of 0.2 V: the sample responds to the AC voltage by charging and discharging the double layer.

With increasing bias, the onset of a second semicircle can be recognized at low frequencies (Fig. 5.3a and b). The diameter of this semicircle decreases when the bias is increased. This is typical of electrodes loosing their electron blocking behavior. The second semicircle depends on the in-plane electrode area A (inset of Fig. 5.3). It is smaller with respect to the first semicircle for samples with a larger ratio A/W (Fig. S4), suggesting that it arises from an interface rather than a bulk phenomenon. In the study of mixed conductors, the appearance of a second semicircle in the low-frequency region of the Nyquist plot and the simultaneous absence of a capacitive low-frequency tail, in absence of electrochemical reactions, is usually taken as evidence of electronic conduction in parallel to ionic conduction [164, 165].

Nevertheless, a number of charge transfer processes at the electrodes can cause a similar low-frequency behavior, in absence of electronic conduction in the bulk. The dependence of the low-frequency semicircle on the applied bias and in-plane electrode area indicates its electrochemical origin.

The conclusions drawn from EIS measurements are supported by the I-V characteristics of hydrated eumelanin thin films measured with the same electrode configuration at different voltage sweep rates (Fig. 5.4a). Currents at $|V| < 0.2$ V are primarily of capacitive origin, as deduced from the weak dependence on voltage and the quasi-linear dependence on sweep rate (Fig. S5). A linear fit of the rate-dependence according to $I = C\frac{dV}{dt}$ yields a capacitance C of about 10^{-7} F (Fig. S5). This corresponds well to typical values of the double-layer capacitance at electrode/electrolyte interfaces (10^{-5} F cm^{-2}), when taking into account not only the film cross section ($W \cdot d$), but also the in-plane electrode area ($A = 0.8$ mm^2) [218]. The capacitive currents are orders of magnitude higher than what is expected from dielectric polarization and are thus an indication of ionic currents in hydrated eumelanin films.

At $|V| > 0.2$ V, currents show a quasi-exponential dependence on V, suggesting a non-capacitive behavior. Figure 5.4b shows the positive branches of the first five I-V cycles at the slowest sweep rate, 0.5 mV s^{-1}. The current decreases with each cycle and shows a broad shoulder above 0.4 V. From an electrochemical perspective, the I-V characteristics suggest the presence of irreversible redox processes at the Pt/eumelanin interfaces. The decrease of the current with each cycle is attributable to the depletion of redox species or the formation of an insulating layer at the electrode interfaces. To further investigate the importance of electrochemical reactions as compared to ionic and electronic conduction in the bulk, we investigated the scaling of the current with interelectrode distance L, film thickness d, and in-plane electrode area A (Fig. S6-S8). While conduction in the bulk should scale with the film cross section ($W \cdot d$) and increase with L^{-1}, electrochemical reactions should be more sensitive to the interface area, and thus A. Our results suggest that both transport in the bulk and processes at the electrodes determine the electrical response of the films.

To shed light on possible redox processes, cyclic voltammetry (CV) measurements were conducted on films of *Sigma melanin*. An intense oxidation peak, located at about 0.5 V vs SCE, is observed (Fig. S9). This peak has an irreversible character. CV measurements were also carried out on films with a more controlled chemical composition, using eumelanins obtained by the polymerization of DHI and DHICA (*DHI melanin* and *DHICA melanin*). Analogously to the case of *Sigma melanin*, an irreversible oxidation peak is observed during the first cycle (Fig. S9) [89, 219]. The irreversibility of the oxidation peak likely originates from the covalent coupling (intramolecular reticulation) of the intermediate species formed at the positive electrode. Indeed, radicals and Q species formed by the oxidation of DHI

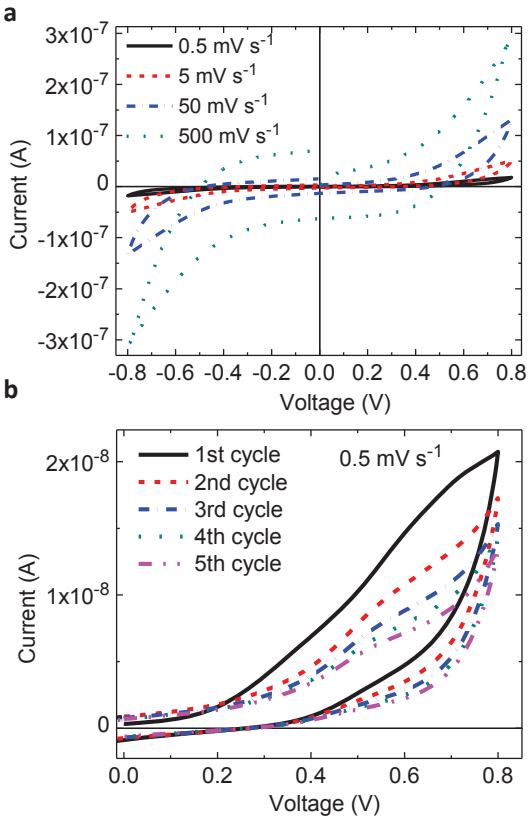

Figure 5.4 Current-voltage characteristics of a eumelanin film (d = 50 nm) at 90% RH, measured with coplanar Pt electrodes (L = 10 μm, W = 24.5 mm). (a) Voltage sweep rate dependence of the first cycle. (b) First five cycles of the 0.5 mV s^{-1} measurements for positive voltages.

moieties are reactive and may undergo coupling processes with other radicals and nucleophilic counterparts [214, 220, 221]. The decrease of the current density with each CV cycle can be interpreted at least in a twofold manner: polymerizing species are depleted under prolonged biasing and/or the reaction products have limited electronic conductivity. We did not observe any reversible redox activity, a prerequisite for efficent electronic conduction.

5.4.4 Discussion on the interplay of proton migration, redox processes, and electronic transport

To propose an explanation for the electrical response of hydrated eumelanin films as observed by EIS and I-V, we consider the interplay of proton migration, redox processes, and electronic transport. Before biasing, the hydrated eumelanin film contains eumelanin building blocks DHI and DHICA in different redox states (H_2Q, SQ, Q, and QI tautomer, Fig. 5.1) as well as protons originating from -COOH, QI, and SQ moieties, homogeneously

distributed within the film (Fig. 5.5a). -COOH groups, not explicitly shown in Fig. 5.5, leave quasi immobile negative moieties when deprotonated. It has recently been proposed that the electronic charge carrier in eumelanin originates from the SQ free radical [42]. The density of SQ moieties is determined by the comproportionation equilibrium [42],

$$H_2Q + Q + 2H_2O \rightleftharpoons 2\ H_3O^+ + 2\ SQ^-. \tag{5.1}$$

We first consider the case of low bias ($|V| < 0.2$ V), where currents are largely capacitive. Protons migrate under the influence of the external electric field and accumulate close to the negative electrode, creating a pH gradient across the film (Fig. 5.5b). The electric field within the bulk is significantly reduced due to formation of space charges. The change in local pH affects protonation and the comproportionation equilibrium. In aqueous suspensions of eumelanin, the SQ^- concentration increases up to a factor of 7 between pH 7 and 11 [85,86]. An increase in SQ^- with pH has also been observed for hydrated pellets [85]. Thus, the density of SQ^- is expected to be higher at the positive than the negative electrode.

At higher bias ($|V| > 0.2$ V), electron transfer processes take place at the electrodes (Fig. 5.5c). The low pH at the negative electrode should favor the reduction of Q and SQ moieties (Fig. 5.1) [88]. The reduction of Q to SQ^- would correspond to the injection of an electron capable to contribute to electronic conduction [42]. Several processes might hinder the efficient injection. If two SQ^- are formed in close proximity, they might recombine by disproportionation to H_2Q and Q, assisted by the presence of protons (Equation 5.1) or undergo free-radical coupling [222]. In addition, SQ^- might be further reduced to H_2Q incorporating H^+. Species such as H^+ and O_2 could also be reduced.

At the positive electrode, the extraction of a mobile electron corresponds to the oxidation of SQ^- to Q, a process that could extend into the bulk of the film. However, tautomer formation from Q to QI followed by deprotonation of QI could limit electron transport. Furthermore, H_2Q could be oxidized to Q in a two-electron process with release of two H^+ that subsequently migrate toward the negative electrode. Irreversible processes as those discussed for CV measurements are also expected to take place.

In this picture, under sufficiently high electrical bias, an increasing number of DHI and DHICA moieties get fully reduced at the negative electrode and fully oxidized at the positive electrode. At least two processes might lead to the continuous decrease of the electronic current in eumelanin: the formation of H_2Q at the negative electrode and QI^- at the positive electrode. Both reduce the number of potential hopping sites for electrons. For a certain time, a non-capacitive current can flow even in absence of a continuous electron path between the two electrodes, the electric circuit being closed by proton migration.

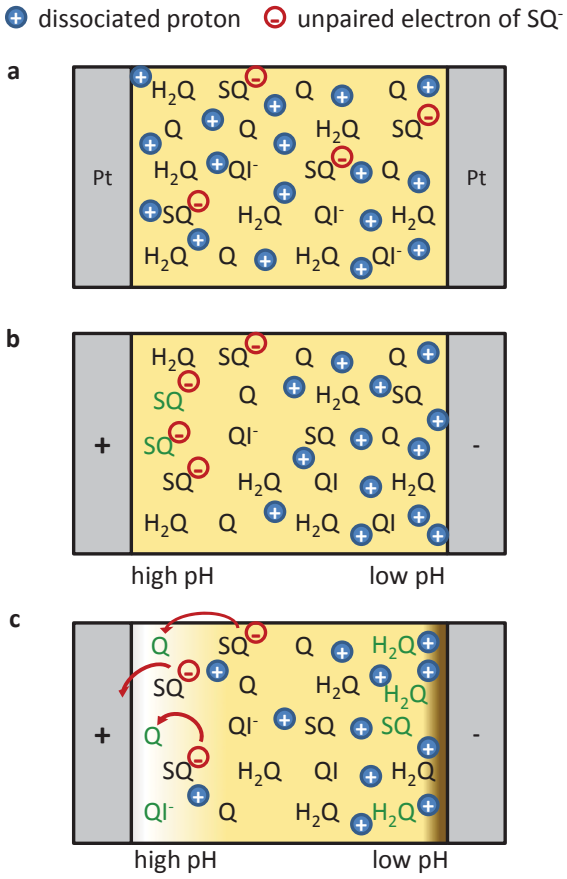

Figure 5.5 Illustration of the most important concepts of the model proposed for the electrical response of hydrated eumelanin films between co-planar Pt electrodes. (a) Composition of the eumelanin film before biasing including the various redox forms of DHI and DHICA (H_2Q, SQ, Q, QI tautomer). (b) Under electrical bias, proton migration affects protonation and the comproportionation equilibrium (Eq. 5.1). (c) Possible electron transfer reactions at higher bias include the oxidation (brighter background) and reduction of eumelanin (darker background) according to Fig. 5.1. Moieties that changed their redox state are marked in green. While H_2Q might form an insulating layer at the negative electrode, Q provides a transport path for the electronic charge carriers.

5.5 Conclusion

In conclusion, we show that eumelanin films are proton conductive over micrometric distances and that the contribution of protons to the electrical current strongly increases with hydration, reaching about 10^{-4} S cm^{-1} at 90% RH. Our results point to the importance of electrochemical reactions in the electrical response of hydrated eumelanin thin films. We propose a qualitative model to describe how the interplay of proton migration, comproportionation equilibrium, and redox processes could limit electron transport through eumelanin films. Reversible and irreversible redox processes have to be properly recognized to improve the understanding of electrical conduction in eumelanin. We are currently carrying out a systematic CV survey considering different pH and electrolyte conditions.

In perspective, two approaches can be adopted to observe electronic currents in eumelanin films. From the structural point of view, electron transport could be enabled by the use of eumelanin derived from DHI. It has recently been suggested that DHI-derived eumelanin forms planar oligomers, which assemble via π-stacking [223]. In contrast, eumelanin derived from DHICA, while leading to superior proton donating and free radical scavenging properties, forms non-planar structures [223]. The high content of -COOH and uncyclized building blocks, as detected by XPS, indicate that there might be room to improve the electronic conduction by engineering the molecular structure of eumelanin. Other H-bonded pigments, which show strong intermolecular π-stacking, have recently emerged as ambipolar semiconductors [20, 151].

Furthermore, electron and hole injection might be enhanced by the use of different electrode materials. The lack of well-defined highest occupied and lowest unoccupied molecular orbital energies for eumelanin makes a rational choice of the electrode material based on energy-level alignment difficult. In this regard, carbon nanotube electrodes, which have been shown to enhance electron and hole injection in different organic semiconductors [224], could help to ensure that electronic currents in eumelanin are not limited by injection.

Our results point to the need for a holistic approach, including chemical, electrochemical, and structural contributions, to uncover the charge transport properties of eumelanin films. A good understanding of these properties holds the potential to reveal bioelectronic applications of eumelanin and to advance the knowledge on the functional properties of eumelanin in biological systems.

5.6 Experimental

5.6.1 Sample preparation

Si/SiO_2 substrates with 50 nm thick co-planar Pt or Pd electrodes patterned by photolithography were wet-cleaned and UV-ozone treated. Eumelanin thin films were deposited from a suspension of synthetic eumelanin (Sigma Aldrich) in dimethyl sulfoxide (sonicated and filtered) by spin-coating (1 min at 1000 rpm + 30 s at 4000 rpm, 30 mg ml^{-1} suspension). Some thicker films were prepared by drop casting a diluted eumelanin suspension. Film thicknesses were determined by atomic force microscopy measurements on a scratch. Films were kept in humid air (90% relative humidity (RH)) without heating for at least 24 h before characterization for evaporation of residual solvent and hydration. The effect of residual DMSO and different thermal treatments on the electrical properties of the films is currently investigated. In measurements with Pt electrodes, two different electrode geometries were compared: an interdigitated circular design with interelectrode distance $L = 10$ μm, electrode width $W = 24.5$ mm, and total in-plane electrode area $A = 0.8$ mm^2, and a design with a straight single channel with $L = 10$ μm, $W = 4$ mm, and $A = 8$ mm^2 (see Fig. 5.3 for definition of sample dimensions). *DHI melanin* and *DHICA melanin* used for CV measurements were obtained from DHI and DHICA by the procedure reported in Ref. [225]. DHI and DHICA were prepared according to Ref. [47]. Suspensions of *DHI melanin* and *DHICA melanin* in methanol (30 mg ml^{-1}) were spin-coated on ITO substrates using a rotation speed gradient from 2000 rpm to 4000 rpm. For CV measurements, *Sigma melanin* was spin-coated on ITO substrates as described above.

5.6.2 Sample characterization

I-V and EIS measurements were performed in a chamber with controlled RH at 90% RH in air. This value of RH corresponds to about 14 wt% sample hydration according to thermogravimetric analysis (Fig. S10). The Pt electodes were contacted with micromanipulated tungsten probes. A software-controlled source/measure unit (Agilent B2902A) was used for *I-V* measurements. EIS data was acquired from 1 MHz to 0.01 Hz (10 points per decade, 50 mV oscillation amplitude) with a potentiostat (Versa STAT 4, Princeton Applied Research). The ion conductivity was evaluated from measurements on five independent samples with L=10 μm (several measurements each). For transient current measurements with proton-transparent electrodes, eumelanin was deposited on Si/SiO_2 substrates with prepatterned Pd electrodes (L=9 μm, W=20 μm). Measurements were conducted with a semiconductor parameter analyser (Agilent 4155C) in an environmental chamber with controlled humidity under N_2 atmosphere, with and without 5% H_2. XPS measurements were taken

with an ESCALAB 3 MKII from VG Scienta with a Mg Kα source. CV measurements were conducted with Versa STAT 4 (Princeton Applied Research) in 0.01 M phosphate-buffered saline solution (PBS, pH 7.4). Eumelanin films were deposited on ITO on glass, used as the working electrode (area 0.63 cm^2). A saturated calomel electrode (SCE) and a Pt foil were used as reference and counter electrode, respectively. The voltage was scanned from 0 V to positive and then to negative voltages at a rate of 50 mV s^{-1}.

5.7 Acknowledgement

The authors thank to J.-P. Lévesque, J. Bouchard, and Y. Drolet for technical support, to J. Lefebvre and S. Poulin for XPS measurements. Part of this work was carried out at the Central Facilities of École Polytechnique/Université de Montréal. J.W. is grateful to NSERC for financial support through a Vanier Canada Graduate Scholarship and to M. Irimia-Vladu and R. Oakley for valuable discussions. C.S. acknowledges financial support by FQRNT (Equipe) and by the Québec MDEIE-PSR-SIIRI. F.C. and C.S. acknowledge financial support by NSERC (Discovery grant). F.S. acknowledges financial support by Alma Mater Studiorum-Università di Bologna under the researcher mobility program within the Italian-Canadian cooperation agreement. M.R. and Y.D. acknowledge support from the National Science Foundation Career award DMR-1150630. J.S. acknowledges financial support by CONACYT and CMC Microsystems.

CHAPTER 6

SUPPLEMENTARY METHODS AND RESULTS

This chapter describes methods and results that have not been incorporated in a peer-reviewed article but are believed to be useful for future work and the general discussion in Chapter 7. The chapter contains information on the solution-processing, the patterning, and the structure of eumelanin thin films, as well as on the RH-dependent water content of eumelanin powder. Finally, two attempts to enhance the conductivity of eumelanin films, by molecular doping and in electrolyte-gated thin film transistor structures, are described.

6.1 Thin film processing: Effect of the molecular structure of eumelanin, substrate, and post-treatments

The film forming properties of eumelanin strongly depend on its synthetic or biological origin. Apart from the differences between *Sigma melanin*, *Dopa melanin*, and *DMSO melanin* described in Article 1, *DMSO melanin* was found to be unstable in air. Once degraded, it has a strongly reduced solubility and results in films with larger aggregates (Fig. 6.1a). This was also recently reported by Graeff *et al.* who developed the synthetic procedure for *DMSO melanin* [128]. Furthermore, it was not possible to deposit continuous films of *Sepia melanin* from DMSO suspension due to strong aggregation (compare Fig. S13 of Appendix B). *DHICA melanin* had a tendency to form dendritic structures on SiO_2 substrates often resulting in discontinuous films (Fig. 6.1b).

Good film adhesion was only obtained on hydrophilic substrates such as glass and thermal SiO_2 on Si wafers. Thin films of *Sigma melanin*, *Dopa melanin*, and *DMSO melanin* readily adhere on glass, while UV-ozone treatment is required to enhance the adhesion on thermal SiO_2. Considering the similar surface chemistry of these substrates, the difference in adhesion is likely due to the difference in surface roughness ($Rq \approx 0.3$ nm for SiO_2 and 0.6 nm for glass). The film forming properties of *Sigma melanin*, *Dopa melanin*, and *DMSO melanin* were reported in *ECS Transactions*, vol. 35, no. 7, pp. 75–81, 2011.

The use of a solvent with low vapor pressure and high boiling point such as DMSO bears several challenges in thin film processing. For example, high rotation speed is needed to remove at least the majority of the solvent during spin-coating, limiting the maximum film thickness that can be obtained. A two-step process using 1000 rpm (1 or 2 min) and 4000 rpm (30 s) was found to yield homogenous films of thicknesses up to 50 nm (for 30 mg ml^{-1}

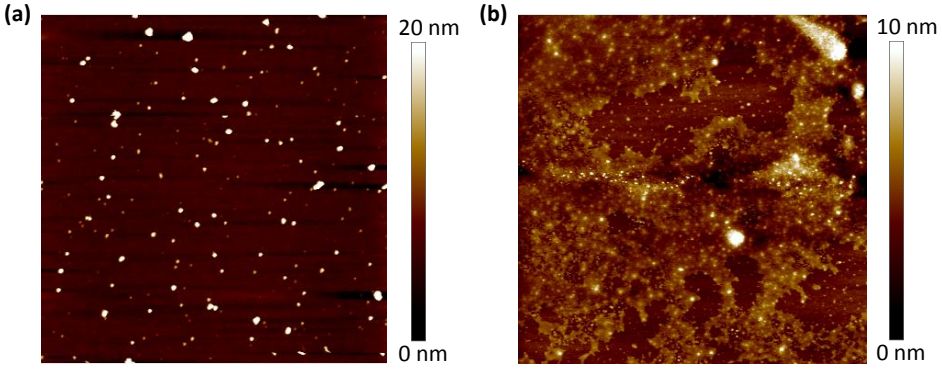

Figure 6.1 10 μm×10 μm AFM images of thin films of degraded *DMSO melanin* spin-coated from 15 mg ml^{-1} NH_3(aq) suspension (a) and *DHICA melanin* spin-coated from 15 mg ml^{-1} DMSO suspension (b).

Table 6.1 Thickness of eumelanin thin films deposited by spin-coating from DMSO suspension at 1000 rpm (2 min) and 4000 rpm (30 s).

Concentration (mg ml^{-1})	Thickness by ellipsometry (nm)	Thickness by AFM (nm)
0.3	8±4	10±4
3	14±7	21±8
15	25±13	34±6
30	40±20	50±10

suspension). Omitting the fast spinning step left drops of suspension on the substrate, which resulted in inhomogeneous films after drying.

The thickness of thin films prepared by spin-coating eumelanin suspensions of different concentrations on SiO_2 were determined by AFM (scratch test) and ellipsometry. For the analysis of ellipsometry data, a refractive index of 1.7 was assumed for eumelanin [226]. Measurements were taken on at least three positions for each sample and technique. The results are shown in Tab. 6.1.

Several post treatments have been explored to remove residues of DMSO after spin-coating. In order to evaluate the success of these treatments, thermogravimetric analysis (TGA) was performed on pristine eumelanin powder (*Sigma melanin*) and eumelanin recovered from post-treated films prepared by drop casting a suspension of eumelanin in DMSO. The TGA curves and their weight loss derivative (DTG) of pristine eumelanin and eumelanin deposited from DMSO suspension without post-treatment are shown in Fig. 6.2a. Measurements were done on powder samples under N_2 with a heating rate of 10 ℃ min^{-1}. The DTG

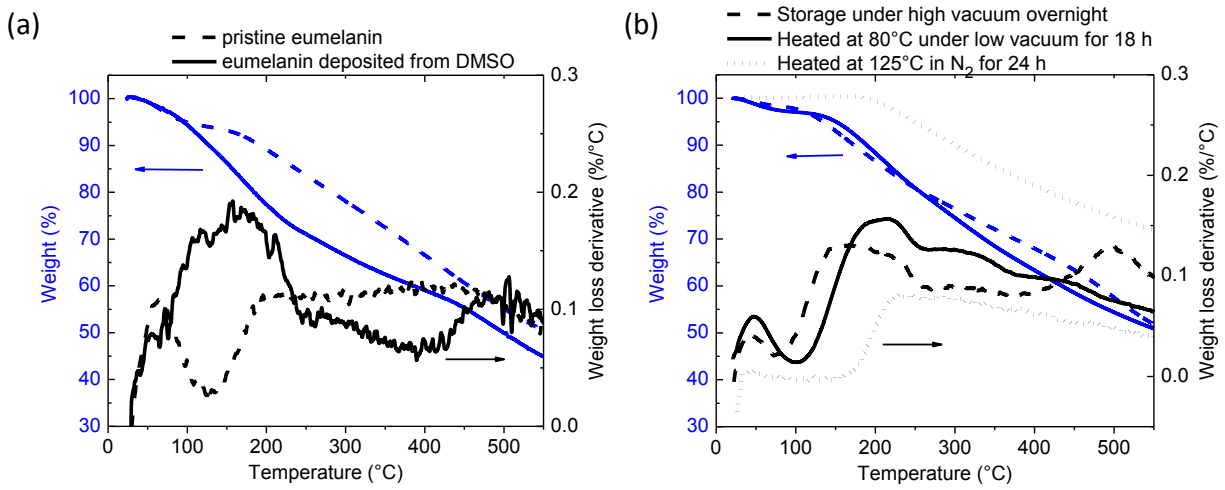

Figure 6.2 TGA (weight) and DTG (weight loss derivative) curves of (a) pristine eumelanin powder and eumelanin deposited from DMSO and (b) eumelanin deposited from DMSO and treated according to the procedures given in the legend.

curve for pristine eumelanin has a first peak below 100 ℃ that can be attributed to the loss of weakly bound water (eumelanin is stored under ambient conditions). This attribution was confirmed by comparing the initial mass of a sample with its mass after heating to 100 ℃ and exposure to ambient atmosphere for several hours, which were almost the same (not shown). The weight loss derivative has a minimum at 125 ℃ and then increases again up to 200 ℃, from where it is approximately constant up to 450 ℃. Eumelanin keeps more than 50% of its mass up to 500 ℃ and is therefore often considered thermally stable [48]. However, our TGA results also show that weight loss starts at much lower temperatures. Part of the weight loss above 125 ℃ is due to strongly adsorbed water [72]. Above 250 ℃ eumelanin decomposes under the release of CO_2 [56]. The thermal decomposition of eumelanin seems to take place gradually up to 500 ℃. Similar results have also been obtained on *DHI melanin* and *DMSO melanin* [41, 131]. The loss of strongly bound water and eumelanin decomposition cannot be distinguished based of the TGA curves. Furthermore, it should be noted that the removal of strongly bound water can also induce irreversible structural modifications [50, 72]. Therefore, eumelanin is considered thermally stable only up to 125 ℃ in this work. The thermal stability of eumelanin was further tested by heating eumelanin (stored under ambient conditions) at 200 ℃ for 3 h under N_2. During this time, the sample lost about 17% of its mass. 5% of the initial mass could be regained by exposure to ambient conditions for 12 h. However, 12% of the mass was permanently lost, indicating the decomposition of eumelanin at 200 ℃.

DMSO residues introduce a broad peak around 170 ℃ to the DTG curve (Fig. 6.2a, the boiling point of DMSO is 189 ℃). Its overlap with the weight loss of pristine eumelanin

above 125 ℃ indicates that DMSO cannot be removed by heating the sample at temperatures above 170 ℃ without risking a degradation of eumelanin. Furthermore, the eumelanin sample deposited from DMSO shows a further peak in DTG around 500 ℃, possibly related to a modification of the macro- or supramolecular structure of eumelanin. Therefore, three different procedures using lower temperatures have been investigated to remove DMSO residues: storage under high vacuum (10^{-5} mbar) overnight, heating at 80 ℃ in low vacuum for 18 h, and heating at 125 ℃ under N_2 for 24 h. The TGA curves of samples treated in this way are given in Fig. 6.2b. Samples stored under vacuum or heated at 80 ℃ still show a peak in the DTG curve around 170-210 ℃. Heating at 80 ℃ shifts this peak to higher temperatures. The origin of this peak are likely DMSO residues. However, it cannot be excluded that structural modifications also play a role because the TGA curves were also affected at higher temperatures. In contrast, heating at 125 ℃ removed the peak attributed to DMSO and resulted in a TGA curve similar to pristine eumelanin (the sample was not exposed to air after heating and thus shows no loss of water below 100 ℃). Heating at 125 ℃ did not affect the morphology or surface roughness of spin-coated films, as investigated by AFM measurements. However, electrical currents through heated eumelanin films were lower than through non-treated films. This could indicate that DMSO assists electrical conduction in eumelanin films and/or that eumelanin is irreversibly affected by the thermal treatment. From these results, heating at 125 ℃ under N_2 appears to be the most promising post treatment of eumelanin thin films to remove the majority of residual DMSO. However, further investigations are required to determine the amount of residual DMSO after heating and to evaluate the effect on the molecular and thin film structure of eumelanin.

6.2 Patterning of eumelanin thin films

Patterning of the eumelanin film limits charge carrier movement on top and around the electrodes and to reduce the area of the eumelanin/electrode interface. In Article 3, it was shown that the electrical response of eumelanin films measured with co-planar electrodes is affected by the in-plane electrode area, not only the film cross section. To facilitate modeling and to obtain a system with well defined boundary conditions, it is advantageous to pattern the eumelanin film with minimal overlap with the electrodes. Furthermore, in this work, the use of Kelvin probe microscopy was envisaged for the investigation of charge carrier accumulation at the electrodes. However, conclusive results can only be obtained if the electrodes are not covered by the ion-conductive film [161]. Therefore, different procedures based on photolithography were explored to pattern eumelanin films without any overlap with the electrodes. It is important to note that standard resists and solvents used in photolithography

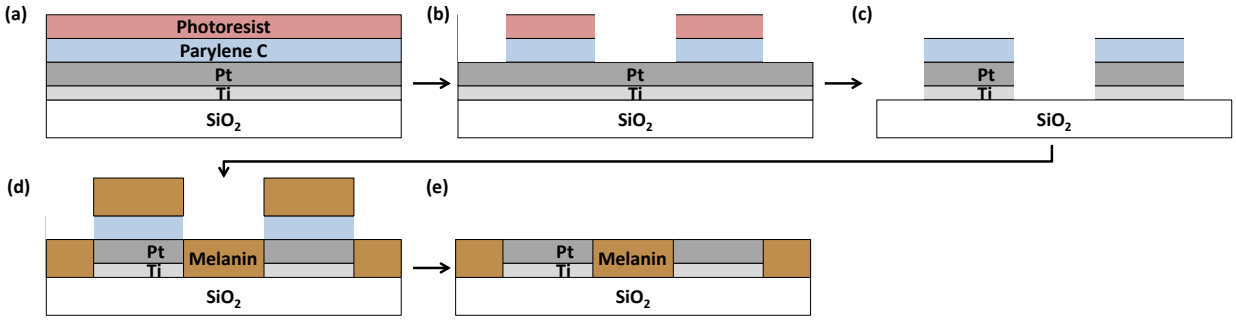

Figure 6.3 Process flow for the preparation of patterned eumelanin thin films between Pt electrodes using a parylene C layer as a mask for metal etching and eumelanin deposition.

are generally not compatible with organic films.

The first process investigated makes use of a parylene C layer as a mask for metal etching and eumelanin deposition. This process is similar to the one reported in Ref. [161]. After wafer cleaning, a 3 nm Ti adhesion layer and a 30 nm thick Pt layer were deposited by e-beam evaporation. 1.6 μm of parylene C was coated on top of the metal layers by thermal deposition (Fig. 6.3a). The parylene C layer was patterned by a standard photolithography process and etched by O_2 reactive ion etching (RIE, 125 mTorr, 10 sccm, 150 W, 10 min) (Fig. 6.3b). Pt was subsequently etched using Ar plasma (75 mTorr, 4 sccm, 200 W, 10 min) in an RIE chamber. Ti was removed by wet etching using a mixture of hydrofluoric acid and deionized water (10:1) in an ultrasonic bath (2 min) (Fig. 6.3c). In this way, Pt electrodes with a spacing of 10 μm were obtained and a sufficiently thick layer of parylene C remained on top of the electrodes to be used as a mask for spin-coating eumelanin (Fig. 6.3d). Subsequently, the parylene C layer can be peeled off mechanically, avoiding the use of any solvents that could affect the eumelanin layer (Fig. 6.3e). Unfortunately, the DMSO suspension did not well wet the substrate in proximity of the parylene C layer, so that the interelectrode region remained largely uncovered by eumelanin. Other solvents might yield better results. However, the selection of possible solvents for eumelanin is very limited. Therefore, the use of parylene C as a method to pattern eumelanin films was discarded.

Recently, fluorinated resists, developed for the patterning of organic layers, became commercially available (OSCoR 4000 from Orthogonal Inc.). They are also referred to as orthogonal resists since they do not interact with conventional polar and non-polar solvents. Developer and stripper are also orthogonal and thus do not severely affect the eumelanin layer, as was verified by AFM and electrical measurements on unpatterned devices. The orthogonal resist can potentially replace both the resist and the parylene C layer in the process described above. The photolithography parameters for the orthogonal resist needed to be

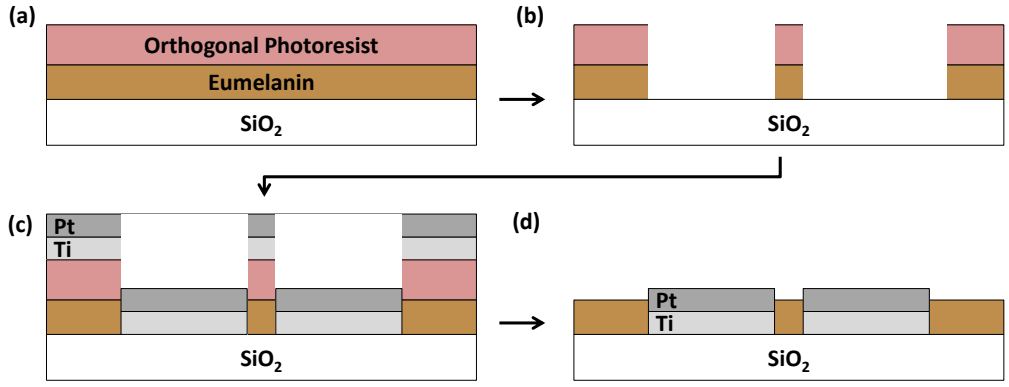

Figure 6.4 Process flow for the preparation of patterned eumelanin thin films between Pt electrodes using an orthogonal resist layer as a mask for the etching of eumelanin and in the lift-off process to pattern the electrodes.

optimized. 60 s soft bake at 90 ℃, 55 mJ/cm^2 exposure dose (365 nm), 40 s post-exposure bake at 80 ℃ and 2×60 s puddle development were found to be suitable for resist films spin-coated at 1000 rpm. The orthogonal resist film was intended as a mask for metal etching as well as eumelanin deposition. However, the resist film was not sufficiently resistant against dry etching of Pt in Ar plasma. Other dry and wet etching procedures for Pt were explored but were not successful.

Due to the challenges related to selective etching of Pt, a lift-off process using the orthogonal resist on top of a predeposited eumelanin film was explored as an alternative. In this process, the orthogonal resist layer acts as a mask for eumelanin etching. First, the eumelanin film and the orthogonal resist were deposited on a wafer by spin-coating (Fig 6.4a). The resist was patterned by the photolithography process described above and eumelanin was etched by O_2 RIE (125 mTorr, 10 sccm, 150 W, 40 s) (Fig 6.4b). Subsequently, metal was deposited (Fig. 6.4c) and the resist layer was removed by sonication in stripper solution (Fig. 6.4d). Unfortunately, the orthogonal resists available so far tend to have an overcut profile, whereas an undercut profile is required for a successful lift-off process. The consequence were metal side walls several hundreds of nanometers high at the Pt/eumelanin interface. Processing parameters for the orthogonal resist were varied in a wide range in an attempt to solve this problem but without success.

Finally, the use of the orthogonal resist as a lift-off resist beneath a layer of conventional negative photoresist was explored. By selective development of the lift-off resist, an undercut profile can be generated. In this way, the formation of metal sidewalls was largely avoided. However, the undercut profile caused another problem. The openings created in the eumelanin film by O_2 RIE were slightly too large as compared to the size of the Pt con-

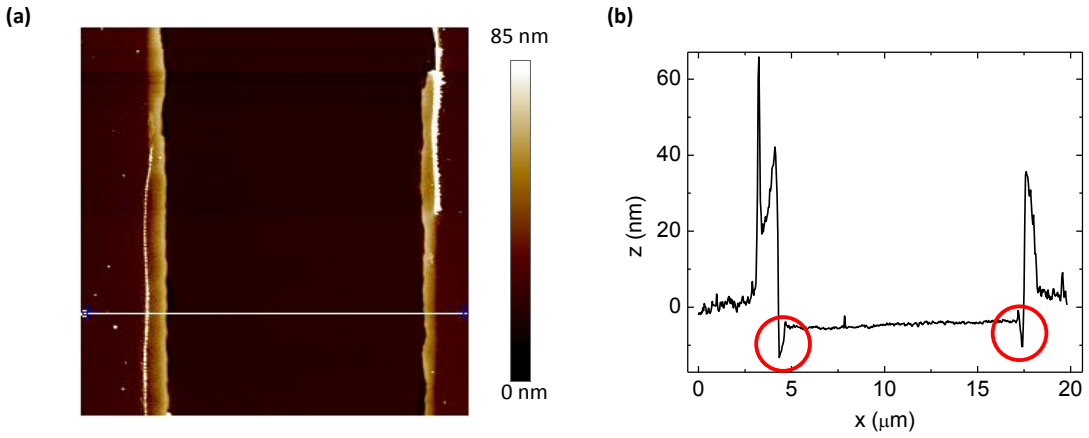

Figure 6.5 20 μm×20 μm AFM image (a) and corresponding height profile (b) of a eumelanin film patterned to fit the interelectrode region between two Pt electrodes. The sample was fabricated by the lift-off process in Fig. 6.4 but using orthogonal resist as a lift-off material and a conventional negative photoresist on top. The red circles indicate interstices between the eumelanin film and the Pt electrode leading to a bad electrical contact.

tacts deposited into these openings. This is a direct consequence of RIE being an isotropic etching process and metal deposition being directional. Thus, the process resulted in a bad contact between eumelanin and Pt, as was observed by AFM (Fig. 6.5) and electrical measurements (not shown). Furthermore, during this process eumelanin is potentially exposed to the developer solvent for the conventional photoresist. Therefore, it is advantageous to work only with an orthogonal resist optimized for lift-off. However, such a resist is not yet commercially available. Etching of eumelanin by a directional process such as ion milling could greatly improve the Pt/eumelanin interface morphology.

6.3 Thin film structure

Preliminary grazing incidence X-ray diffraction measurements were performed by collaborators in the group of Prof. Alberto Salleo at the synchrotron facility of Stanford University on *Sigma melanin* films drop cast from DMSO suspension onto Si substrates with native oxide (Fig. 6.6). The 2D diffraction pattern shows a weak broad arc, which has its strongest intensity close to the y-axis of the 2D plot (Fig. 6.6a), corresponding to the diffraction of the X-ray beam on molecular planes parallel to the substrate. The intensity profile along the y axis reveals that the maximum occurs at a scattering vector $q_z = 1.7$ Å^{-1} (Fig. 6.6b). This corresponds to a spacing $d = 2\pi/q_z = 0.37$ nm of the scattering planes, which is in good agreement with the stacking distance of eumelanin in powder and pellet samples reported in

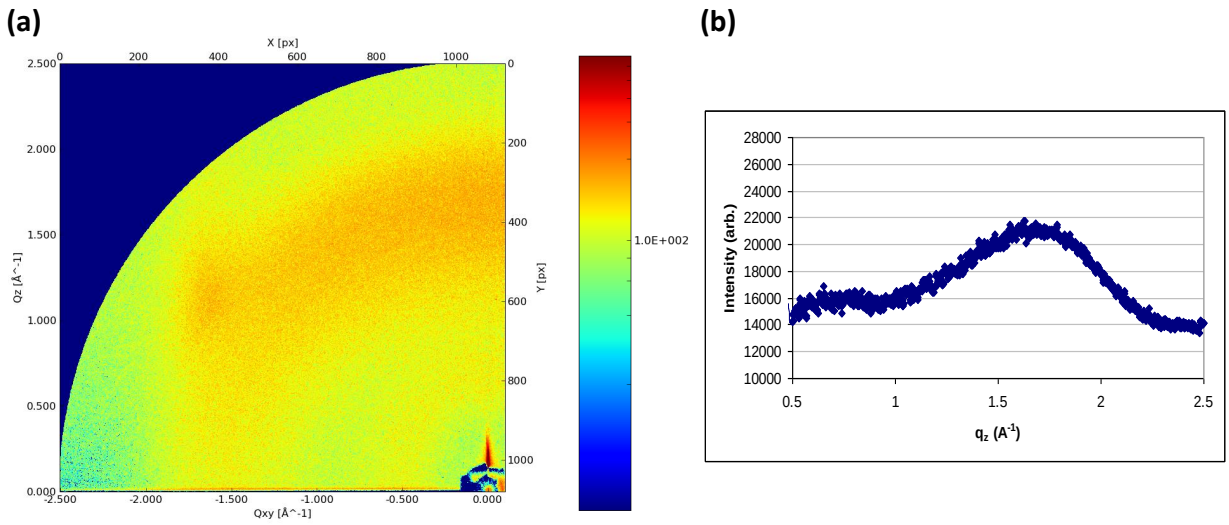

Figure 6.6 2D plot (a) and intensity profile along the y-axis (b) of GIXRD data taken on a drop cast film of *Sigma melanin* on a Si substrate.

literature [48, 61].

The broad peak in Fig. 6.6b and the extension of the arc to larger angles from the y-axis indicate a large variation in both stacking distance and orientation of the oligomer sheets of eumelanin. The XRD peak width is related to crystallite size, paracrystalline disorder within the crystallites (the degree of disorder in the π-stacking direction), and variations in the average lattice spacing [7]. In the case of high-molecular weight polymers, the paracrystalline disorder g often dominates and can be estimated from the XRD peak width (Δ_q) by $g = \sqrt{\Delta_q / 2\pi q_z}$. Polymers with $g > 10\%$ are considered amorphous. At this degree of paracrystalline disorder, the density-of-states can be described by a single broad distribution of localized states [7]. Fig. 6.6b, suggests $g \approx 25\%$ for the eumelanin films. This value is an overestimation, since the small size of the eumelanin nano-aggregates (limiting the size of crystallites), as observed by AFM in Article 1, also contributes to peak broadening [7]. Nevertheless, this comparison indicates the large degree of disorder in *Sigma melanin* deposited from DMSO. Synchrotron XRD measurements on deposits of *Sigma melanin* from DMSO suspension have also been conducted by Borghetti *et al.*. No diffraction peak could be identified for drop-cast films on Au, whereas electrodeposited films showed a peak corresponding to a spacing $d = 0.38$ nm.

GIXRD measurements should be repeated on spin-coated eumelanin films on thermal SiO_2, as used for the electrical measurements, for a more reliable correlation of film structure and charge transport.

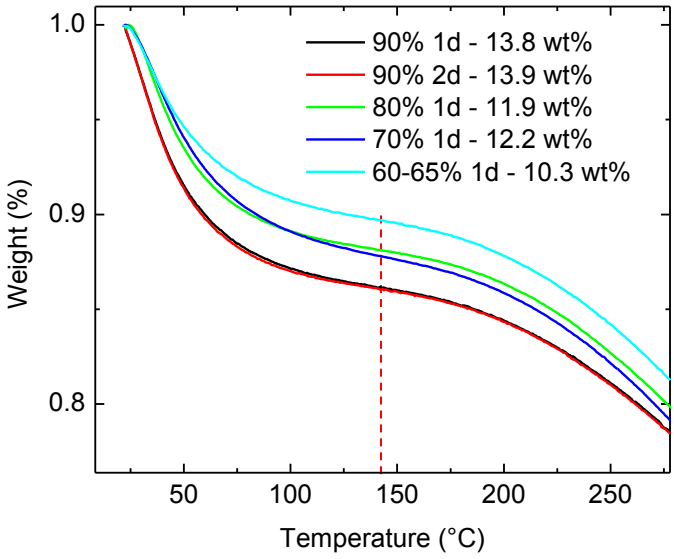

Figure 6.7 TGA data of eumelanin powder hydrated at the RH as indicated in the legend. The water content, also given in the legend, was determined from the weight loss up to 140 ℃.

6.4 Degree of hydration for different relative humidities

TGA was performed on powder samples of *Sigma melanin* hydrated at constant humidity during 24 h to estimate their water content (Fig. 6.7). Powder samples were used since spin-coated thin films did not provide enough mass of eumelanin when scratched off and scratching would have to be performed in the humidity chamber. The samples had to be exposed to ambient air for a few minutes during sample transfer. Therefore, the initial water content might have been slightly higher than indicated by the TGA curves. The water content was determined by the weight loss up to 140 ℃, where the derivative (DTG) had a minimum for these samples. The results are given in the legend of Fig. 6.7. At 90% RH, one sample was hydrated for two days to verify that hydration had saturated. The water content shows a clear increase from 60% to 70% RH and then again from 80% to 90% RH. In contrast, the hydration of samples at 70% and 80% RH is almost the same. This indicates a plateau in water adsorption, which has also been observed in studies based on infrared absorption [72].

6.5 The effect of molecular dopants on the electrical properties of eumelanin

A common strategy to increase the conductivity of organic semiconductors by several orders of magnitude is doping with strong electron acceptors (for p-type transport) or strong electron donors (for n-type transport) [4]. Doping shifts the Fermi level closer to the transport

states and thus leads to an increase of the density of mobile electrons or holes. Furthermore, it improves charge injection from the electrodes into the organic film. Typical molar doping ratios vary between 1:100 and 1:10 [227]. Since reliable HOMO and LUMO energies are not reported for eumelanin (indeed there should be a broad distribution of energies [73]), a rational choice of dopants based on energy level alignment is not possible. Two molecules successfully employed in the doping of organic semiconductors and carbon nanotubes are 2,3-dichloro-5,6-dicyano-1,4-benzoquinone (DDQ, for p-doping) and tetrathiafulvalene (TTF, for n-doping) [228–231]. These molecules were used to explore the possibility of doping eumelanin thin films.

Eumelanin, DDQ, TTF were separately dissolved/dispersed in DMSO to yield three solutions with a concentration of 15 mg ml^{-1}, 2 mg ml^{-1}, and 2 mg ml^{-1}, respectively. The solutions were mixed to yield a ratio of one DDQ or TTF molecule to 30 monomers of eumelanin (DHI:DHICA assumed to be 1:1). The pristine eumelanin solution, the eumelanin-DDQ, and eumelanin-TTF solution were spin-coated as described in Section 6.1 on Si/SiO_2 substrates with patterned Pt electrodes (25 nm thick on a 5 nm Ti adhesion layer) for electrical characterization and AFM. For Fourier transform infrared spectroscopy (FT-IR), films were deposited onto intrinsic Si substrates (UV-ozone treated) due to the strong IR absorption of SiO_2. Processing was conducted under controlled N_2 atmosphere to minimize the introduction of additional H_2O and O_2 to the samples.

FT-IR was conducted to investigate any charge transfer between the dopant molecules and eumelanin, which should lead to an energetic shift or the enhancement of certain vibrational modes [232, 233]. IR absorption spectra were taken under vacuum (1.6 Torr, RH<1%) with a Vertex 80v IR spectrometer from Bruker directly after sample preparation. The sample was left 10 min under vacuum before starting the measurement. The spectrum of a bare Si substrate was subtracted from all spectra. FTIR spectra of films of pristine eumelanin, eumelanin:DDQ, and eumelanin:TTF are shown in Fig. 6.8. The absorption peaks are listed in Tab. 6.2 together with a tentative assignment of vibrational modes. As expected, the main features of the spectra include C=C stretching from the phenyl ring, C-N stretching from the indole ring, C=O and C-OH contributions from the catechol and phenolic hydroxyl groups, respectively. In addition, peaks corresponding to the stretching of alphatic C-H (2870-3020 cm^{-1}) are observed. Peaks below 1500 cm^{-1} are strongly asymmetric. The asymmetry is much more pronounced than in other FT-IR spectra of eumelanin reported in literature and is subject of further investigations. Comparison of the spectra is difficult due to the different background and absolute intensity of the spectra, which should be mainly due to the inhomogeneity of the deposits on Si. Overall, the spectra appear similar. Notable differences are the enhancement of all peaks in the spectrum of eumelanin:DDQ, probably

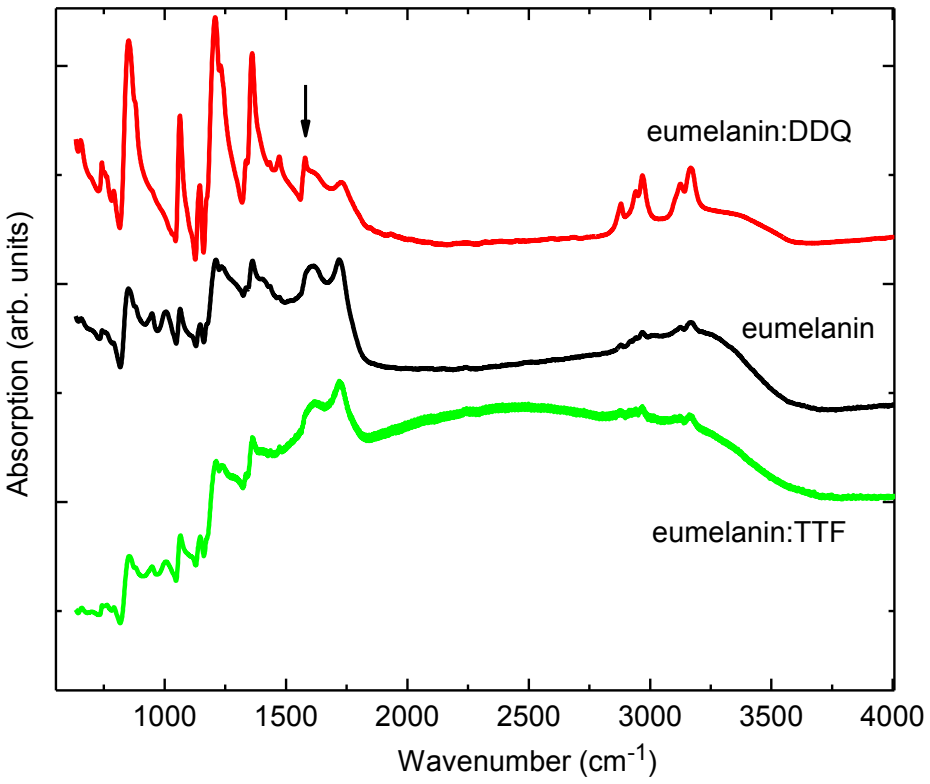

Figure 6.8 FT-IR measurements on pristine eumelanin, eumelanin with DDQ and TTF (molar ratio 1:30). The spectra are normalized and shifted along the absorption axis for better comparability.

attributable to a higher local film thickness, and a large background peak centered at about 2400 cm^{-1} in the spectrum of eumelanin:TTF, possibly related to scattering. Tab. 6.2 reveals that the FT-IR peak positions are almost identical for the pristine and doped eumelanin films. The most remarkable change in peak position is observed for C=O stretching, which is found at 1730 cm^{-1} for eumelanin:DDQ as compared to about 1720 cm^{-1} for the other two films. Taking a closer look at this wavelength region, a sharp peak at about 1580 cm^{-1} can be noticed in the spectrum of eumelanin:DDQ (marked by an arrow in Fig. 6.8). This peak can be assigned to C=C aromatic/pyrrole ring stretching [234]. The enhancement of C=C stretching can be an indication for the transfer of a positive charge (a hole) from DDQ to the π-conjugated portion of the eumelanin macromolecule [233]. Smaller changes in peak position can also be observed for the peaks assigned to C-OH stretching and bending and C=C ring vibrations. The latter were associated with a larger error, however. These changes suggest an interaction of DDQ with the DHI or DHICA phenyl ring and its –OH and =O groups. This FT-IR analysis is preliminary and preferably measurements should be repeated

on homogenous deposits with consistent film thickness.

Table 6.2 FT-IR peak positions for a pristine eumelanin films and eumelanin films with DDQ and TTF (molar ratio 1:30) and their possible assignments [234–236].

Peak position Eumelanin (cm^{-1})	Peak position Eumelanin:DDQ (cm^{-1})	Peak position Eumelanin:TTF (cm^{-1})	Possible assignment
657	656	657	Aromatic ring deformation
742	742	743	C-H stretching, indole ring vibration
763	763	763	C-H stretching, indole ring vibration
792	791	792	$[NH_2]^+$ rocking
852	852	855	C-H stretching
882	882	882	Pyrrole ring vibrations
949	951	950	Pyrrole C-H out-of-plane deformation, O-H bending
1007	≈1007	1008	C-H in-plane deformation
1065	1063	1065	C-H in/out-of-plane deformation
1146	1146	1146	C-OH phenolic stretching
1212	1209	1213	C-OH phenolic stretching, C-O stretching
1234	1231	1238	C-OH phenolic stretching, C-O stretching
1336	1335	1335	C-N stretching, indole ring
1362	1361	1361	C-N stretching, indole ring
1472	1472	1473	Pyrrole ring vibrations
≈1580	1579	≈1575	C=C aromatic/pyrrole ring stretching
≈1618	1623	≈1620	C=C aromatic ring vibration
1719	1730	1722	C=O stretching in COOH or quinone
2880	2881	≈2876	-CH_3 sym. stretching
≈2920, ≈2940	2940	≈2920, ≈2940	-CH_2 stretching
2970, ≈3016	2968	≈2969, ≈3014	-CH_3 assym. stretching
3125	3126	≈3104, ≈3123	=C-H stretching
3169	3168	≈3166	N-H stretching, indole ring
3000-3500	3000-3500	Hidden by background	-O-H stretching, also due to water residues in films

The morphology of pristine eumelanin, eumelanin:DDQ, and eumelanin:TTF films on SiO_2 was investigated by AFM. All films were homogeneous, smooth, and showed no sign of phase segregation on a length scale of tens of nanometers to micrometers. To verify if DDQ and TTF had an effect on the conductivity of dry eumelanin films, *I-V* measurements were conducted under high vacuum ($<10^{-5}$ mbar). Samples were stored overnight under the same conditions to remove residual water. Currents remained below noise level for voltages up to 50 V for all samples (Fig. 6.9a). An upper limit for the conductivity of about 10^{-11} S cm^{-1} can be estimated, in agreement with other studies on dry pristine eumelanin films [41,48,130]. DDQ and TTF at a 30:1 molar doping ratio do not increase the conductivity of dry eumelanin

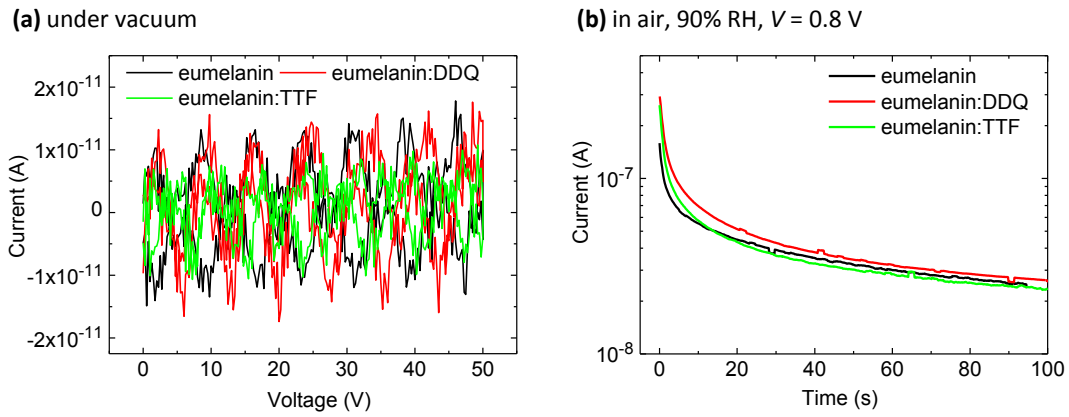

Figure 6.9 (a) I-V measurement for thin films of eumelanin, eumelanin:DDQ (30:1), and eumelanin:TTF (30:1) under vacuum. $L = 10$ μm, $W = 24.5$ mm, $d = 30$ nm. Currents are below noise level . (b) Measurement of current vs time at 90% RH for the same samples. The applied voltage is 0.8 V.

films beyond that limit. Transient current measurements were conducted in air at 90% RH on the same samples (Fig. 6.9a). There is no significant difference between the currents measured in pristine eumelanin, eumelanin:DDQ, and eumelanin:TTF films.

6.6 Electrical characterization of eumelanin thin films in thin film transistor configuration with ionic liquid as gating medium

In undoped organic semiconductors, high carrier densities can be achieved when incorporating the semiconductor as the channel material in organic thin film transistors (OTFT) (Fig. 6.10). In OTFTs, a third electrode, the gate, is separated from the channel by an electronically insulating gating medium. The charge carrier density in the channel and thereby the current between source and drain electrode (I_{DS}) is modulated by the gate voltage via electrostatic and/or electrochemical doping [237]. In electrostatic doping, charge carriers (injected from source or drain electrode) accumulate at the interface of the channel and the gating medium. The number of accumulated charges depends on the capacitance of the gating medium sandwiched between the gate and the transistor channel. Ionic liquid (IL) electrolytes have been used as gating media because of the very high capacitance of the electric double layers at the gate/IL and the IL/semiconductor interfaces [238]. The capacitance also depends on the area of these interfaces. To avoid having the gating efficiency limited by the size of the gate electrode, high surface area activated carbon has recently been employed as gate electrode [239]. If ions from the gating medium enter the channel material, electrochemical doping of the bulk can occur in addition to electrostatic doping [237]. The

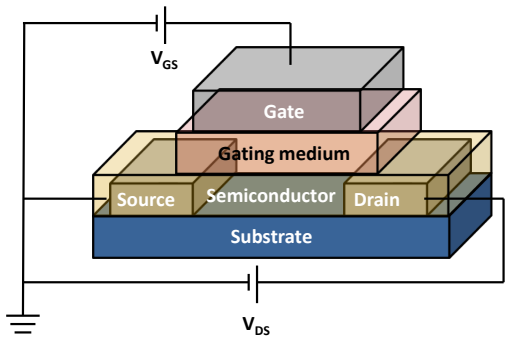

Figure 6.10 OTFT structure as used in this work, with bottom source and drain electrodes (Pt), unpatterned channel material (eumelanin), gating medium (BMPyrr-TFSI ionic liquid in Durapore® filter), and top gate (high surface-area activated carbon). Voltages are shown for n-type operation but p-type operation was also tested.

combination of IL as gating medium and carbon gate electrode has recently been reported to be very efficient in making organic transistor channels conductive at low gate voltage [239]. In collaboration with Jonathan Sayago (École Polytechnique de Montréal), this approach was explored for eumelanin.

30 nm thick films of *Sigma melanin* were deposited by spin-coating DMSO suspension on SiO_2 substrates with co-planar pre-patterned Pt electrodes (L = 10 μm, W = 4 mm). Processing was conducted under inert atmosphere and anhydrous DMSO was used. However, it should be noted that eumelanin was stored under ambient conditions. A Durapore® filter soaked in the ionic liquid 1-butyl-1-methylpyrrolidinium bis(trifluoromethylsulfonyl)imide (BMPyrr-TFSI, IoLiTec) was placed on top of the eumelanin channel as the gating medium. An activated carbon gate electrode (prepared according to the procedure in Ref. [239]) was added on top of the Durapore® filter. Devices were stored overnight under high vacuum ($<10^{-5}$ mbar) to remove residual water and characterized under the same conditions. Drain-source (V_{DS}) and gate-source (V_{GS}) voltages up to $\pm$1.5 V were applied (the maximum voltage is limited by the electrochemical stability window of the IL). No modulation of I_{DS} could be observed. The only measurable currents were leakage currents between the gate and source/drain suggesting that ions penetrated the eumelanin film.

CHAPTER 7

GENERAL DISCUSSION

In the following, the results of Chapter 3 to 6 are discussed as a whole with reference to the literature presented in Chapter 2. Although only a small part of the complex properties of eumelanin could be investigated in this work, several insights were gained. These insights are discussed with respect to processibility and chemical identity of eumelanin, charge carrier transport properties, and the role of electrochemistry in the electrical response of eumelanin.

7.1 Processibility and chemical identity of eumelanin

Eumelanin is a natural, insoluble pigment with strong hierarchical aggregation [45, 63, 64]. Indeed, natural *Sepia melanin* does not form fine suspensions in DMSO (Section 6.1). Problems were also encountered during the processing of *DHICA melanin* obtained by biomimetic synthesis. In contrast, synthetic *DMSO melanin*, *dopa melanin*, and *Sigma melanin* readily disperse in DMSO and NH_3(aq) and yield smooth and continuous films in most cases (Article 1). It is well known that different synthesis routes yield chemically distinct eumelanins [47, 50, 59]. As mentioned in Article 1 and 2, it has recently been reported that the monomers of *DMSO melanin* are sulfonated, a significant modification of the molecular structure of eumelanin that results in a better solubility [128]. This is supported by the XPS data in Article 1, which also show that a considerable amount of N is incorporated into the eumelanin structure during solubilization in NH_3(aq). Thus, Article 1 reveals that the first two procedures reported in literature for the preparation of eumelanin films [48, 49] lead to changes in chemical composition.

It is important to note that the solubilization (or the fine dispersion) of eumelanin requires at least the interruption of its supramolecular aggregation. For example, the analysis of film growth and morphology in Article 1 suggests that DMSO preserves the nanoaggregate/protomolecule structure of eumelanin but prevents the formation of larger aggregates. Although the elemental composition of *Sigma melanin* is in agreement with a macromolecule of DHI and DHICA, *Sigma melanin* is different from natural eumelanin, for example, in its content of uncyclized structures (XPS results of Article 3 and Ref. [59]).

The comparison of eumelanins from different sources suggest that there is a trade-off between (solution) processibility of eumelanin and a chemical composition closely resembling the natural pigment. The choice of the synthesis route or natural source of eumelanin

and the procedure employed for processing should be guided by the objective of the study. In view of bioelectronic applications, it is strongly desirable to have a solution-processable eumelanin/eumelanin-inspired material to readily obtain homogeneous and smooth films that can be incorporated into devices. For example, the great adhesion and film-forming properties of polydopamine enabled its use in many biomedical applications [40]. Apart from good processibility, film structure is essential for potential applications because it strongly affects the functional properties of the film. Therefore, a larger variety of eumelanins with different supramolecular structures and further processing techniques/conditions should be explored. In contrast, in studies aimed at a better understanding of the bio-functionality of eumelanin, the use of a natural eumelanin or a bio-mimetic synthesis route might have priority over good film-forming properties. In any case, it is important to investigate the effect of synthesis route and film processing on the molecular or supramolecular structure as well as on the film properties.

7.2 Charge carrier transport properties

Article 3 showed that protons are the dominant charge carriers in solution-processed thin films of *Sigma melanin* at 90% RH. The proton conductivity of about 10^{-4} S cm^{-1} is in the range of the DC conductivity of strongly hydrated eumelanin films and pellets reported in literature [39, 49, 71, 187]. This suggests the possibility that protonic currents might have been dominant in these measurements. Previous studies were conducted with proton-blocking electrodes. However, at the high voltages employed ($\geq$ 5 V and up to 100 V), water electrolysis could occur and protons could thus contribute to the DC current.

Among proton conductors, eumelanin can be classified as a hydrated acidic polymer (disregarding questions about the macromolecular structure) [171]. The proton conduction mechanism of acidic polymers depends on their hydration state [171]. At low hydration, the vehicle mechanism dominates, whereas at high hydration, when a continuous hydrogen-bond network exist, protons migrate mostly by structure diffusion (the Grotthus mechanism) [171]. The transition between the two mechanisms can be described by percolation theory and strongly depends upon the morphology of the material [175]. At 90% RH, eumelanin contains about 14 wt% water, which corresponds to 1.35-1.75 water molecules per monomer, depending on the ratio of DHI and DHICA. Infrared absorption studies have shown that water is in the liquid-phase (i.e. hydrogen-bonded) in synthetic eumelanin drop cast from aqueous suspensions [72]. Furthermore, the conductivity of eumelanin pellets shows a strong increase with hydration only beyond 10 wt% [42], which resembles the power-law dependence, beyond a certain threshold, predicted by percolation theory [173]. These observations suggest

that proton conduction via structure diffusion could dominate in strongly hydrated synthetic eumelanin pellets/films. To assess the contribution of the two transport mechanisms to proton conduction in hydrated eumelanin thin films, the dependence of the proton conductivity on hydration and the morphology of water domains should be investigated.

Many experimental observations on eumelanin can be explained by proton migration and hence without assuming electron transport according to the amorphous semiconductor model:

- A strong hydration dependence is expected for protonic conduction. This dependence was indeed observed in Article 3. With increasing hydration, the density of dissociated protons increases and the hydrogen-bond network providing proton transport paths becomes more dense. The hydration dependence of the proton density is due not only to the comproportionation equilibrium but also to a varying degree of protonation of moieties other than SQ. Indeed, Gonçalves *et al.* reported the trapping of protons in -COOH groups during dehydration [41].
- The long RC time constants observed in transient current (Article 1) and photoconductivity measurements are typical of ionic charge carriers [42, 53]. The photoconductivity itself is possibly related to excited-state proton transfer, which has been suggested to cause efficient non-radiative relaxation in eumelanin [74, 76]. Heating of the sample during illumination can also contribute to the observation of photoconductivity [36].
- The high polarization currents observed for eumelanin pellets [70], the hysteresis in the I-V characteristics of ITO/eumelanin/Au structures in ambient air [53], and the capacitive currents in hydrated eumelanin films reported in Article 3 are likely caused by protonic currents blocked by the electrodes.
- The non-capacitive currents in hydrated eumelanin films observed at 0.2 V$< V <$0.8 V in Article 3 can be explained by electrochemical reactions, enabled by proton migration.
- Like electronic conduction in semiconductors, protonic conduction is a thermally activated process and, hence, can give rise to the Arrhenius-type temperature dependence of the eumelanin conductivity [36, 41].

It should be noted that ions other than protons are also likely to contribute to the electrical current. ToF-SIMS measurements in Article 2 (Fig. S18, Appendix B) show the accumulation of Cl^- ions at the positively biased electrode. NAA measurements, conducted to quantify the Cl^- content, also revealed the presence of Na and K, likely present in the cationic form. The contribution of these ions to the capacitive and non-capacitive currents in hydrated eumelanin films should be investigated systematically, e.g., by varying their concentration.

In the following, experimental results from literature and this thesis will be discussed with regard to the possibility of electronic conduction in eumelanin pellets/films. In the dry state, the number of dissociated protons should be very low. Hence, one could expect

that electron transport dominates the electrical properties of dry eumelanin pellets/films. The conductivities measured so far for nearly dry eumelanin samples are very low, in the range of $10^{-13} - 10^{-10}$ S cm^{-1} [41, 48, 71]. Measurements of activation energies E_A under vacuum or N_2 are partly affected by sample dehydration but consistently indicate rather large values. E_A of 0.4-1.5 eV and 0.8-1.3 eV have been reported for pellets and thin films, respectively [36, 38, 41, 48, 71]. Hence, if we assume that the electrical current under dry atmosphere is dominated by electronic conduction, the mobility of the electronic charge carrier would be very low in dry samples [142]. The question arises if water could increase the electron/hole mobility. Ambrico *et al.* suggested that water might form bridges between eumelanin molecules for electron/hole transport [44]. The only report found on the activation energy or charge carrier mobility of hydrated eumelanin dates back to 1969 [179] and indicates 1.2 eV for partially hydrated pellets vs 1.5 eV for dry pellets. The model of Mostert *et al.* suggests that the density of mobile electrons increases with hydration but does not predict the dependence of the mobility of the electronic charge carrier on hydration. Indeed, as pointed out by the authors, the model does not assume any specific electron transport mechanism. In contrast to these hypotheses, water is detrimental to electron transport in many organic materials due to the creation of trap states [148, 240].

So far, classical approaches to increase the conductivity of organic semiconductors by increasing the density of electronic charge carriers such as chemical and field-effect doping have not been successful for eumelanin (Section 6.5) [35,241]. The development of an effective doping strategy suffers from the lack of well-defined HOMO and LUMO levels for eumelanin, among others. For the same reason, a rational choice of an electrode material optimized for hole or electron injection based on energy-level alignment is difficult at this point. Carbon nanotube electrodes have been shown to enhance electron and hole injection in different organic semiconductors [224] and could help to ensure that electronic currents in eumelanin are not limited by injection.

One of the requirements of efficient electronic conduction in organic semiconductors is that the constituent molecules have to be easily oxidized and reduced. In Article 3, only irreversible redox reactions were clearly observed. In contrast, partly reversible redox processes have been observed for electropolymerized eumelanin films [58]. This redox activity was weak though.

Apart from the influence of atmosphere and electrode material, briefly discussed above, electron transport in organic materials is largely determined by structure: from molecular structure to molecular packing on the nanoscale to film microstructure [7]. All eumelanins have a π-conjugated backbone but the extension of the π-conjugation varies with the synthesis route. An important parameter is the ratio of DHICA vs DHI. Panzella *et al.* have suggested that eumelanin based on DHICA units forms non-planar rod-like structures with in-

terrupted π-conjugation, whereas *DHI melanin* forms planar oligomer sheets with enhanced π-conjugation and stacking [223]. Although the XPS data of Article 3 indicates a high -COOH content in *Sigma melanin*, round-shaped nanoaggregates dominate its film morphology (Article 1). Furthermore, the optical absorption spectrum of *Sigma melanin* was found to resemble more the spectrum of *DHI melanin* than *DHICA melanin* (Wünsche *et al.*, *ECS Transactions*, vol. 35, no. 7, pp. 75–81, 2011). This indicates the need for further structural characterization. The presence of uncyclized units as found in *Sigma melanin* interrupts π-conjugation and should thus be limited.

Intermolecular electron transfer is greatly enhanced by π-stacking [7]. Recently, efficient electron and hole transport has been reported in films of highly purified H-bonded pigments, which have limited intramolecular π-conjugation but strong intermolecular π-stacking [20, 151]. XRD measurements indicate weak graphite-like π-stacking but a large degree of disorder in *Sigma melanin* deposited from DMSO suspension (Section 6.3). The preferential orientation of π-stacking is perpendicular to the substrate and hence unfavorable for in-plane electron transport. The large degree of structural disorder in eumelanin is likely promoted by the large number of different coexisting oligomers.

AFM images in Article 1 show that eumelanin films processed in DMSO are composed of nano-aggregates 1-2 nm high and 10-30 nm large. A small aggregate size does not necessarily impede electron transport if the aggregates are well interconnected [7]. In the AFM images (Article 1), the connectivity of aggregates appears to be generally good due to their small and compact size, although some interstices can be seen. Further studies are required to conclude about the electronic connectivity, which depends on intermolecular distances and orientations [242].

The strong degree of structural disorder at the molecular and supramolecular level translates into energetic disorder, which is believed to be the origin of the broad-band optical absorption of eumelanin [73, 77]. The tail states of this broad distribution of HOMO and LUMO levels act as traps for electronic charge carriers. Further trap states can be introduced by impurities. Along this line of thought, a reduction in the chemical and structural disorder might enhance electronic conduction in eumelanin films. It is possible though that the remaining degree of disorder, inherent to eumelanin, and the self-assembly to nanoaggregates continue to limit electron transport.

This discussion points out that electron conductivity in eumelanin is not an intrinsic material property. It strongly depends on film structure, material purity, and atmosphere. Furthermore, the electrode material and the sample dimensions have an effect on the electrical properties of the sample. A particularity of eumelanin is its high structural diversity depending on the (bio-)synthetic origin. Eumelanins with different monomer composition,

macro-, and/or supramolecular structure could show different electron transport properties. Therefore, while no clear evidence of electronic conduction was found in this thesis, there are several approaches that should be explored in order to determine if eumelanin or eumelanin-inspired materials can conduct electrons under different conditions.

7.3 The role of electrochemistry

Recognizing and investigating the role of electrochemistry in the electrical response of hydrated eumelanin films was a major part of this work. As discussed in Section 2.4.1, the presence of water and mobile ions enables electrochemical reactions. Electrochemical reactions play an important role in the working mechanism of various organic devices based on mixed conduction. Nevertheless, an electrochemical perspective on the electrical properties of eumelanin is largely missing in literature. Early coulometric measurements on the mixed conduction in eumelanin pellets were based on hydrogen evolution [43] but other redox processes that might occur in parallel were not discussed. Redox processes at the Au/eumelanin interface are considered in a recent EIS study on p-Si/eumelanin/Au and ITO/eumelanin/Au samples [189] but not further specified and their role in DC electrical measurements was not evaluated.

Both Articles 2 and 3 clearly indicate the presence of electrochemical processes at $V \leq 1$ V. Under certain conditions, these processes dominate the electrical response of *Sigma melanin*. The chemistry and electrochemistry of eumelanin films is without doubt very complex. Several efforts were made to shed light on the various reactions occurring. CV measurements in Article 3 indicate the importance of irreversible oxidative processes in hydrated eumelanin films, possibly involving further polymerization of the film. The change of film height after biasing points to pH-induced disaggregation. Furthermore, the possible involvement of reversible redox reactions of eumelanin and the comproportionation equilibrium is considered in the model in Article 3.

Article 2 reveals that the electrode material itself can participate in electrochemical reactions. Chloride traces could promote the electrochemical oxidation of Au, underlining the importance to consider impurities in the electrical response of hydrated eumelanin films. Traces of chloride were present in all eumelanins investigated. It should be noted that eumelanin is difficult to purify due to its low solubility, varying molecular weight, and metal chelation properties. Furthermore, chloride is ubiquitous in biological systems. In view of bioelectronic applications, it is thus important to consider the effects of halides on typical electrode materials such as Au. Article 2 also suggests that the metal chelation properties of eumelanin play a role in Au dissolution and aggregate formation. The analysis of ToF-SIMS

data is ongoing to identify Au-eumelanin complexes forming at the interface of the hydrated eumelanin film and the positively biased Au electrode.

In summary, this thesis reveals the rich chemistry and electrochemistry of hydrated eumelanin films and makes several hypotheses for the processes occurring. Further studies are required to clearly identify the reactions taking place.

CHAPTER 8

CONCLUSION AND PERSPECTIVES

In this thesis, new insights were gained on

- the solution-processing and growth of eumelanin thin films,
- the electrical response of hydrated eumelanin films including their interaction with Au electrodes,
- the charge carrier transport properties of eumelanin films.

Due to the largely insoluble character of eumelanin, only few eumelanin synthesis routes and processing solvents have been reported as suitable for the preparation of thin films. In this work, these synthesis routes and solvents are compared with respect to their effect on film morphology and chemical composition, studied by AFM and XPS, respectively. Homogeneous and smooth eumelanin films are obtained by spin-coating suspensions of *Sigma melanin* in DMSO. These films show good adhesion on hydrophilic substrates and an elemental composition in agreement with the molecular structure of eumelanin. In contrast, film deposition from NH_3(aq) suspension severely affects the chemical composition. The use of the low volatile solvent DMSO has the drawback of solvent residues in the film. TGA measurements suggest that heating the films at 125 ℃ could be a suitable method to remove DMSO residues without risking the thermal decomposition of eumelanin. *Sigma melanin* has a much better processibility than natural eumelanins, which is likely related to differences in molecular structure. XPS measurements indicate that *Sigma melanin* has a high content of DHICA units and uncyclized monomers. The morphology and the growth of films deposited from DMSO was studied by AFM. Films are composed of nanoaggregates 1–2 nm high and 10–30 nm large, supporting the stacked-oligomer model for the supramolecular structure of eumelanin. The nanoaggregates assemble according to a quasi layer-by-layer mode, yielding films with surface roughnesses as low as 0.4 nm. Preliminary GIXRD measurements indicate a large degree of disorder in the films and weak π-stacking with a preferential orientation perpendicular to the substrate.

This thesis contains the first detailed investigation of the electrical properties of strongly hydrated eumelanin films. The electrical characterization of eumelanin in thin film form and in a strongly hydrated state is especially important in view of bioelectronic applications. The strong hydration-dependence of the conductivity of eumelanin was confirmed for thin films.

Transient current measurements with proton-transparent PdH_x electrodes, rate-dependent I-V, and EIS measurements were employed to distinguish between the contributions of ionic conduction, electronic conduction, and electrochemical reactions. For the first time, evidence is provided for protonic conduction in eumelanin thin films and an estimate for the proton conductivity (10^{-4} S cm^{-1}) is given. Furthermore, the important role of electrochemical processes in the electrical response of hydrated eumelanin films is revealed. In the case of eumelanin films between coplanar Au electrodes, a combination of AFM, SEM, and ToF-SIMS measurements could show that electrochemical processes lead to the dissolution of Au from the positive electrode, followed by the growth of Au-eumelanin dendrites between the electrodes. A comparison of eumelanins from different sources suggest that chloride traces as well as the metal chelation properties of eumelanin play a role in this process. The dendrites cause a sudden change of the electrical resistance of the sample. In analogy to resistive switching memory devices based on electrochemical metallization, this phenomenon can possibly be employed for biocompatible memory devices. Even in absence of a transformation of the electrode material, electrochemical processes strongly contribute to the electrical current in hydrated eumelanin films measured with coplanar Pt electrodes. In contrast, no evidence is found for a significant contribution of electronic conduction. A model is proposed to explain this observation, based on proton migration, the redox properties of eumelanin, and the recent insight that the electronic charge carrier density is directly linked to the concentration of the semi-oxidized semiquinone form of the eumelanin building blocks.

Future work on the electrical properties of eumelanin thin films should aim at a correlation of structure and electron transport at different length scales. The relative portion of the various eumelanin building blocks, the macro- and supramolecular structure, as well as the thin film texture are expected to affect charge transport. To this end, it would be instructive to compare the structure and the charge carrier transport properties of films of eumelanins obtained by the polymerization of DHI and DHICA. *DHI melanin* and *DHICA melanin* not only have a better defined chemical composition but they are also reported to have very different macro- and supramolecular structures. The use of *DHI melanin* and *DHICA melanin* will require further efforts in the development of suitable film processing techniques. Films of eumelanin with a higher content of DHI, promoting the formation of planar oligomers and π-stacking, might show better electronic conduction than *Sigma melanin*. Furthermore, electropolymerized eumelanin films seem to show enhanced molecular ordering and redox activity compared to spin-coated films. However, their applications seem limited since they have to be deposited on conductive substrates. To explore the limits of electron transport in eumelanin, it would be helpful to prepare highly ordered films of one specific eumelanin monomer or oligomer with strong π-stacking in the direction of current flow. In analogy to

semiconducting films of other H-bonded pigments such as indigo, this strategy might provide an efficient electron transport path. However, it has to be noted that such well-ordered eumelanin-derived structures, if processable, might have very different properties than natural eumelanin, with its inherent chemical and structural disorder. In addition, efforts could be extended to innovative electrode materials other than thermally evaporated noble metals. A promising candidate are carbon nanotubes because of their superior charge injecting properties. In the case of enhanced electronic conduction, it would be very interesting to re-investigate the effect of hydration on the density and mobility of electronic charge carriers.

A further avenue of research put forth by this thesis is the investigation of the various electrochemical processes that take place at the interface of hydrated eumelanin films and metal electrodes. Apart from further CV studies with a conventional electrochemical cell, it would be useful to integrate a (quasi-)reference electrode directly into the thin film sample. In this way, the electrochemical potential at the electrodes can be determined and electrochemical reactions can be studied in-situ. In addition, the use of various spatially resolved spectroscopy techniques should be explored to detect local chemical changes. Infrared spectroscopy coupled to AFM seems to be a promising new technique for this purpose.

For a better understanding of the interplay of ion/proton accumulation and charge transfer at the electrodes, it would be useful to investigate the electric field distribution in hydrated eumelanin films by Kelvin probe microscopy. For this purpose and for quantitative modeling of the electrical response of eumelanin films, it is necessary to obtain films with well defined dimensions and little overlap with the electrodes. Therefore, capitalizing on the experiments performed in this work, a procedure for the patterning of eumelanin films by photolithography using fluorinated photoresists should be developed.

The demonstration of proton conduction in eumelanin films in this thesis could be the starting point for the design of eumelanin-based protonic devices. Complementary field-effect transistors based on purely protonic conduction in biomolecular materials have recently been reported. Protonic conduction in combination with the peculiar properties of eumelanin such as metal chelation could be a unique platform for new sensing devices.

In order to explore the feasibility and performance of Au-eumelanin based resistive switching memory devices, one of the two electrodes should be made of another conducting material, inert in the range of voltages applied. Promising candidates for the inert electrode are non-metallic materials such as graphene or the conducting polymer poly(3,4-ethylenedioxythiophene) polystyrene sulfonate. The electrode distance should be decreased to reduce writing times. Furthermore, a substitute for DMSO with higher boiling point should be found to enable aggregate migration over prolonged device operation.

In summary, this thesis reports solution-processed eumelanin thin films that are proton-conductive and show interesting electrochemical interactions with Au electrodes in the hydrated state. New insights are gained on the origin of electrical currents in hydrated eumelanin films, based on chemical, electrochemical, and electrical characterization. The necessity of a combined approach, including electrochemical and structural characterization, to uncover the charge carrier transport properties of eumelanin is discussed. A good understanding of the charge carrier transport properties of eumelanin can contribute to the elucidation of the diverse biological functions of eumelanin. Furthermore, the characterization of protonic and electronic conduction in hydrated eumelanin films, as well as their interaction with metal electrodes is essential to evaluate the potential of eumelanin for bioelectronic applications. As a contribution to the emerging field of organic bioelectronics, this work emphasizes the need to consider electrochemical processes in the electrical response of organic bioelectronic devices and to carefully assess the effect of ionic impurities and water on the electrical properties of the organic active layer.

REFERENCES

[1] H. Shirakawa and E. Louis, "Synthesis of electrically conducting organic polymers: halogen derivatives of polyacetylene,$(CH)_x$," *Journal of the Chemical Society, Chemical Communications*, vol. 1977, no. 16, pp. 578–580, 1977.

[2] C. K. Chiang, C. R. Fincher, Y. W. Park, A. J. Heeger, H. Shirakawa, E. J. Louis, S. C. Gau, and A. G. MacDiarmid, "Electrical conductivity in doped polyacetylene," *Physical Review Letters*, vol. 39, no. 17, p. 1098, 1977.

[3] B. Bolto, R. McNeill, and D. Weiss, "Electronic Conduction in Polymers III. Electronic Properties of Polypyrrole," *Australian Journal of Chemistry*, vol. 16, no. 6, pp. 1090–1130, 1963.

[4] B. Lüssem, M. Riede, and K. Leo, "Doping of organic semiconductors," *Physica Status Solidi (a)*, vol. 210, no. 1, pp. 9–43, 2013.

[5] A. Facchetti, "π-Conjugated Polymers for Organic Electronics and Photovoltaic Cell Applications," *Chemistry of Materials*, vol. 23, no. 3, pp. 733–758, 2011.

[6] T. Sekitani and T. Someya, "Stretchable, large-area organic electronics," *Advanced Materials*, vol. 22, no. 20, pp. 2228–2246, 2010.

[7] R. Noriega, J. Rivnay, K. Vandewal, F. P. V. Koch, N. Stingelin, P. Smith, M. F. Toney, and A. Salleo, "A general relationship between disorder, aggregation and charge transport in conjugated polymers," *Nature Materials*, vol. 12, no. 11, pp. 1038–1044, 2013.

[8] R. A. J. Janssen and J. Nelson, "Factors limiting device efficiency in organic photovoltaics," *Advanced Materials*, vol. 25, no. 13, pp. 1847–1858, 2013.

[9] J. Perelaer, P. J. Smith, D. Mager, D. Soltman, S. K. Volkman, V. Subramanian, J. G. Korvink, and U. S. Schubert, "Printed electronics: the challenges involved in printing devices, interconnects, and contacts based on inorganic materials," *Journal of Materials Chemistry*, vol. 20, no. 39, p. 8446, 2010.

[10] J. E. Anthony, A. Facchetti, M. Heeney, S. R. Marder, and X. Zhan, "n-Type organic semiconductors in organic electronics," *Advanced Materials*, vol. 22, no. 34, pp. 3876–3892, 2010.

[11] M. Zhu and C. Yang, "Blue fluorescent emitters: design tactics and applications in organic light-emitting diodes," *Chemical Society Reviews*, vol. 42, no. 12, pp. 4963–4976, 2013.

[12] R. R. Sø ndergaard, M. Hösel, and F. C. Krebs, "Roll-to-Roll fabrication of large area functional organic materials," *Journal of Polymer Science Part B: Polymer Physics*, vol. 51, no. 1, pp. 16–34, 2013.

[13] J. Rivnay, R. M. Owens, and G. G. Malliaras, "The rise of organic bioelectronics," *Chemistry of Materials*, vol. 26, no. 1, pp. 679–685, 2014.

[14] L. Kergoat, B. Piro, M. Berggren, G. Horowitz, and M.-C. Pham, "Advances in organic transistor-based biosensors: from organic electrochemical transistors to electrolyte-gated organic field-effect transistors," *Analytical and Bioanalytical Chemistry*, vol. 402, no. 5, pp. 1813–1826, 2012.

[15] R. M. Owens and G. G. Malliaras, "Organic electronics at the interface with biology," *MRS Bulletin*, vol. 35, no. 06, pp. 449–456, 2010.

[16] K. Svennersten, K. C. Larsson, M. Berggren, and A. Richter-Dahlfors, "Organic bioelectronics in nanomedicine," *Biochimica et Biophysica Acta (BBA) - General Subjects*, vol. 1810, no. 3, pp. 276–285, 2011.

[17] M. Irimia-Vladu, ""Green" electronics: biodegradable and biocompatible materials and devices for sustainable future," *Chemical Society Reviews*, vol. 43, no. 2, pp. 588–610, 2014.

[18] P. Meredith, C. J. Bettinger, M. Irimia-Vladu, a. B. Mostert, and P. E. Schwenn, "Electronic and optoelectronic materials and devices inspired by nature," *Reports on Progress in Physics*, vol. 76, no. 3, p. 034501, 2013.

[19] C. J. Bettinger and Z. A. Bao, "Biomaterials-based organic electronic devices," *Polymer International*, vol. 59, no. 5, pp. 563–567, 2010.

[20] M. Irimia-Vladu, E. D. Głowacki, P. A. Troshin, G. Schwabegger, L. Leonat, D. K. Susarova, O. Krystal, M. Ullah, Y. Kanbur, M. A. Bodea, V. F. Razumov, H. Sitter, S. Bauer, and N. S. Sariciftci, "Indigo - a natural pigment for high performance ambipolar organic field effect transistors and circuits," *Advanced Materials*, vol. 24, pp. 375–380, 2012.

[21] C. Zhong, Y. Deng, A. F. Roudsari, A. Kapetanovic, M. P. Anantram, and M. Rolandi, "A polysaccharide bioprotonic field-effect transistor," *Nature Communications*, vol. 2, p. 476, 2011.

[22] H. Longuet-Higgins, "On the origin of the free radical property of melanins," *Archives of Biochemistry and Biophysics*, vol. 86, no. 2, pp. 231–232, 1960.

[23] A. Pullman and B. Pullman, "The band structure of melanin," *Biochimica et Biophysica Acta*, vol. 54, no. 2, pp. 384–385, 1961.

[24] J. E. McGinness, "Mobility gaps: a mechanism for band gaps in melanins," *Science*, vol. 177, no. 52, pp. 896–897, 1972.

[25] J. McGinness, P. Corry, and P. Proctor, "Amorphous semiconductor switching in melanins." *Science*, vol. 183, no. 127, pp. 853–855, 1974.

[26] G. Prota, "Progress in the chemistry of melanins and related metabolites," *Medicinal Research Reviews*, vol. 8, no. 4, pp. 525–556, 1988.

[27] P. Riley, "Melanin," *International Journal of Biochemistry and Cell Biology*, vol. 29, no. 11, pp. 1235–1239, 1997.

[28] F. A. Zucca, G. Giaveri, M. Gallorini, A. Albertini, M. Toscani, G. Pezzoli, R. Lucius, H. Wilms, D. Sulzer, S. Ito, K. Wakamatsu, and L. Zecca, "The neuromelanin of human substantia nigra: physiological and pathogenic aspects," *Pigment Cell Research*, vol. 17, no. 6, pp. 610–617, 2004.

[29] H. Fedorow, F. Tribl, G. Halliday, M. Gerlach, P. Riederer, and K. L. Double, "Neuromelanin in human dopamine neurons: comparison with peripheral melanins and relevance to Parkinson's disease," *Progress in Neurobiology*, vol. 75, no. 2, pp. 109–124, 2005.

[30] M. Youdim, D. Ben-Shachar, and P. Riederer, "Is Parkinson's disease a progressive siderosis of substantia nigra resulting in iron and melanin induced neurodegeneration?" *Acta Neurologica Scandinavica*, vol. 80, pp. 47–54, 1989.

[31] H. Z. Hill, W. Li, P. Xin, and D. L. Mitchell, "Melanin: a two edged sword?" *Pigment Cell Research*, vol. 10, no. 3, pp. 158–161, 1997.

[32] B. Commoner, J. Townsend, and G. E. Pake, "Free radicals in biological materials," *Nature*, vol. 174, no. 4432, pp. 689–691, 1954.

[33] P. Crippa, V. Cristofoletti, and N. Romeo, "A band model for melanin deduced from optical absorption and photoconductivity experiments," *Biochimica et Biophysica Acta (BBA) - General Subjects*, vol. 538, no. 1, pp. 164–170, 1978.

[34] A. M. Potts and P. C. Au, "The photoconductivity of melanin," *Agressologie*, vol. 9, no. 2, pp. 225–230, 1968.

[35] M. M. Jastrzebska, H. Isotalo, J. Paloheimo, H. Stubb, and B. Pilawa, "Effect of Cu^{2+}-ions on semiconductor properties of synthetic DOPA melanin polymer," *Journal of Biomaterials Science, Polymer Edition*, vol. 7, no. 9, pp. 781–793, 1996.

[36] M. Abbas, F. D'Amico, L. Morresi, N. Pinto, M. Ficcadenti, R. Natali, L. Ottaviano, M. Passacantando, M. Cuccioloni, M. Angeletti, and R. Gunnella, "Structural, electrical, electronic and optical properties of melanin films," *European Physical Journal E*, vol. 28, no. 3, pp. 285–291, 2009.

[37] M. Piacenti da Silva, J. C. Fernandes, N. B. de Figueiredo, M. Congiu, M. Mulato, and C. F. de Oliveira Graeff, "Melanin as an active layer in biosensors," *AIP Advances*, vol. 4, no. 3, p. 037120, 2014.

[38] T. Ligonzo, M. Ambrico, V. Augelli, G. Perna, L. Schiavulli, M. A. Tamma, P. F. Biagi, A. Minafra, and V. Capozzi, "Electrical and optical properties of natural and synthetic melanin biopolymer," *Journal of Non-Crystalline Solids*, vol. 355, no. 22-23, pp. 1221–1226, 2009.

[39] C. J. Bettinger, J. P. Bruggeman, A. Misra, J. T. Borenstein, and R. Langer, "Biocompatibility of biodegradable semiconducting melanin films for nerve tissue engineering," *Biomaterials*, vol. 30, no. 17, pp. 3050–3057, 2009.

[40] M. E. Lynge, R. van der Westen, A. Postma, and B. Städler, "Polydopamine–a nature-inspired polymer coating for biomedical science," *Nanoscale*, vol. 3, no. 12, pp. 4916–4928, 2011.

[41] P. J. Gonçalves, O. B. Filho, and C. F. O. Graeff, "Effects of hydrogen on the electronic properties of synthetic melanin," *Journal of Applied Physics*, vol. 99, no. 10, p. 104701, 2006.

[42] A. B. Mostert, B. J. Powell, F. L. Pratt, G. R. Hanson, T. Sarna, I. R. Gentle, and P. Meredith, "Role of semiconductivity and ion transport in the electrical conduction of melanin," *Proceedings of the National Academy of Sciences*, vol. 109, no. 23, pp. 8943–8947, 2012.

[43] M. R. Powell and B. Rosenberg, "The nature of the charge carriers in solvated biomacromolecules," *Journal of Bacteriology*, vol. 1, no. 6, pp. 493–509, 1970.

[44] M. Ambrico, P. F. Ambrico, A. Cardone, T. Ligonzo, S. R. Cicco, R. D. Mundo, V. Augelli, and G. M. Farinola, "Melanin layer on silicon: an attractive structure for a possible exploitation in bio-polymer based metal-insulator-silicon devices," *Advanced Materials*, vol. 23, no. 29, pp. 3332–3336, 2011.

[45] M. D'Ischia, A. Napolitano, A. Pezzella, P. Meredith, and T. Sarna, "Chemical and structural diversity in eumelanins: unexplored bio-optoelectronic materials," *Angewandte Chemie (International Edition)*, vol. 48, no. 22, pp. 3914–3921, 2009.

[46] P. Meredith and T. Sarna, "The physical and chemical properties of eumelanin," *Pigment Cell Research*, vol. 19, no. 6, pp. 572–594, 2006.

[47] M. D'Ischia, K. Wakamatsu, A. Napolitano, S. Briganti, J.-C. Garcia-Borron, D. Kovacs, P. Meredith, A. Pezzella, M. Picardo, T. Sarna, J. D. Simon, and S. Ito, "Melanins and melanogenesis: methods, standards, protocols," *Pigment Cell & Melanoma Research*, vol. 26, no. 5, pp. 616–633, 2013.

[48] S. N. Dezidério, C. A. Brunello, M. I. N. da Silva, M. A. Cotta, and C. F. O. Graeff, "Thin films of synthetic melanin," *Journal of Non-Crystalline Solids*, vol. 338-340, pp. 634–638, 2004.

[49] J. P. Bothma, J. de Boor, U. Divakar, P. E. Schwenn, and P. Meredith, "Device-quality electrically conducting melanin thin films," *Advanced Materials*, vol. 20, no. 18, pp. 3539–3542, 2008.

[50] A. Pezzella and J. Wünsche, "Eumelanin: an old natural pigment – a new material for organic electronics. Chemical, physical, and structural properties in relation to potential applications," in *Organic Electronics: Emerging Concepts and Technologies*, F. Cicoira and C. Santato, Eds. Weinheim, Germany: Wiley-VCH Verlag GmbH & Co. KGaA, 2013.

[51] P. Meredith, K. Tandy, and A. B. Mostert, "A hybrid ionic–electronic conductor: melanin, the first organic amorphous semiconductor?" in *Organic Electronics: Emerging Concepts and Technologies*, F. Cicoira and C. Santato, Eds. Weinheim, Germany: Wiley-VCH Verlag GmbH & Co. KGaA, 2013.

[52] Y. J. Kim, W. Wu, S.-E. Chun, J. F. Whitacre, and C. J. Bettinger, "Biologically derived melanin electrodes in aqueous sodium-ion energy storage devices," *Proceedings of the National Academy of Sciences*, vol. 110, no. 52, pp. 20 912–20 917, 2013.

[53] M. Ambrico, A. Cardone, and T. Ligonzo, "Hysteresis-type current–voltage characteristics in Au/eumelanin/ITO/glass structure: Towards melanin based memory devices," *Organic Electronics*, vol. 11, no. 11, pp. 1809–1814, 2010.

[54] A. González Orive, Y. Gimeno, A. Creus, D. Grumelli, C. Vericat, G. Benitez, and R. Salvarezza, "Electrochemical preparation of metal–melanin functionalized graphite surfaces," *Electrochimica Acta*, vol. 54, no. 5, pp. 1589–1596, 2009.

[55] H. Lee, S. M. Dellatore, W. M. Miller, and P. B. Messersmith, "Mussel-inspired surface chemistry for multifunctional coatings," *Science*, vol. 318, no. 5849, pp. 426–430, 2007.

[56] G. Prota, *Melanins and melanogenesis*. San Diego: Academic Press, 1992.

[57] A. Pezzella, A. Iadonisi, S. Valerio, L. Panzella, A. Napolitano, M. Adinolfi, and M. D'Ischia, "Disentangling eumelanin "black chromophore": visible absorption changes as signatures of oxidation state- and aggregation-dependent dynamic interactions in a model water-soluble 5,6-dihydroxyindole polymer," *Journal of the American Chemical Society*, vol. 131, no. 42, pp. 15 270–15 275, 2009.

[58] S. Gidanian and P. J. Farmer, "Redox behavior of melanins: direct electrochemistry of dihydroxyindole-melanin and its Cu and Zn adducts," *Journal of Inorganic Biochemistry*, vol. 89, no. 1-2, pp. 54–60, 2002.

[59] M. R. Chedekel, A. B. Ahene, and L. Zeise, "Melanin standard method: Empirical formula 2," *Pigment Cell Research*, vol. 5, no. 5, pp. 240–246, 1992.

[60] S. Reale, M. Crucianelli, A. Pezzella, M. D'Ischia, and F. De Angelis, "Exploring the frontiers of synthetic eumelanin polymers by high-resolution matrix-assisted laser/desorption ionization mass spectrometry," *Journal of Mass Spectroscopy*, vol. 47, no. 1, pp. 49–53, 2012.

[61] J. Cheng, S. C. Moss, M. Eisner, and P. Zschack, "X-Ray Characterization of Melanins—I," *Pigment Cell Research*, vol. 7, no. 4, pp. 255–262, 1994.

[62] G. Zajac, J. Gallas, J. Cheng, M. Eisner, S. Moss, and A. Alvaradoswaisgood, "The fundamental unit of synthetic melanin: a verification by tunneling microscopy of X-ray scattering results," *Biochimica et Biophysica Acta (BBA) - General Subjects*, vol. 1199, no. 3, pp. 271–278, 1994.

[63] C. M. R. Clancy and J. D. Simon, "Ultrastructural organization of eumelanin from Sepia officinalis measured by atomic force microscopy," *Biochemistry*, vol. 40, no. 44, pp. 13 353–13 360, 2001.

[64] A. A. R. Watt, J. P. Bothma, and P. Meredith, "The supramolecular structure of melanin," *Soft Matter*, vol. 5, no. 19, p. 3754, 2009.

[65] C.-T. Chen, V. Ball, J. J. de Almeida Gracio, M. K. Singh, V. Toniazzo, D. Ruch, and M. J. Buehler, "Self-assembly of tetramers of 5,6-dihydroxyindole explains the primary physical properties of eumelanin: experiment, simulation, and design," *ACS Nano*, vol. 7, no. 2, pp. 1524–1532, 2013.

[66] E. Kaxiras, A. Tsolakidis, G. Zonios, and S. Meng, "Structural model of eumelanin," *Physical Review Letters*, vol. 97, p. 218102, 2006.

[67] N. F. Della Vecchia, R. Avolio, M. Alfè, M. E. Errico, A. Napolitano, and M. D'Ischia, "Building-Block Diversity in Polydopamine Underpins a Multifunctional Eumelanin-Type Platform Tunable Through a Quinone Control Point," *Advanced Functional Materials*, vol. 23, no. 10, pp. 1331–1340, 2013.

[68] A. B. Mostert, K. J. P. Davy, J. L. Ruggles, B. J. Powell, I. R. Gentle, and P. Meredith, "Gaseous adsorption in melanins: hydrophilic biomacromolecules with high electrical conductivities," *Langmuir*, vol. 26, no. 1, pp. 412–416, 2009.

[69] G. Albanese, M. G. Bridelli, and A. Deriu, "Structural dynamics of melanin investigated by Rayleigh scattering of Mössbauer radiation," *Biopolymers*, vol. 23, no. 8, pp. 1481–1498, 1984.

[70] M. G. Bridelli, R. Capeletti, and P. R. Crippa, "Electret state and hydrated structure of melanin," *Journal of Electroanalytical Chemistry*, vol. 128, pp. 555–567, 1981.

[71] M. M. Jastrzebska, H. Isotalo, J. Paloheimo, and H. Stubb, "Electrical conductivity of synthetic DOPA-melanin polymer for different hydration states and temperatures," *Journal of Biomaterials Science, Polymer Edition*, vol. 7, no. 7, pp. 577–586, 1995.

[72] M. G. Bridelli and P. R. Crippa, "Infrared and water sorption studies of the hydration structure and mechanism in natural and synthetic melanin," *Journal of Physical Chemistry B*, vol. 114, pp. 9381–9390, 2010.

[73] M. L. Tran, B. J. Powell, and P. Meredith, "Chemical and structural disorder in eumelanins: A possible explanation for broadband absorbance," *Biophysical Journal*, vol. 90, no. 3, pp. 743–752, 2006.

[74] S. Meng and E. Kaxiras, "Mechanisms for ultrafast nonradiative relaxation in electronically excited eumelanin constituents," *Biophysical Journal*, vol. 95, no. 9, pp. 4396–4402, 2008.

[75] A. Huijser, A. Pezzella, and V. Sundström, "Functionality of epidermal melanin pigments: current knowledge on UV-dissipative mechanisms and research perspectives." *Physical Chemistry Chemical Physics : PCCP*, vol. 13, no. 20, pp. 9119–9127, 2011.

[76] S. Olsen, J. Riesz, I. Mahadevan, A. Coutts, J. P. Bothma, B. J. Powell, R. H. McKenzie, S. C. Smith, and P. Meredith, "Convergent proton-transfer photocycles violate mirror-image symmetry in a key melanin monomer," *Journal of the American Chemical Society*, vol. 129, no. 21, pp. 6672–6673, 2007.

[77] P. Meredith, B. J. Powell, J. Riesz, S. P. Nighswander-Rempel, M. R. Pederson, and E. G. Moore, "Towards structure–property–function relationships for eumelanin," *Soft Matter*, vol. 2, pp. 37–44, 2006.

[78] S. P. Nighswander-Rempel, J. Riesz, J. Gilmore, and P. Meredith, "A quantum yield map for synthetic eumelanin," *The Journal of Chemical Physics*, vol. 123, no. 19, p. 194901, 2005.

[79] S. P. Nighswander-Rempel, I. B. Mahadevan, H. Rubinsztein-Dunlop, and P. Meredith, "Time-resolved and steady-state fluorescence spectroscopy of eumelanin and indolic polymers," *Photochemistry and Photobiology*, vol. 83, no. 6, pp. 1449–1454, 2007.

[80] C. C. Felix, J. S. Hyde, T. Sarna, and R. C. Sealy, "Interactions of melanin with metal ions. Electron spin resonance evidence for chelate complexes of metal ions with free radicals," *Journal of the American Chemical Society*, vol. 100, no. 12, pp. 3922–3926, 1978.

[81] S.-S. Chio, J. S. Hyde, and R. C. Sealy, "Paramagnetism in melanins: pH dependence," *Archives of Biochemistry and Biophysics*, vol. 215, no. 1, pp. 100–106, 1982.

[82] M. Zdybel, E. Chodurek, and B. Pilawa, "EPR studies of DOPA–melanin complexes with Fe(III)," *Applied Magnetic Resonance*, vol. 40, no. 1, pp. 113–123, 2010.

[83] T. Sarna, W. Froncisz, and J. S. Hyde, "Cu$ˆ{2+}$ probe of metal-ion binding sites in melanin using electron paramagnetic resonance spectroscopy," *Archives of Biochemistry and Biophysics*, vol. 202, no. 1, pp. 304–313, 1980.

[84] R. J. Sever, F. W. Cope, and B. D. Polis, "Generation by visible light of labile free radicals in the melanin granules of the eye," *Science*, vol. 137, no. 3524, pp. 128–129, 1962.

[85] A. B. Mostert, G. R. Hanson, T. Sarna, I. R. Gentle, B. J. Powell, and P. Meredith, "Hydration-controlled X-band EPR spectroscopy: a tool for unravelling the complexities of the solid-state free radical in eumelanin," *Journal of Physical Chemistry B*, vol. 117, no. 17, pp. 4965–4972, 2013.

[86] B. Szpoganicz, S. Gidanian, P. Kong, and P. Farmer, "Metal binding by melanins: studies of colloidal dihydroxyindole-melanin, and its complexation by Cu(II) and Zn(II) ions," *Journal of Inorganic Biochemistry*, vol. 89, no. 1-2, pp. 45–53, 2002.

[87] E. Jacobson and J. Hong, "Redox buffering by melanin and Fe(II) in Cryptococcus neoformans," *Journal of Bacteriology*, vol. 179, no. 17, pp. 5340–5346, 1997.

[88] T. Sarna, W. Korytowski, and R. Sealy, "Nitroxides as redox probes of melanins: Dark-induced and photoinduced changes in redox equilibria," *Archives of Biochemistry and Biophysics*, vol. 239, no. 1, pp. 226–233, 1985.

[89] C.-L. Serpentini, D. D. Montauzon, M. Comtat, J. Ginestar, N. Paillous, and P. Sabatier, "First electrochemical investigation of the redox properties of DOPA – melanins by means of a carbon paste electrode," *Electrochimica Acta*, vol. 45, pp. 1663–1668, 2000.

[90] P. Díaz, Y. Gimeno, P. Carro, S. González, P. L. Schilardi, G. Benítez, R. C. Salvarezza, and A. H. Creus, "Electrochemical self-assembly of melanin films on gold," *Langmuir*, vol. 21, no. 13, pp. 5924–5930, 2005.

[91] Y. Liu, L. Hong, V. R. Kempf, K. Wakamatsu, S. Ito, and J. D. Simon, "Ion-exchange and adsorption of Fe(III) by Sepia melanin," *Pigment Cell Research*, vol. 17, no. 3, pp. 262–269, 2004.

[92] L. K. Charkoudian and K. J. Franz, "Fe(III)-coordination properties of neuromelanin components: 5,6-dihydroxyindole and 5,6-dihydroxyindole-2-carboxylic acid," *Inorganic Chemistry*, vol. 45, no. 9, pp. 3657–3664, 2006.

[93] C. C. Felix and R. C. Sealy, "Photolysis of melanin precursors: formation of semiquinone radicals and their complexation with diamagnetic metal ions," *Photochemistry and photobiology*, vol. 34, pp. 423–429, 1981.

[94] L. Hong and J. D. Simon, "Current understanding of the binding sites, capacity, affinity, and biological significance of metals in melanin," *The Journal of Physical Chemistry B*, vol. 111, no. 28, pp. 7938–7947, 2007.

[95] S. Chen, C. Xue, J. Wang, H. Feng, Y. Wang, Q. Ma, and D. Wang, "Adsorption of Pb(II) and Cd(II) by squid ommastrephes bartrami melanin," *Bioinorganic Chemistry and Applications*, vol. 2009, p. 901563, 2009.

[96] K. Sono, D. Lye, C. A. Moore, W. C. Boyd, T. A. Gorlin, and J. M. Belitsky, "Melanin-based coatings as lead-binding agents," *Bioinorganic Chemistry and Applications*, vol. 2012, p. 361803, 2012.

[97] T. Sarna, J. Hyde, and H. Swartz, "Ion-exchange in melanin: an electron spin resonance study with lanthanide probes," *Science*, vol. 192, no. 4244, pp. 1132–1134, 1976.

[98] L. Hong and J. D. Simon, "Insight into the binding of divalent cations to Sepia eumelanin from IR absorption spectroscopy," *Photochemistry and Photobiology*, vol. 82, no. 5, pp. 1265–1269, 2006.

[99] A. Samokhvalov, Y. Liu, and J. D. Simon, "Characterization of the Fe(III)-binding site in Sepia eumelanin by resonance Raman confocal microspectroscopy," *Photochemistry and Photobiology*, vol. 80, pp. 84–88, 2004.

[100] S. Meng and E. Kaxiras, "Theoretical models of eumelanin protomolecules and their optical properties," *Biophysical Journal*, vol. 94, no. 6, pp. 2095–2105, 2008.

[101] M. D'Ischia, A. Napolitano, and A. Pezzella, "5,6-Dihydroxyindole chemistry: Unexplored opportunities beyond eumelanin," *European Journal of Organic Chemistry*, vol. 2011, no. 28, pp. 5501–5516, 2011.

[102] B. Simonovic, V. Vucelic, A. Hadzi-Pavlovic, K. Stepien, T. Wilczok, and D. Vucelic, "Thermogravimetry and differential scanning calorimetry of natural and synthetic melanins," *Journal of Thermal Analysis*, vol. 36, no. 7-8, pp. 2475–2482, 1990.

[103] F. Schreiber, "Organic Molecular Beam Deposition: Growth Studies beyond the First Monolayer," in *Physics of Organic Semiconductors*, W. Brütting, Ed. Wiley-VCH Verlag GmbH & Co. KGaA, 2006, pp. 15–40.

[104] R. Ruiz, D. Choudhary, B. Nickel, T. Toccoli, K.-C. Chang, A. C. Mayer, P. Clancy, J. M. Blakely, R. L. Headrick, S. Iannotta, and G. G. Malliaras, "Pentacene Thin Film Growth," *Chemistry of Materials*, vol. 16, no. 23, pp. 4497–4508, 2004.

[105] G. Witte and C. Woell, "Growth of aromatic molecules on solid substrates for applications in organic electronics," *ChemInform*, vol. 35, no. 51, 2004.

[106] J. H. Kang and X.-Y. Zhu, "Layer-by-layer growth of incommensurate, polycrystalline, lying-down pentacene thin films on Au(111)," *Chemistry of Materials*, vol. 18, no. 5, pp. 1318–1323, 2006.

[107] J. Fraxedas, "Perspectives on thin molecular organic films," *Advanced Materials*, vol. 14, no. 22, pp. 1603–1614, 2002.

[108] Y. Zheng, A. T. Shen Wee, and N. Chandrasekhar, "Structural analysis of pentacene thin film growth on polycrystalline Ox-Au surfaces using scanning tunneling microscopy," *ACS Nano*, vol. 4, no. 4, pp. 2104–2108, 2010.

[109] S. Kowarik, A. Gerlach, and F. Schreiber, "Organic molecular beam deposition: fundamentals, growth dynamics, and in situ studies," *Journal of Physics: Condensed Matter*, vol. 20, no. 18, p. 184005, 2008.

[110] C. Reese, W.-J. Chung, M.-m. Ling, M. Roberts, and Z. Bao, "High-performance microscale single-crystal transistors by lithography on an elastomer dielectric," *Applied Physics Letters*, vol. 89, no. 20, pp. 202 103–202 108, 2006.

[111] J. Peet, M. L. Senatore, A. J. Heeger, and G. C. Bazan, "The role of processing in the fabrication and optimization of plastic solar cells," *Advanced Materials*, vol. 21, no. 14-15, pp. 1521–1527, 2009.

[112] M. Heuken and N. Meyer, "Organic vapor phase deposition," *Organic Electronics: Materials, Manufacturing and Applications*, pp. 203–232, 2006.

[113] F. So, B. Krummacher, M. K. Mathai, D. Poplavskyy, S. A. Choulis, and V.-E. Choong, "Recent progress in solution processable organic light emitting devices," *Journal of Applied Physics*, vol. 102, no. 9, p. 091101, 2007.

[114] S. R. Forrest, "The path to ubiquitous and low-cost organic electronic appliances on plastic," *Nature*, vol. 428, no. 6986, pp. 911–918, 2004.

[115] J. Mei and Z. Bao, "Side chain engineering in solution-processable conjugated polymers," *Chemistry of Materials*, vol. 26, pp. 604–615, 2014.

[116] S. Allard, M. Forster, B. Souharce, H. Thiem, and U. Scherf, "Organic semiconductors for solution-processable field-effect transistors (OFETs)," *Angewandte Chemie (International Edition)*, vol. 47, no. 22, pp. 4070–4098, 2008.

[117] Y. Li, P. Sonar, S. P. Singh, M. S. Soh, M. van Meurs, and J. Tan, "Annealing-free high-mobility diketopyrrolopyrrole-quaterthiophene copolymer for solution-processed organic thin film transistors," *Journal of the American Chemical Society*, vol. 133, no. 7, pp. 2198–2204, 2011.

[118] J. Zhou, X. Wan, Y. Liu, Y. Zuo, Z. Li, G. He, G. Long, W. Ni, C. Li, X. Su, and Y. Chen, "Small molecules based on benzo[1,2-b:4,5-b']dithiophene unit for high-performance solution-processed organic solar cells," *Journal of the American Chemical Society*, vol. 134, no. 39, pp. 16 345–16 351, 2012.

[119] B. Zhang, G. Tan, C.-S. Lam, B. Yao, C.-L. Ho, L. Liu, Z. Xie, W.-Y. Wong, J. Ding, and L. Wang, "High-efficiency single emissive layer white organic light-emitting diodes based on solution-processed dendritic host and new orange-emitting iridium complex," *Advanced Materials*, vol. 24, no. 14, pp. 1873–1877, 2012.

[120] H. Usta, A. Facchetti, and T. J. Marks, "Air-stable, solution-processable n-channel and ambipolar semiconductors for thin-film transistors based on the indenofluorenebis(dicyanovinylene) core," *Journal of the American Chemical Society*, vol. 130, no. 27, pp. 8580–8581, 2008.

[121] Y. Cao, P. Smith, and A. J. Heeger, "Counter-ion induced processibility of conducting polyaniline and of conducting polyblends of polyaniline in bulk polymers," *Synthetic Metals*, vol. 48, no. 1, pp. 91–97, 1992.

[122] L. Groenendaal, F. Jonas, D. Freitag, H. Pielartzik, and J. R. Reynolds, "Poly(3,4-ethylenedioxythiophene) and its derivatives: past, present, and future," *Advanced Materials*, vol. 12, no. 7, pp. 481–494, 2000.

[123] E. D. Głowacki, L. Leonat, G. Voss, M.-A. Bodea, Z. Bozkurt, A. M. Ramil, M. Irimia-Vladu, S. Bauer, and N. S. Sariciftci, "Ambipolar organic field effect transistors and inverters with the natural material Tyrian Purple," *AIP Advances*, vol. 1, no. 4, p. 042132, 2011.

[124] Y. Deng, E. Josberger, J. Jin, A. F. Rousdari, B. Helms, C. Zhong, M. P. Anantram, and M. Rolandi, "H^+-type and OH^- -type biological protonic semiconductors and complementary devices," *Scientific Reports*, vol. 3, p. 2481, 2013.

[125] Y. Okahata and T. Kobayashi, "Anisotropic electric conductivity in an aligned DNA cast film," *Journal of the American Chemical Society*, vol. 120, pp. 6165–6166, 1998.

[126] M. I. N. da Silva, S. N. Deziderio, J. C. Gonzalez, C. F. O. Graeff, and M. A. Cotta, "Synthetic melanin thin films: Structural and electrical properties," *Journal of Applied Physics*, vol. 96, no. 10, p. 5803, 2004.

[127] G. S. Lorite, V. R. Coluci, M. I. N. da Silva, S. N. Deziderio, C. F. O. Graeff, D. S. Galvao, and M. A. Cotta, "Synthetic melanin films: Assembling mechanisms, scaling behavior, and structural properties," *Journal of Applied Physics*, vol. 99, no. 11, pp. 113 511–113 516, 2006.

[128] E. S. Bronze-Uhle, A. Batagin-Neto, P. H. P. Xavier, N. I. Fernandes, E. R. de Azevedo, and C. F. O. Graeff, "Synthesis and characterization of melanin in DMSO," *Journal of Molecular Structure*, vol. 1047, pp. 102–108, 2013.

[129] M. Abbas, M. Ali, S. K. Shah, F. D'Amico, P. Postorino, S. Mangialardo, M. C. Guidi, A. Cricenti, and R. Gunnella, "Control of structural, electronic, and optical properties of eumelanin films by electrospray deposition," *Journal of Physical Chemistry B*, vol. 115, no. 38, pp. 11 199–11 207, 2011.

[130] F. Bloisi, A. Pezzella, M. Barra, F. Chiarella, A. Cassinese, and L. Vicari, "Matrix assisted pulsed laser deposition of melanin thin films," *Journal of Applied Physics*, vol. 110, no. 2, p. 026105, 2011.

[131] F. Bloisi, A. Pezzella, M. Barra, M. Alfè, F. Chiarella, A. Cassinese, and L. Vicari, "Effect of substrate temperature on MAPLE deposition of synthetic eumelanin films," *Applied Physics A*, vol. 105, no. 3, pp. 619–627, 2011.

[132] P. Borghetti, A. Goldoni, C. Castellarin-Cudia, L. Casalis, F. Herberg, L. Floreano, A. Cossaro, A. Verdini, R. Gebauer, P. Ghosh, and L. Sangaletti, "Effects of potassium on the supramolecular structure and electronic properties of eumelanin thin films," *Langmuir*, vol. 26, no. 24, pp. 19 007–19 013, 2010.

[133] S. Subianto, G. Will, and P. Meredith, "Electrochemical synthesis of melanin free-standing films," *Polymer*, vol. 46, no. 25, pp. 11 505–11 509, 2005.

[134] M. Pope and C. E. Swenberg, *Electronic processes in organic crystals and polymers*. Oxford University Press, 1999.

[135] N. Koch, "Electronic structure of interfaces with conjugated organic materials," in *Physics of Organic Semiconductors*. Wiley-VCH Verlag GmbH Co. KGaA, 2012, pp. 35–63.

[136] M. Pfeiffer, "Controlled doping of organic vacuum deposited dye layers: Basics and applications," Ph.D. dissertation, Technische Universität Dresden, 1999.

[137] H. Yersin, "Triplet emitters for OLED applications. Mechanisms of exciton trapping and control of emission properties," in *Transition Metal and Rare Earth Compounds SE - 1*, ser. Topics in Current Chemistry. Springer Berlin Heidelberg, 2004, vol. 241, pp. 1–26.

[138] N. Ueno, "Electronic structure of molecular solids: Bridge to the electrical conduction," in *Physics of Organic Semiconductors*. Wiley-VCH Verlag GmbH & Co. KGaA, 2012, pp. 65–89.

[139] B. D'Andrade, S. Datta, S. Forrest, P. Djurovich, E. Polikarpov, and M. Thompson, "Relationship between the ionization and oxidation potentials of molecular organic semiconductors," *Organic Electronics*, vol. 6, no. 1, pp. 11–20, 2005.

[140] J. Wünsche, "Investigation of triplet-exciton diffusion in organic semiconductors," Diploma thesis, TU Dresden, 2009.

[141] R. A. Marcus, "On the theory of oxidation-reduction reactions involving electron transfer. I," *The Journal of Chemical Physics*, vol. 24, no. 5, p. 966, 1956.

[142] V. Coropceanu, J. Cornil, D. A. da Silva Filho, Y. Olivier, R. Silbey, and J.-L. Brédas, "Charge transport in organic semiconductors," *Chemical Reviews*, vol. 107, no. 4, pp. 926–952, 2007.

[143] A. Salleo, R. J. Kline, D. M. DeLongchamp, and M. L. Chabinyc, "Microstructural characterization and charge transport in thin films of conjugated polymers," *Advanced Materials*, vol. 22, no. 34, pp. 3812–3838, 2010.

[144] G. Horowitz, "Organic field-effect transistors," *Advanced Materials*, vol. 10, no. Compendex, pp. 365–377, 1998.

[145] H. Klauk, "Organic thin-film transistors," *Chemical Society Reviews*, vol. 39, no. 7, pp. 2643–2666, 2010.

[146] H. S. White, G. P. Kittlesen, and M. S. Wrighton, "Chemical derivatization of an array of three gold microelectrodes with polypyrrole: fabrication of a molecule-based transistor," *Journal of the American Chemical Society*, vol. 106, no. 18, pp. 5375–5377, 1984.

[147] N. Koch, "Organic electronic devices and their functional interfaces," *Chemphyschem*, vol. 8, no. 10, pp. 1438–1455, 2007.

[148] C. M. Aguirre, P. L. Levesque, M. Paillet, F. Lapointe, B. C. St-Antoine, P. Desjardins, and R. Martel, "The role of the oxygen/water redox couple in suppressing electron conduction in field-effect transistors," *Advanced Materials*, vol. 21, no. 30, pp. 3087–3091, 2009.

[149] H. T. Nicolai, M. Kuik, G. A. H. Wetzelaer, B. de Boer, C. Campbell, C. Risko, J. L. Brédas, and P. W. M. Blom, "Unification of trap-limited electron transport in semiconducting polymers," *Nature Materials*, vol. 11, no. 10, pp. 882–887, 2012.

[150] T. Steiner, "The hydrogen bond in the solid state," *Angewandte Chemie (International Edition)*, vol. 41, no. 1, pp. 49–76, 2002.

[151] E. D. Głowacki, M. Irimia-Vladu, M. Kaltenbrunner, J. Gsiorowski, M. S. White, U. Monkowius, G. Romanazzi, G. P. Suranna, P. Mastrorilli, T. Sekitani, S. Bauer,

T. Someya, L. Torsi, and N. S. Sariciftci, "Hydrogen-bonded semiconducting pigments for air-stable field-effect transistors," *Advanced Materials*, vol. 25, no. 11, pp. 1563–1569, 2013.

[152] E. D. Głowacki, M. Irimia-Vladu, S. Bauer, and N. S. Sariciftci, "Hydrogen-bonds in molecular solids – from biological systems to organic electronics," *Journal of Materials Chemistry B*, vol. 1, no. 31, pp. 3742–3753, 2013.

[153] M. Gsänger, J. H. Oh, M. Könemann, H. W. Höffken, A.-M. Krause, Z. Bao, and F. Würthner, "A crystal-engineered hydrogen-bonded octachloroperylene diimide with a twisted core: an n-channel organic semiconductor," *Angewandte Chemie (International Edition)*, vol. 122, no. 4, pp. 752–755, 2010.

[154] Q. Tang, Z. Liang, J. Liu, J. Xu, and Q. Miao, "N-heteroquinones: quadruple weak hydrogen bonds and n-channel transistors," *Chemical Communications*, vol. 46, no. 17, pp. 2977–2979, 2010.

[155] Y.-W. Kwon, C. H. Lee, D.-H. Choi, and J.-I. Jin, "Materials science of DNA," *Journal of Materials Chemistry*, vol. 19, no. 10, p. 1353, 2009.

[156] O. Inganäs, "Hybrid electronics and electrochemistry with conjugated polymers," *Chemical Society Reviews*, vol. 39, no. 7, pp. 2633–2642, 2010.

[157] M. Berggren and A. Richter-Dahlfors, "Organic bioelectronics," *Advanced Materials*, vol. 19, no. 20, pp. 3201–3213, 2007.

[158] R. Baughman, "Conducting polymer artificial muscles," *Synthetic Metals*, vol. 78, no. 3, pp. 339–353, 1996.

[159] P. M. Beaujuge and J. R. Reynolds, "Color control in pi-conjugated organic polymers for use in electrochromic devices," *Chemical Reviews*, vol. 110, no. 1, pp. 268–320, 2010.

[160] D. A. Bernards, D. J. Macaya, M. Nikolou, J. A. DeFranco, S. Takamatsu, and G. G. Malliaras, "Enzymatic sensing with organic electrochemical transistors," *Journal of Materials Chemistry*, vol. 18, no. 1, pp. 116–120, 2008.

[161] J. D. Slinker, J. a. DeFranco, M. J. Jaquith, W. R. Silveira, Y.-w. Zhong, J. M. Moran-Mirabal, H. G. Craighead, H. D. Abruña, J. a. Marohn, and G. G. Malliaras, "Direct measurement of the electric-field distribution in a light-emitting electrochemical cell," *Nature Materials*, vol. 6, no. 11, pp. 894–899, 2007.

[162] J. Isaksson, P. Kjäll, D. Nilsson, N. D. Robinson, M. Berggren, and A. Richter-Dahlfors, "Electronic control of Ca^{2+} signalling in neuronal cells using an organic electronic ion pump," *Nature Materials*, vol. 6, no. 9, pp. 673–679, 2007.

[163] E. Stavrinidou, P. Leleux, H. Rajaona, D. Khodagholy, J. Rivnay, M. Lindau, S. Sanaur, and G. G. Malliaras, "Direct measurement of ion mobility in a conducting polymer," *Advanced Materials*, vol. 25, no. 32, pp. 4488–4493, 2013.

[164] R. A. Huggins, "Simple method to determine electronic and ionic components of the conductivity in mixed conductors a review," *Ionics*, vol. 8, no. 3-4, pp. 300–313, 2002.

[165] S. N. Patel, A. E. Javier, G. M. Stone, S. A. Mullin, and N. P. Balsara, "Simultaneous conduction of electronic charge and lithium ions in block copolymers," *ACS Nano*, vol. 6, no. 2, pp. 1589–1600, 2012.

[166] T. Saha and P. Purkait, "Investigation of polarization and depolarization current measurements for the assessment of oil-paper insulation of aged transformers," *IEEE Transactions on Dielectrics and Electrical Insulation*, vol. 11, no. 1, pp. 144–154, 2004.

[167] I. Riess, "Mixed ionic–electronic conductors—material properties and applications," *Solid State Ionics*, vol. 157, pp. 1–17, 2003.

[168] X. Wang, B. Shapiro, and E. Smela, "Visualizing Ion Currents in Conjugated Polymers," *Advanced Materials*, vol. 16, no. 18, pp. 1605–1609, 2004.

[169] P. Mitchell, "Coupling of phosphorylation to electron and hydrogen transfer by a chemi-osmotic type of mechanism," *Nature*, vol. 191, pp. 144–148, 1961.

[170] S. M. E. Smith, D. Morgan, B. Musset, V. V. Cherny, A. R. Place, J. W. Hastings, and T. E. Decoursey, "Voltage-gated proton channel in a dinoflagellate," *Proceedings of the National Academy of Sciences of the United States of America*, vol. 108, no. 44, pp. 18 162–18 167, 2011.

[171] K.-D. Kreuer, S. J. Paddison, E. Spohr, and M. Schuster, "Transport in proton conductors for fuel-cell applications: simulations, elementary reactions, and phenomenology," *Chemical Reviews*, vol. 104, no. 10, pp. 4637–4678, 2004.

[172] K.-D. Kreuer, "Proton conductivity : materials and applications," *Chemistry of Materials*, vol. 8, pp. 610–641, 1996.

[173] V. K. Shante and S. Kirkpatrick, "An introduction to percolation theory," *Advances in Physics*, vol. 20, no. 85, pp. 325–357, 1971.

[174] G. Careri, A. Giansanti, and J. A. Rupley, "Proton percolation on hydrated lysozyme powders," *Proceedings of the National Academy of Sciences*, vol. 83, no. 18, pp. 6810–6814, 1986.

[175] K.-D. Kreuer and G. Portale, "A critical revision of the nano-morphology of proton conducting ionomers and polyelectrolytes for fuel cell applications," *Advanced Functional Materials*, vol. 23, no. 43, pp. 5390–5397, 2013.

[176] L. Glasser, "Proton conduction and injection in solids," *Chemical Reviews*, vol. 75, no. 1, pp. 21–65, 1975.

[177] M. Eigen and L. de Maeyer, "Self-Dissociation and Protonic Charge Transport in Water and Ice," *Proceedings of the Royal Society A: Mathematical, Physical and Engineering Sciences*, vol. 247, no. 1251, pp. 505–533, 1958.

[178] H. Morgan, R. Pethig, and G. T. Stevens, "A proton-injecting technique for the measurement of hydration-dependent protonic conductivity," *Journal of Physics E: Scientific Instruments*, vol. 19, no. 1, pp. 80–82, 1986.

[179] B. Rosenberg and E. Postow, "Semiconduction in proteins and lipids – its possible biological importance," *Annals of the New York Academy of Sciences*, vol. 158, pp. 161–190, 1969.

[180] B. Rosenberg, "Electrical conductivity of proteins," *Nature*, vol. 193, no. 4813, pp. 364–365, 1962.

[181] P. R. Gascoyne, R. Pethig, and A. Szent-Györgyi, "Water structure-dependent charge transport in proteins," *Proceedings of the National Academy of Sciences of the United States of America*, vol. 78, no. 1, pp. 261–265, 1981.

[182] N. Mott, "Electrons in disordered structures," *Advances in Physics*, vol. 16, no. 61, pp. 49–144, 1967.

[183] T. Strzelecka, "A band model for synthetic dopa-melanin," *Physiological Chemistry and Physics*, vol. 14, no. 3, pp. 219–222, 1982.

[184] M. M. Jastrzebska and T. Wilczok, "Thermoelectric effect in synthetic dopa-melanin," *Studia Biophysica*, vol. 132, pp. 39–46, 1987.

[185] M. M. Jastrzebska and S. Jussila, "Dielectric response and A.C. conductivity of synthetic dopa-melanin polymer," *Journal of Materials Science*, vol. 33, no. 16, pp. 4023–4028, 1998.

[186] M. Jastrzebska, A. Kocot, J. K. Vij, J. Zalewska-Rejdak, and T. Witecki, "Dielectric studies on charge hopping in melanin polymer," *Journal of Molecular Structure*, vol. 606, no. 1-3, pp. 205–210, 2002.

[187] A. Mostert, B. J. Powell, I. R. Gentle, and P. Meredith, "On the origin of electrical conductivity in the bio-electronic material melanin," *Applied Physics Letters*, vol. 100, no. 9, p. 093701, 2012.

[188] M. Ambrico, P. F. Ambrico, T. Ligonzo, A. Cardone, S. R. Cicco, A. Lavizzera, V. Augelli, and G. M. Farinola, "Memory-like behavior as a feature of electrical signal transmission in melanin-like bio-polymers," *Applied Physics Letters*, vol. 100, no. 25, p. 253702, 2012.

[189] M. Ambrico, P. F. Ambrico, A. Cardone, S. R. Cicco, F. Palumbo, T. Ligonzo, R. Di Mundo, V. Petta, V. Augelli, P. Favia, and G. M. Farinola, "Melanin-like polymer layered on a nanotextured silicon surface for a hybrid biomimetic interface," *Journal of Materials Chemistry C*, vol. 2, no. 3, pp. 573–582, 2014.

[190] C. M. R. Clancy, J. B. Nofsinger, R. K. Hanks, and J. D. Simon, "A hierarchical self-assembly of eumelanin," *Journal of Physical Chemistry B*, vol. 104, no. 33, pp. 7871–7873, 2000.

[191] T. Sarna, "Interaction of radicals from water radiolysis with melanin," *Biochimica et Biophysica Acta*, vol. 883, no. 1, pp. 162–167, 1986.

[192] H. Lee, J. Rho, and P. B. Messersmith, "Facile conjugation of biomolecules onto surfaces via mussel adhesive protein inspired coatings," *Advanced Materials*, vol. 21, no. 4, pp. 431–434, 2009.

[193] F. Bernsmann, J.-C. Voegel, and V. Ball, "Different synthesis methods allow to tune the permeability and permselectivity of dopamine–melanin films to electrochemical probes," *Electrochimica Acta*, vol. 56, no. 11, pp. 3914–3919, 2011.

[194] A. González Orive, D. Grumelli, C. Vericat, J. M. Ramallo-López, L. Giovanetti, G. Benitez, J. C. Azcárate, G. Corthey, M. H. Fonticelli, F. G. Requejo, A. Hernández Creus, R. C. Salvarezza, and A. G. Orive, ""Naked" gold nanoparticles supported on HOPG: melanin functionalization and catalytic activity." *Nanoscale*, vol. 3, no. 4, pp. 1708–1716, 2011.

[195] F. Li, L. Yang, C. Zhao, and Z. Du, "Electroactive gold nanoparticles/polyaniline/polydopamine hybrid composite in neutral solution as high-performance sensing platform," *Analytical Methods*, vol. 3, no. 7, p. 1601, 2011.

[196] G. S. Huang, M.-T. Wang, C.-W. Su, Y.-S. Chen, and M.-Y. Hong, "Picogram detection of metal ions by melanin-sensitized piezoelectric sensor," *Biosensors and Bioelectronics*, vol. 23, no. 3, pp. 319–325, 2007.

[197] R. Waser, R. Dittmann, G. Staikov, and K. Szot, "Redox-based resistive switching memories - nanoionic mechanisms, prospects, and challenges," *Advanced Materials*, vol. 21, no. 25-26, pp. 2632–2663, 2009.

[198] T. A. Witten, "Diffusion-Limited Aggregation, a kinetic critical phenomenon," *Physical Review Letters*, vol. 47, no. 19, p. 1400, 1981.

[199] J. M. Gallas and M. Eisner, "Fluorescence of melanin-dependence upon excitation wavelength and concentration," *Photochemistry and Photobiology*, vol. 45, no. 5, pp. 595–600, 1987.

[200] C. V. Durgadas, C. P. Sharma, and K. Sreenivasan, "Fluorescent gold clusters as nanosensors for copper ions in live cells," *Analyst*, vol. 136, no. 5, pp. 933–940, 2011.

[201] W. Lu, W.-M. Kwok, C. Ma, C. T.-L. Chan, M.-X. Zhu, and C.-M. Che, "Organic triplet excited states of gold(I) complexes with oligo(o- or m-phenyleneethynylene) ligands: conjunction of steady-state and time-resolved spectroscopic studies on exciton delocalization and emission pathways," *Journal of the American Chemical Society*, vol. 133, no. 35, pp. 14 120–14 135, 2011.

[202] C.-A. J. Lin, T.-Y. Yang, C.-H. Lee, S. H. Huang, R. A. Sperling, M. Zanella, J. K. Li, J.-L. Shen, H.-H. Wang, H.-i. Yeh, W. J. Parak, and W. H. Chang, "Bioconjugation of fluorescent gold nanoclusters toward biological labeling applications," *ACS Nano*, vol. 3, no. 2, pp. 395–401, 2009.

[203] N. Agraït, A. L. Yeyati, and J. M. van Ruitenbeek, "Quantum properties of atomic-sized conductors," *Physics Reports*, vol. 377, no. 2-3, pp. 81–279, 2003.

[204] S. Csonka, A. Halbritter, G. Mihály, E. Jurdik, O. Shklyarevskii, S. Speller, and H. van Kempen, "Fractional Conductance in Hydrogen-Embedded Gold Nanowires," *Physical Review Letters*, vol. 90, no. 11, pp. 4–7, 2003.

[205] R. Edge, M. D'Ischia, E. J. Land, A. Napolitano, S. Navaratnam, L. Panzella, A. Pezzella, C. A. Ramsden, and P. A. Riley, "Dopaquinone redox exchange with dihydroxyindole and dihydroxyindole carboxylic acid," *Pigment Cell Research*, vol. 19, no. 5, pp. 443–450, 2006.

[206] R. P. Frankenthal, "The anodic corrosion of gold in concentrated chloride solutions," *Journal of The Electrochemical Society*, vol. 129, no. 6, p. 1192, 1982.

[207] R. Kissner, "Halide catalysis of the electrochemical oxidation of gold in acetonitrile," *Journal of Electroanalytical Chemistry*, vol. 385, pp. 71–75, 1995.

[208] C.-C. Yu, Y.-C. Liu, K.-H. Yang, C.-C. Li, and C.-C. Wang, "A new and clean method on synthesis of gold nanoparticles from bulk gold substrates," *Materials Chemistry and Physics*, vol. 125, no. 1-2, pp. 109–112, 2011.

[209] J. Stainsack, A. S. Mangrich, C. M. Maia, V. G. Machado, J. C. dos Santos, and S. Nakagaki, "Spectroscopic investigation of hard and soft metal binding sites in synthetic melanin," *Inorganica Chimica Acta*, vol. 356, pp. 243–248, 2003.

[210] W.-G. Qu, S.-M. Wang, Z.-J. Hu, T.-Y. Cheang, Z.-H. Xing, X.-J. Zhang, and A.-W. Xu, "In situ synthesis of gold @ 3,4-dihydroxy-L-phenylalanine core-shell nanospheres used for cell imaging," *Journal of Physical Chemistry C*, vol. 114, pp. 13 010–13 016, 2010.

[211] B. Fei, B. Qian, Z. Yang, R. Wang, W. Liu, C. Mak, and J. H. Xin, "Coating carbon nanotubes by spontaneous oxidative polymerization of dopamine," *Carbon*, vol. 46, no. 13, pp. 1795–1797, 2008.

[212] G. Tourillon and F. Garnier, "New electrochemically generated organic conducting polymers," *Journal of Electroanalytical Chemistry and Interfacial Electrochemistry*, vol. 135, no. 1, pp. 173–178, 1982.

[213] B. B. Berkes and G. Inzelt, "Electrochemical nanogravimetric studies on the electropolymerization of indole and on polyindole," *Electrochimica Acta*, vol. 122, pp. 11–15, 2014.

[214] M. Arzillo, G. Mangiapia, A. Pezzella, R. K. Heenan, A. Radulescu, L. Paduano, and M. D'Ischia, "Eumelanin buildup on the nanoscale: aggregate growth/assembly and visible absorption development in biomimetic 5,6-dihydroxyindole polymerization," *Biomacromolecules*, vol. 13, no. 8, pp. 2379–2390, 2012.

[215] J. Wünsche, F. Cicoira, C. F. O. Graeff, and C. Santato, "Eumelanin thin films: solution-processing, growth, and charge transport properties," *Journal of Materials Chemistry B*, vol. 1, pp. 3836–3842, 2013.

[216] J. Wünsche, L. Cardenas, F. Rosei, F. Cicoira, R. Gauvin, C. F. O. Graeff, S. Poulin, A. Pezzella, and C. Santato, "In situ formation of dendrites in eumelanin thin films between gold electrodes," *Advanced Functional Materials*, vol. 23, no. 45, pp. 5591–5598, 2013.

[217] I. D. Raistrick, D. R. Franceschetti, and J. R. Macdonald, "Theory," in *Impedance spectroscopy: theory , experiment, and applications*, 2nd ed., E. Barsoukov and J. R. Macdonald, Eds. Hoboken, New Jersey: John Wiley & Sons, Inc., 2005.

[218] T. Pajkossy and D. Kolb, "Double layer capacitance of Pt(111) single crystal electrodes," *Electrochimica Acta*, vol. 46, no. 20-21, pp. 3063–3071, 2001.

[219] G. Tarabella, A. Pezzella, A. Romeo, P. D'Angelo, N. Coppedè, M. Calicchio, M. D'Ischia, R. Mosca, and S. Iannotta, "Irreversible evolution of eumelanin redox states detected by an organic electrochemical transistor: en route to bioelectronics and biosensing," *Journal of Materials Chemistry B*, vol. 1, no. 31, pp. 3843–3849, 2013.

[220] A. Pezzella, M. D'Ischia, A. Napolitano, A. Palumbo, and G. Prota, "An integrated approach to the structure of Sepia melanin. Evidence for a high proportion of degraded 5,6-dihydroxyindole-2-carboxylic acid units in the pigment backbone," *Tetrahedron*, vol. 53, no. 24, pp. 8281–8286, 1997.

[221] A. Napolitano, A. Pezzella, M. D'Ischia, and G. Prota, "New pyrrole acids by oxidative degradation of eumelanins with hydrogen peroxide. Further hints to the mechanism of pigment breakdown," *Tetrahedron*, vol. 52, no. 26, pp. 8775–8780, 1996.

[222] A. Pezzella, O. Crescenzi, L. Panzella, A. Napolitano, E. J. Land, V. Barone, and M. D'Ischia, "Free radical coupling of o-semiquinones uncovered," *Journal of the American Chemical Society*, vol. 135, no. 32, pp. 12 142–12 149, 2013.

[223] L. Panzella, G. Gentile, G. D'Errico, N. F. Della Vecchia, M. E. Errico, A. Napolitano, C. Carfagna, and M. D'Ischia, "Atypical structural and π-electron features of a melanin polymer that lead to superior free-radical-scavenging properties," *Angewandte Chemie (International Edition)*, vol. 125, no. 48, pp. 12 916–12 919, 2013.

[224] I. Valitova, M. Amato, F. Mahvash, G. Cantele, A. Maffucci, C. Santato, R. Martel, and F. Cicoira, "Carbon nanotube electrodes in organic transistors," *Nanoscale*, vol. 5, no. 11, pp. 4638–4646, 2013.

[225] A. Pezzella, M. Barra, P. Manini, S. Parisi, A. Navarra, A. Cassinese, and M. A. D'Ischia, "Water-switchable stem cell-compatible eumelanin biointerface by chemically-controlled solid state polymerization," *Angewandte Chemie (International Edition)*, p. submitted.

[226] F. Bernsmann, A. Ponche, C. Ringwald, J. Hemmerle, J. Raya, B. Bechinger, J. C. Voegel, P. Schaaf, and V. Ball, "Characterization of dopamine-melanin growth on silicon oxide," *Journal of Physical Chemistry C*, vol. 113, no. 19, pp. 8234–8242, 2009.

[227] S. Olthof, S. Mehraeen, S. K. Mohapatra, S. Barlow, V. Coropceanu, J.-L. Brédas, S. R. Marder, and A. Kahn, "Ultralow doping in organic semiconductors: evidence of trap filling," *Physical Review Letters*, vol. 109, no. 17, p. 176601, 2012.

[228] Y. Takahashi, Y. Nakagawa, K. Hayakawa, T. Inabe, and T. Naito, "Carrier doping to the organic Mott insulator by conjugating with tetrathiafulvalene," *Applied Physics Letters*, vol. 101, no. 10, p. 103303, 2012.

[229] J. Lu, S. Nagase, D. Yu, H. Ye, R. Han, Z. Gao, S. Zhang, and L. Peng, "Amphoteric and controllable doping of carbon nanotubes by encapsulation of organic and organometallic molecules," *Physical Review Letters*, vol. 93, no. 11, p. 116804, 2004.

[230] F. Lapointe, E. Gaufrès, I. Tremblay, N. Y.-W. Tang, R. Martel, and P. Desjardins, "Fano resonances in the midinfrared spectra of single-walled carbon nanotubes," *Physical Review Letters*, vol. 109, no. 9, p. 097402, 2012.

[231] A. Brown, C. Jarrett, D. de Leeuw, and M. Matters, "Field-effect transistors made from solution-processed organic semiconductors," *Synthetic Metals*, vol. 88, no. 1, pp. 37–55, 1997.

[232] M. Pfeiffer, K. Leo, X. Zhou, J. Huang, M. Hofmann, A. Werner, and J. Blochwitz-Nimoth, "Doped organic semiconductors: Physics and application in light emitting diodes," *Organic Electronics*, vol. 4, no. 2-3, pp. 89–103, 2003.

[233] J. Casado, H. Katz, V. Hernandez, and J. Lopez Navarrete, "Infrared spectra of two sexithiophenes in neutral and doped states: a theoretical and spectroscopic study," *Vibrational Spectroscopy*, vol. 30, pp. 175–189, 2002.

[234] S. A. Centeno and J. Shamir, "Surface enhanced Raman scattering (SERS) and FTIR characterization of the sepia melanin pigment used in works of art," *Journal of Molecular Structure*, vol. 873, no. 1-3, pp. 149–159, 2008.

[235] M. G. Bridelli, D. Tampellini, and L. Zecca, "The structure of neuromelanin and its iron binding site studied by infrared spectroscopy," *FEBS letters*, vol. 457, no. 1, pp. 18–22, 1999.

[236] A. Pezzella, L. Capelli, A. Costantini, G. Luciani, F. Tescione, B. Silvestri, G. Vitiello, and F. Branda, "Towards the development of a novel bioinspired functional material: synthesis and characterization of hybrid TiO_2/DHICA-melanin nanoparticles," *Materials Science and Engineering: C*, vol. 33, no. 1, pp. 347–355, 2013.

[237] S. H. Kim, K. Hong, W. Xie, K. H. Lee, S. Zhang, T. P. Lodge, and C. D. Frisbie, "Electrolyte-gated transistors for organic and printed electronics," *Advanced Materials*, vol. 25, no. 13, pp. 1822–1846, 2013.

[238] T. Fujimoto and K. Awaga, "Electric-double-layer field-effect transistors with ionic liquids," *Physical Chemistry Chemical Physics : PCCP*, vol. 15, no. 23, pp. 8983–9006, 2013.

[239] J. Sayago, F. Soavi, Y. Sivalingam, F. Cicoira, and C. Santato, "Low voltage electrolyte-gated polymer transistors making use of high surface area activated carbon gate electrodes," *Journal of Materials Chemistry C*, vol. 2, no. 28, pp. 5690–5694, 2014.

[240] G. Gu and M. G. Kane, "Moisture induced electron traps and hysteresis in pentacene-based organic thin-film transistors," *Applied Physics Letters*, vol. 92, no. 5, pp. 53 303–53 305, 2008.

[241] W. Osak, K. Tkacz-Śmiech, M. Elbanowski, and J. Sławiński, "Dielectric and electric properties of synthetic melanin: the effect of europium ions," *Journal of Biological Physics*, vol. 21, no. 1, pp. 51–65, 1995.

[242] J. Rivnay, L. H. Jimison, J. E. Northrup, M. F. Toney, R. Noriega, S. Lu, T. J. Marks, A. Facchetti, and A. Salleo, "Large modulation of carrier transport by grain-boundary molecular packing and microstructure in organic thin films," *Nature Materials*, vol. 8, no. 12, pp. 952 – 958, 2009.

A - Supporting Information for Article 1

Supporting Information

Eumelanin thin films: solution-processing, growth, and charge transport properties

Julia Wünsche, Fabio Cicoira, Carlos F. O. Graeff, and Clara Santato

J. Mater. Chem. B, vol. 1, pp. 3836–3842, 2013

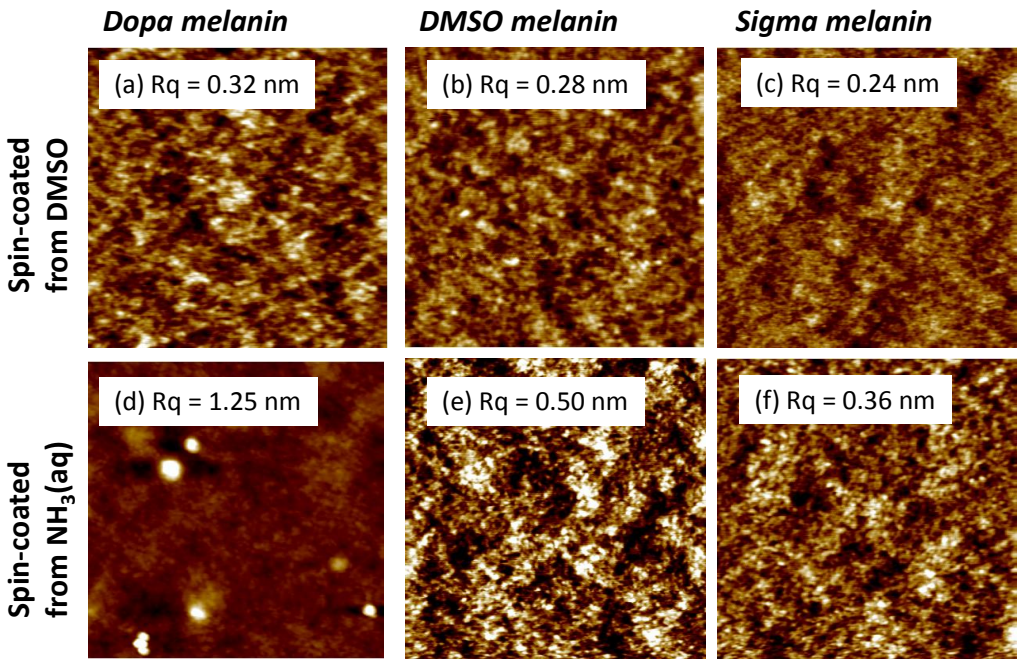

Fig S1 1 μm ×1 μm AFM images of 30 nm thick films of different eumelanins spin-coated from DMSO and $NH_{3(aq)}$ suspensions as indicated. Z-scale 2 nm ((a-c), (e-f)) and 11.5 nm (d). The root mean square roughness Rq is indicated for each film.

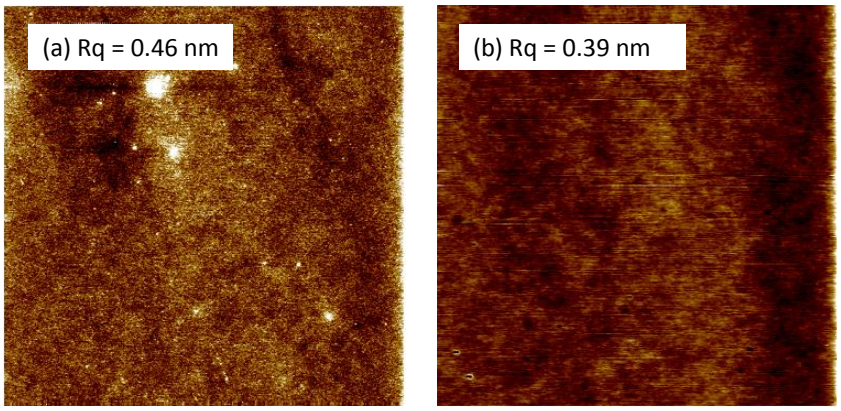

Fig. S2 10 μm ×10 μm AFM images of drop cast films of (a) *DMSO melanin* on glass and (b) *Sigma melanin* on Si. In both cases, a DMSO suspension of 3mg/ml concentration was used. Z-scale: 3 nm. The root mean square roughness Rq is indicated for each film.

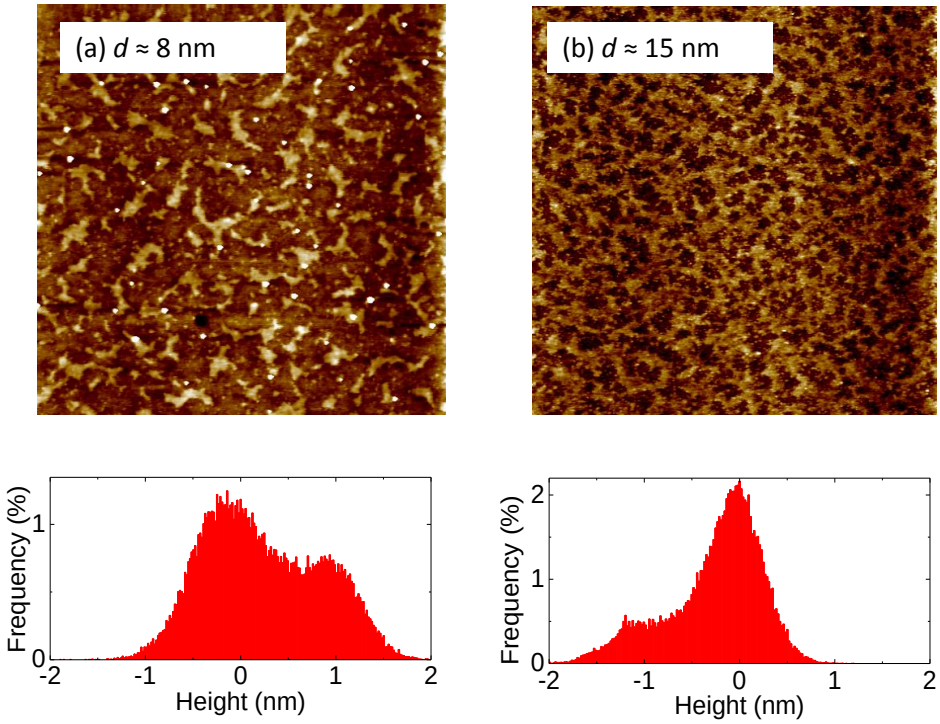

Fig. S3 10 µm ×10 µm AFM images of *DMSO melanin* films of about 8 and 15 nm thickness, spin-coated from DMSO suspension (top) and the corresponding height histograms (bottom). Z-scale: 4 nm. The morphology is dominated by planar islands, about 1 nm high.

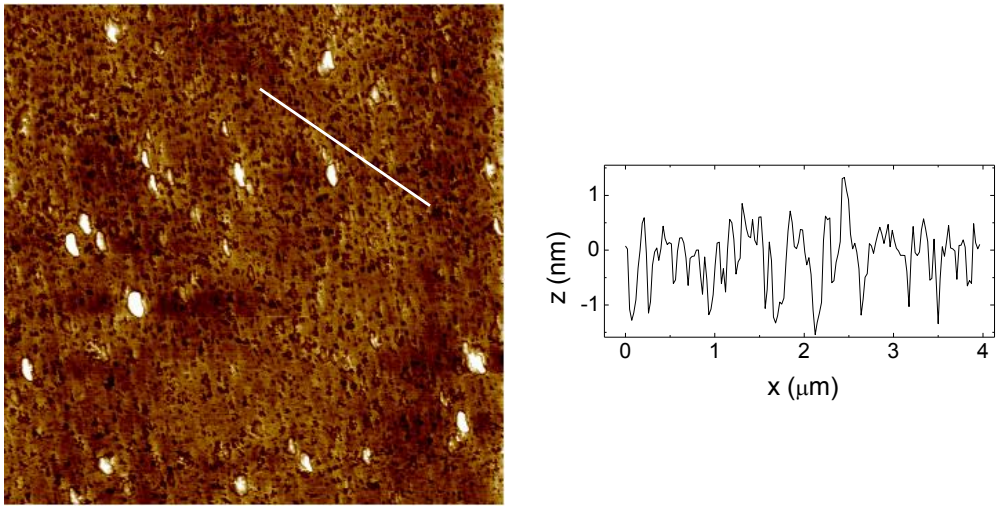

Fig. S4 10 µm ×10 µm AFM image of a *Dopa melanin* drop cast from DMSO suspension (3 mg/ml) on SiO_2 and height profile corresponding to the white line. Z-scale: 5 nm. The surface of the film is covered with holes, about 1.5 nm deep.

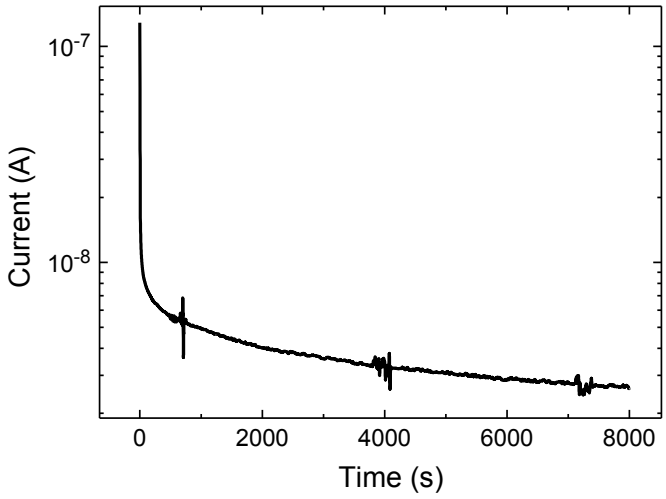

Fig. S5 Transient current measurement on a *Sigma melanin* film, about 30 nm thick, at 90% RH and an electrical bias of 0.6 V. L = 10 μm and W = 7810 μm. The current decreases more and more slowly without reaching a steady state.

B - Supporting Information for Article 2

Supporting Information

In situ formation of dendrites in eumelanin thin films between gold electrodes

Julia Wünsche, Luis Cardenas, Federico Rosei, Fabio Cicoira, Reynald Gauvin, Carlos F.O. Graeff, Suzie Poulin, Alessandro Pezzella, and Clara Santato

Adv. Funct. Mater., vol. 23, no. 45, pp. 5591–5598, 2013

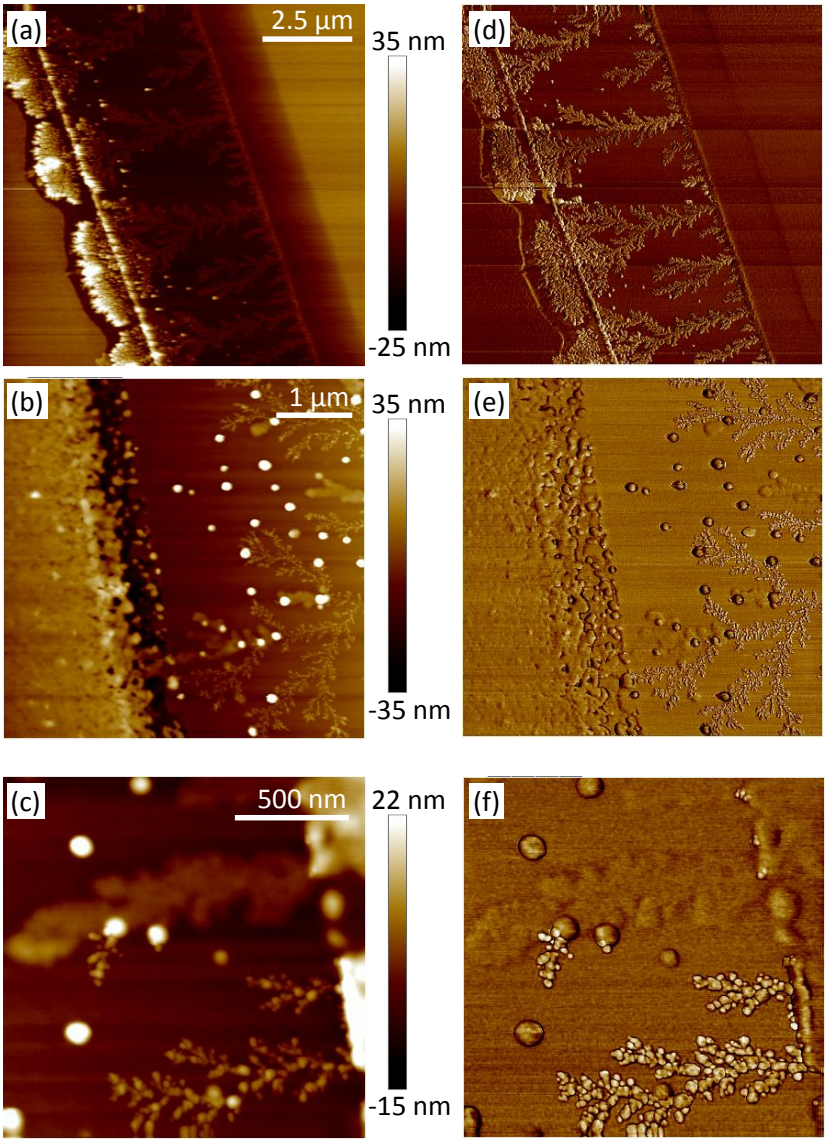

Figure S1. AFM images of the dendrite growth on eumelanin films between Au electrodes. (a)-(c) Height images, (d)-(f) corresponding phase images. (a) and (d) show how the dendrites continue to grow under consumption of Au at the positive (left) electrode once they crossed the entire interelectrode region. Due to the larger amount of Au available, the dendrites easily grow much higher than in the interelectrode region. In (b) and (e), the decomposition of the material at the positive electrode edge into nanoaggregates can be seen. (c) and (f) show how differently dendrites can appear in AFM images. The dendrite at the bottom of the image has thin brunches composed of small nanoaggregates. The brunch-like structure above has a much broader, more compact structure, is generally lower and it shows almost no contrast in the phase image. Possibly, the nanoaggregates merge or sink into the eumelanin film.

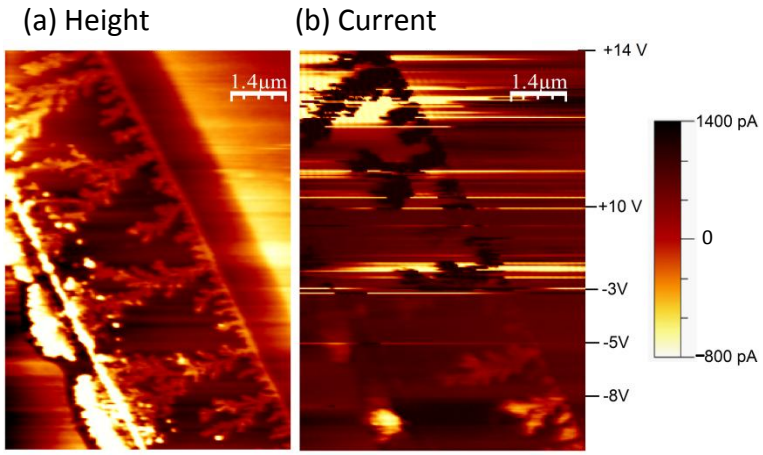

Figure S2: Conductive AFM height (a) and current (b) image of the dendrite structures on a eumelanin film between Au electrodes. The voltage applied to the AFM tip was varied during the scan to demonstrate the voltage dependence.

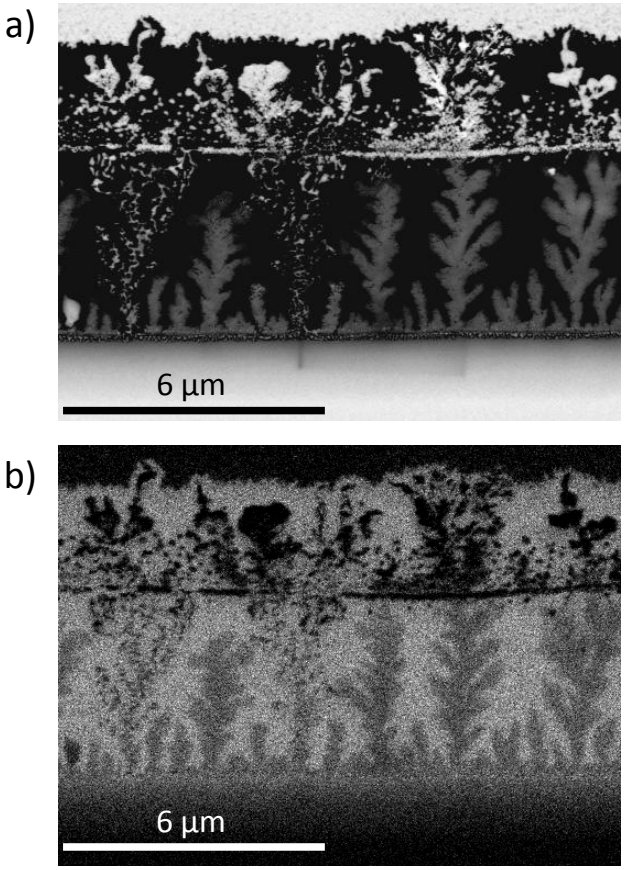

Figure S3. SEM image in back-scattered electron mode (a) and Si mapping (b) of the nanostructures grown between Au electrodes. The region shown is identical to the region of the Au mapping in Fig. 4 (d). (a) shows the same contrast as the Au mapping, while the contrast of the Si mapping is inversed since the Au structures block the electron beam from the SiO_2 substrate.

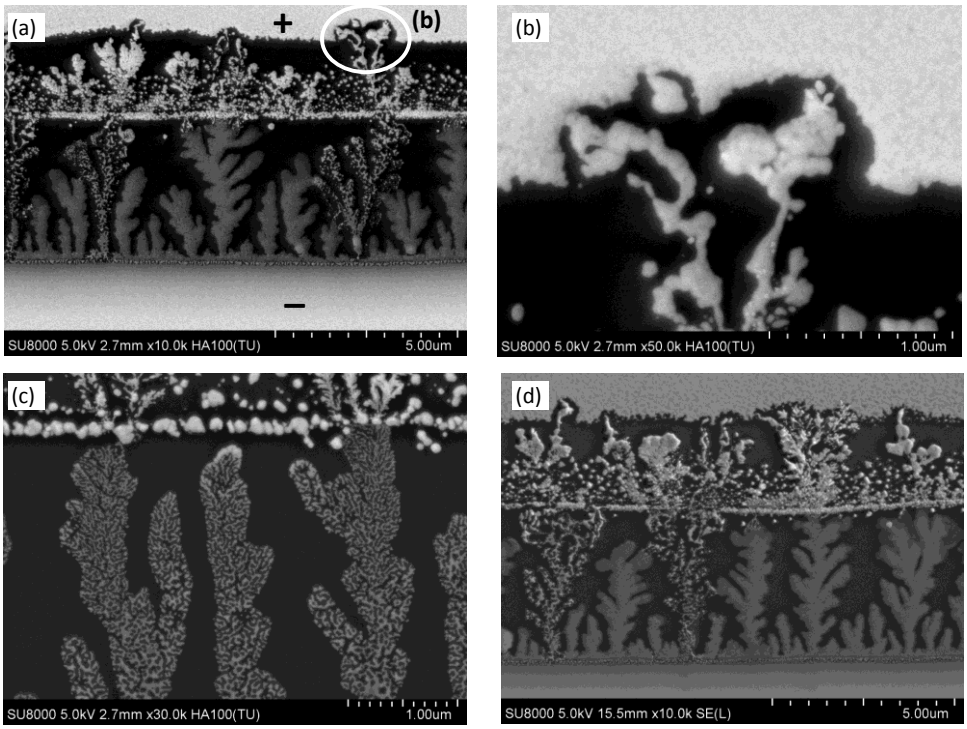

Figure S4. SEM images in backscattered electron mode ((a)-(c)) and secondary electron mode (d) of the Au dendrites between the electrodes. The contrast in images (a)-(c) is caused by sample composition mostly, while (d) contains topographical information. (b) shows the delicate connection of the dendrites to the positive electrode. (d) reveals that the dendrites are higher and have more 3-dimensional morphology beyond the positive electrode edge.

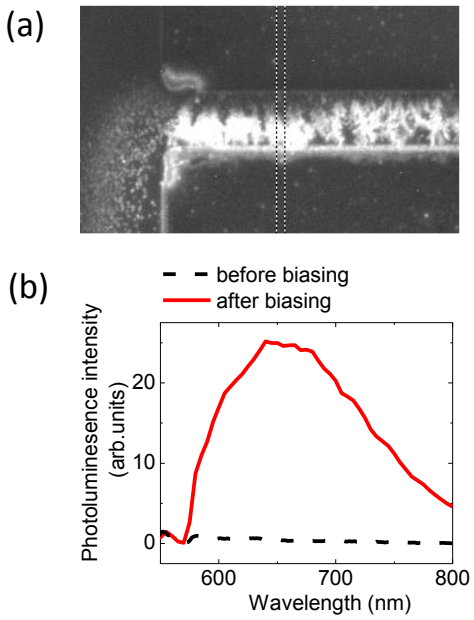

Figure S5. (a) Fluorescence microscopy images of the nanostructures grown on a eumelanin film between Au electrodes taken with (550±10) nm excitation light from a short arc lamp. (b) Fluorescence spectra of the interelectrode region before and after electrical biasing.

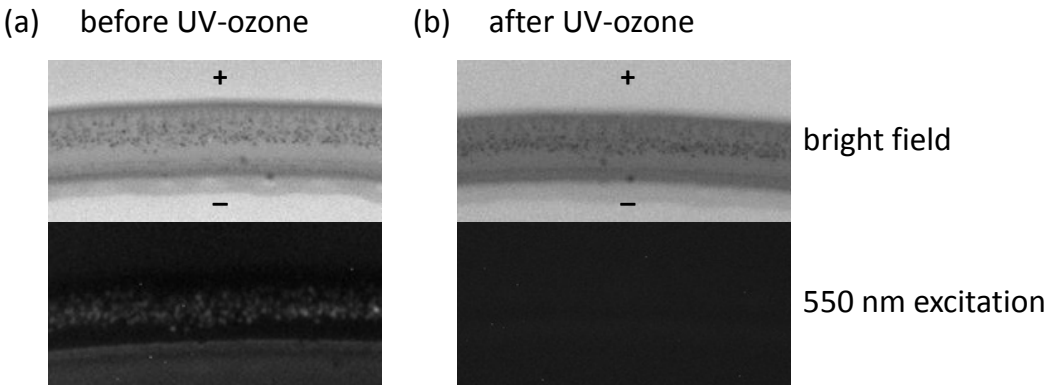

Figure S6. (a) Fluorescence microscopy images of the interelectrode region of eumelanin film after biasing in bright field and with (550±10) nm excitation light from a short arc lamp. (b) Corresponding images after removal of eumelanin by 1 h UV-ozone treatment.

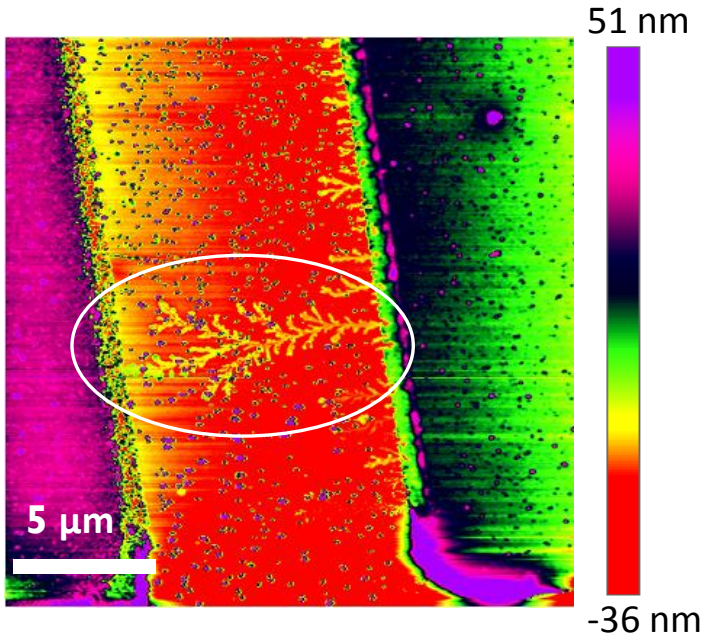

Figure S7. AFM image of a eumelanin film between Au electrodes (L=10 µm, W=200 µm) biased at 1 V for 1.2 h. The electrical measurement was stopped when the sample switched to the highly conductive state. Exactly one dendrite crossing the interelectrode region could be found. The color scale of the AFM image was changed to improve the visibility of the dendrite.

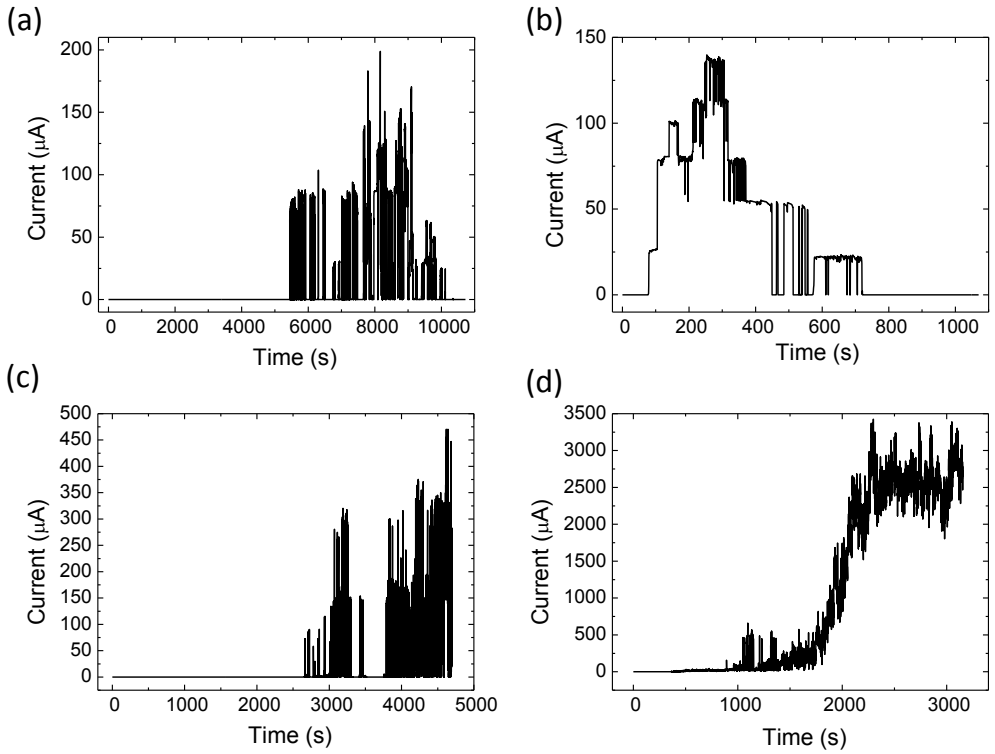

Figure S8. Different current transients for eumelanin films on Au electrodes (L= 6 μm, W= 4 mm) at V=1 V. (a), (c), (d) are the *I-t* curves for the first biasing for three different samples with the same geometry. The time to the first increase of current, the height and shape of the current steps varies. (b) A second measurement on sample (a).

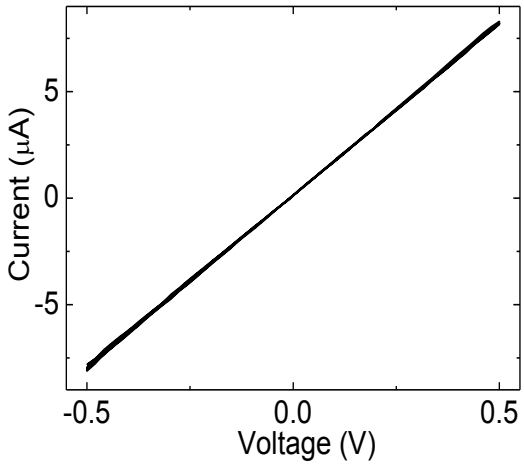

Figure S9. Current-voltage measurement for a eumelanin film between Au electrodes with dendrites in the highly conductive state. The voltage was cycled from -0.5 V to 0.5 V. The current-voltage dependency is highly linear and independent of the sweeping rate between 0.02 V s^{-1} and 2 V s^{-1}.

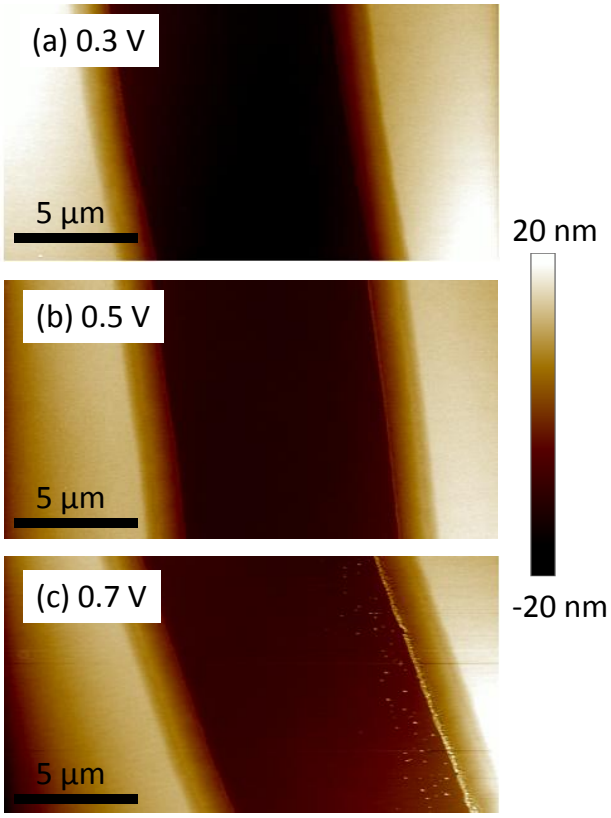

Figure S10. AFM images of eumelanin films between Au electrodes (L=10 µm) biased at 0.3 V (a), 0.5 V (b), and 0.7 V (c). The duration of biasing was 5.5 h for (a) and (c), and 1.7 h for (b). Only at 0.7 V NA formation can be observed.

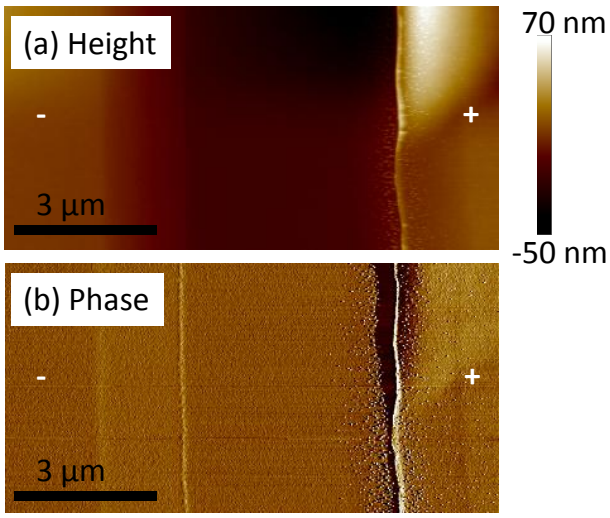

Figure S11. AFM height and phase image of a eumelanin film on Au electrodes (L=6 µm), deposited from DMSO suspension, heated at 125°C for 46 h and biased at 1 V for 20 h. NAs form close to the edge of the positively biased electrode but no dendrite formation is observed.

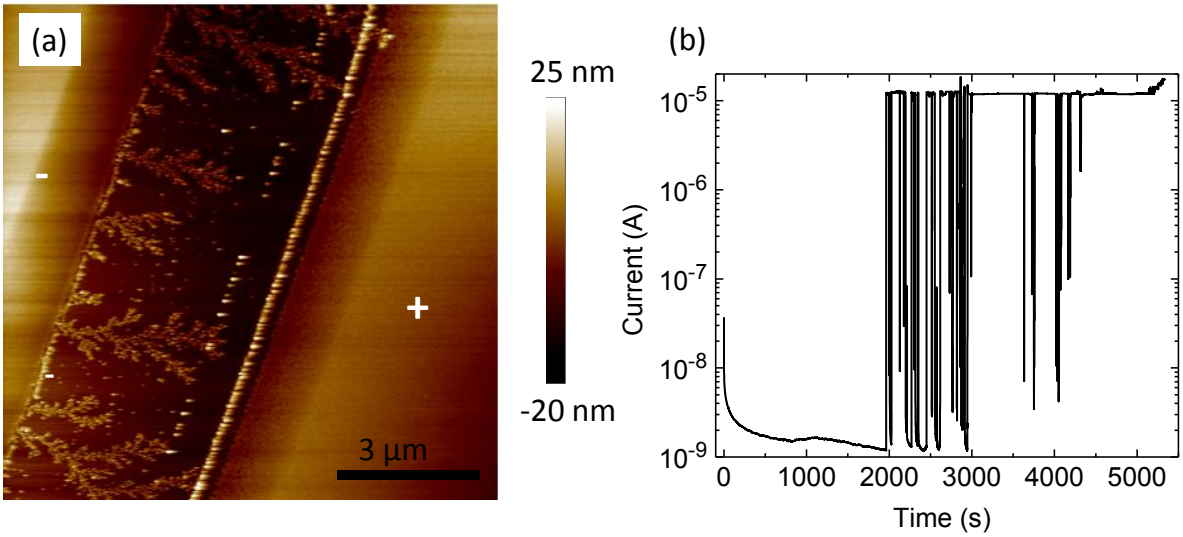

Figure S12. AFM image (a) and current transient (b) for a eumelanin film between Au electrodes (L=6 µm) deposited from DMF and biased at 1 V. Dendrite growth and the resistive change similar to eumelanin films deposited from DMSO were observed.

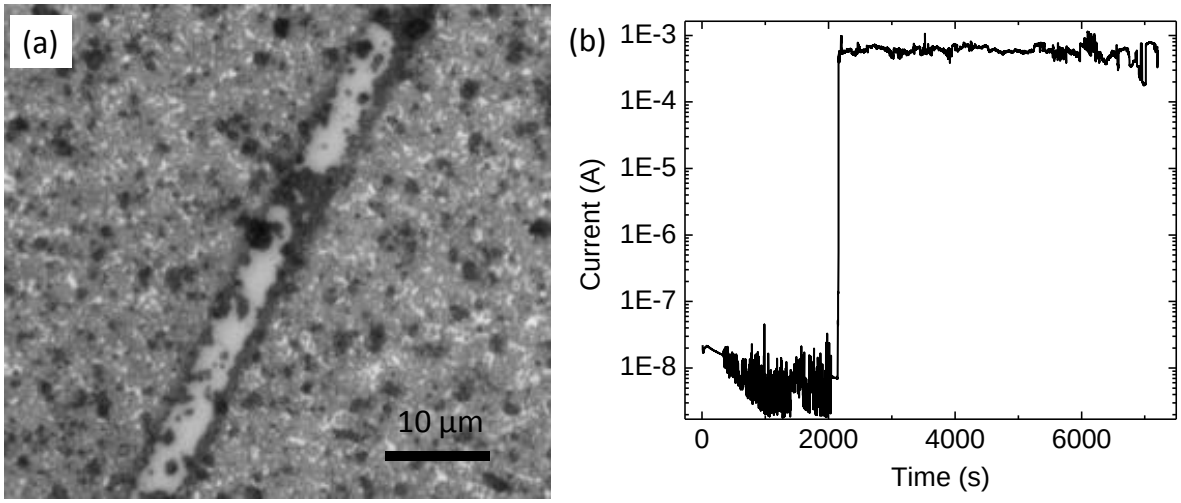

Figure S13. Optical microscopy image (a) for a film of *Sepia melanin* after 2 h of biasing (L=6 µm) at 1 V and corresponding current transient measurement (b). Sepia melanin films were composed of large particles and covered only partly the interelectrode region, which made the localization and imaging of dendrites difficult. However, the sudden increase in current clearly indicates bridging of the interelectrode region by Au-eumelanin nanostructures. The instabilities in the current are likely related to the bad film quality.

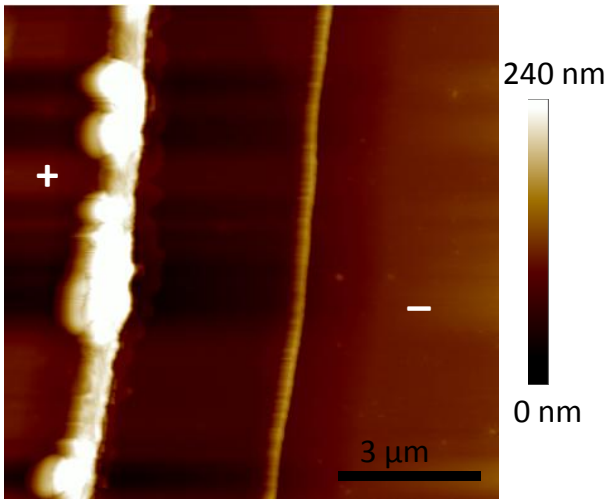

Figure S14. AFM image of a *DHICA melanin* film between Au electrodes (*L*=6 µm) biased at 1 V for 2 h. A strong accumulation, most likely due to Au dissolution, is formed at the edge of the positive electrode. No dendrites or resistive change were observed possibly due to a high degree of polymerization and insufficient film formation.

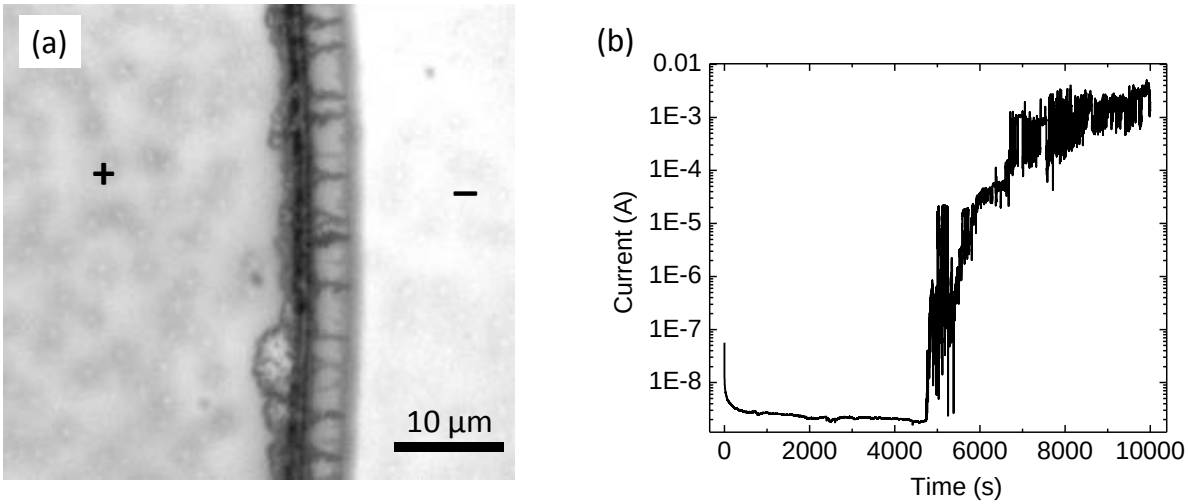

Figure S15. Optical microscopy image (a) of a film deposited from a suspension of the *DHICA monomer* between Au electrodes (*L*=6 µm) after biasing at 1 V for 2.8 h. DHICA partly polymerized during processing as indicated by a darkening of the solution. The growth of dendrites and the sudden increase of current within less than 2 h are clearly visible.

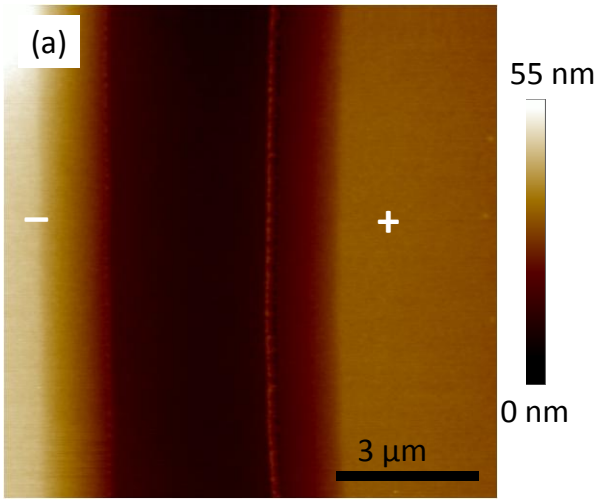

Figure S16. AFM image of a film of *DMSO melanin* after 2 h biasing at 1 V (*L*=6 µm). The experimental conditions were exactly the same as for *DHICA melanin* in Figure S14. Only the formation of a thin line close to the positive electrode can be observed. No larger accumulation or dendrites were formed. No resistive change was observed. Even after 14 h of electrical biasing no significant changes were observed.

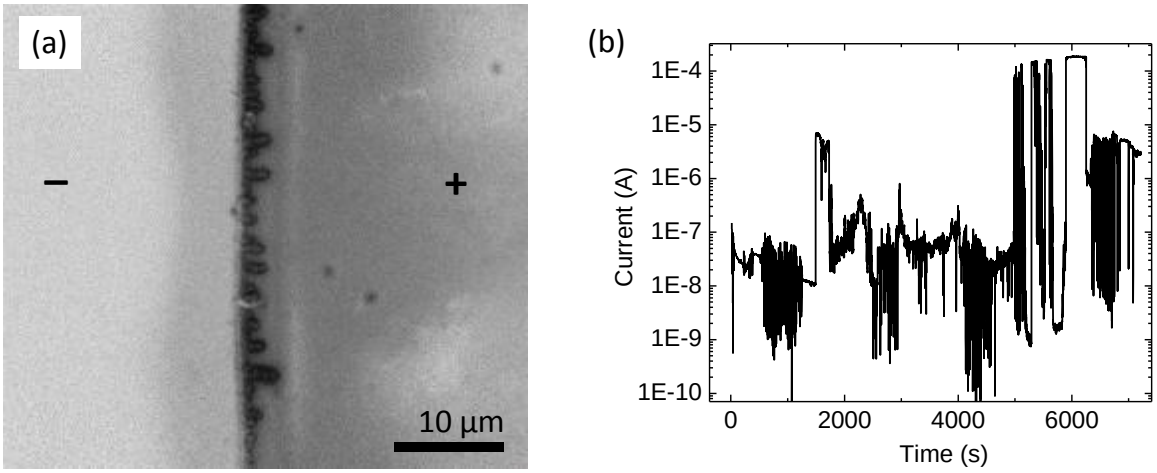

Figure S17. Optical microscopy image (a) and current transient (b) of a film of NaOH-treated *DMSO melanin* biased for 2 h at 1 V (*L*=6 µm). Nanostructures were formed between the Au electrodes during biasing, which lead to sudden increases in the current, particularly around 1800 s and 5000 s. The current transient shows strong instabilities, which we ascribe to the inhomogeneous and bad film quality of NaOH-treated *DMSO eumelanin*.

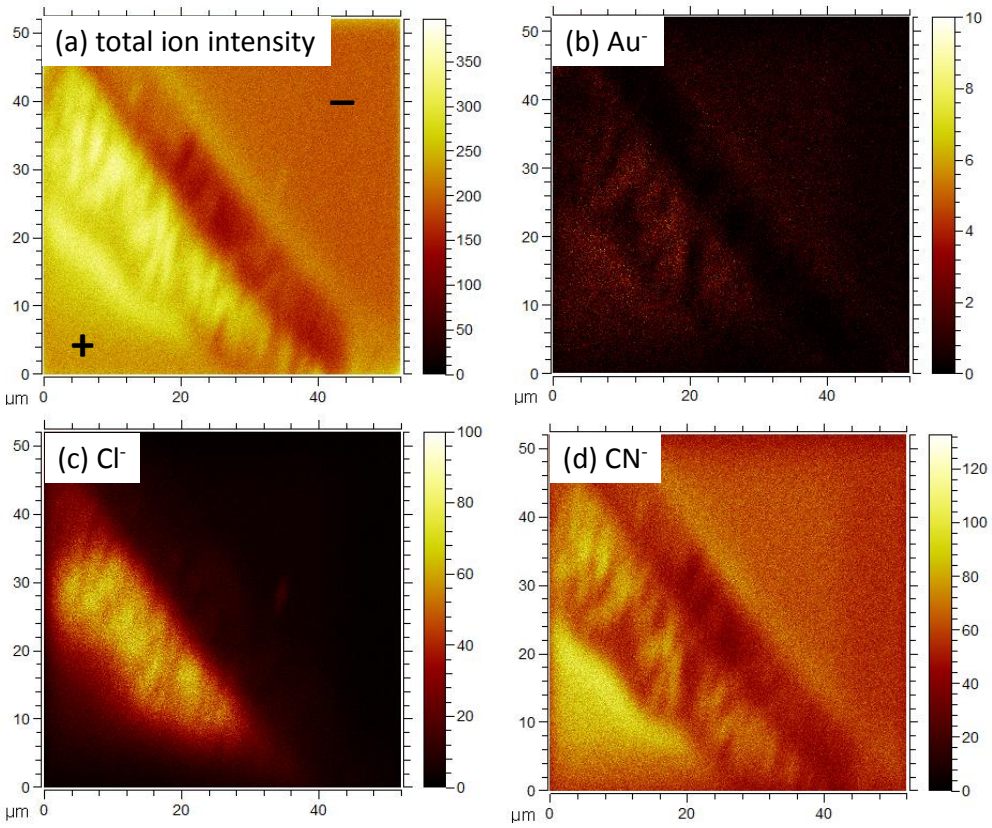

Figure S18. Reconstructed ToF-SIMS images of dendrites forming between two Au electrodes on a *Sigma melanin* film showing the total ion intensity (a) and the distribution of Au^- (b), Cl^- (c), and CN^- ions (d). The presence of Cl^- in the dendrite region is clearly visible. It seems to be more intense around the dendrites than on top of them in contrast to some organic ions such as CN^-.

C - Supporting Information for Article 3

Supporting Information

Proton conduction and transient nature of electronic currents in hydrated eumelanin thin films

J. Wünsche, Y. Deng, P. Kumar, E. Di Mauro, J. Sayago, F. Cicoira, M. Rolandi, F. Soavi, A. Pezzella, and C. Santato

submitted 2014

Proton current

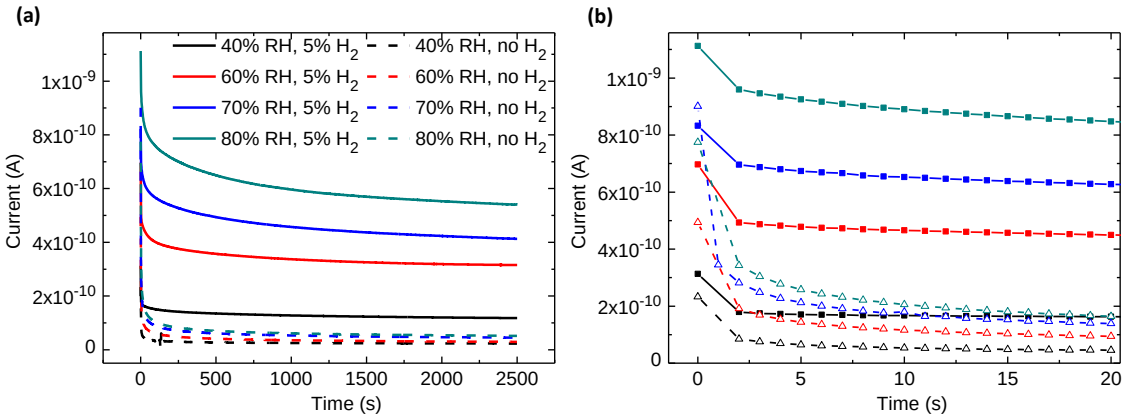

Figure S1: (a) Transient current measurements ($V = 0.5$ V) on a drop-cast sample of eumelanin with Pd electrodes ($W = 20$ μm, $L = 6$ μm) under proton- and electron-injecting (5% H_2 in atmosphere) and only electron-injecting conditions (no H_2) for different values of relative humidity. The film thickness is about 1 μm. (b) First 20 s of same current measurements showing that the transient component is weaker under H_2 exposure. While protons are blocked by Pd electrodes without exposure to H_2 and thus contribute to the transient current, they contribute to the steady-state current when measured with PdH_x electrodes.

X-ray photoelectron spectroscopy

The elemental composition of *Sigma melanin* films deposited from DMSO as obtained by a XPS wide-scan survey is given in Tab. S1. High-resolution spectra of the C1s, N1s, and O1s core levels are displayed in Fig. S3. Binding energies and identification of the components used for peak fitting can be found in Tab.S2. The peak fitting and the analysis of the data regarding the monomer composition of *Sigma melanin* was guided by the standard oxidative pathway for eumelanin from tyrosine (Fig. S2). We also included the possibility that pyrrolic acids form due to oxidative degradation, as well as that they can be incorporated in the macromolecular structure [1] (see end of SI). Thus, we considered the possible presence of the species A-G as given in Fig. S2. To estimate the relative contribution of these units to *Sigma melanin*, we solved a system of equations based on the theoretical (for the monomers) and experimental (for *Sigma melanin*) values of the elemental ratios [C]/[N], [O]/[N], the portion of C bound in carboxyl groups, and the portion of N in pyrrole rings vs. uncyclized structures (Tab. S3). These quantities were judged the most reliable from the XPS spectra and the most useful to distinguish the species A-G. Based on our assumptions, the values given in Tab. S3 do not allow a significant content of pyrrolic acids, E-G. Indeed, we obtain a composition of 22% DHI units, 41%

DHICA units, 37% of L-dopa or tyrosine based on [C]/[N], [C in COOH], and [N in pyrrole]. This composition corresponds to [O]/[N]=3.6, which is lower than the measured ratio but within the experimental error, considering also the presence of impurities. The result can change if other N-containing uncyclized molecules or hydrocarbon contamination are taken into account. Further structural characterization is required to obtain a complete picture of the chemical composition of *Sigma melanin*.

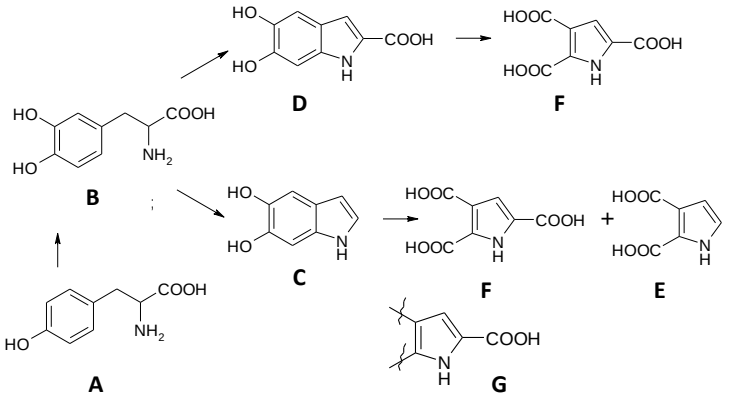

Figure S2: Standard oxidative pathway for the formation of eumelanin from tyrosine (A), via L-dopa (B), DHI (C), and DHICA (D). DHI and DHICA polymerized to give eumelanin. Pyrrole-2,3-dicarboxylic acid (E) and pyrrole-2,3,5-tricarboxylic acid (F) are the main oxidative degradation products of eumelanin and can also be incorporated into the macromolecular structure in the form of specie G.

Table S1: XPS wide scan survey results for a thin film of commercial synthetic eumelanin deposited from dimethyl sulfoxide.

	Binding energy	Atomic %
Pt4f	74.1	0.1
S2p	167.1	0.4
Cl2p	198.7	0.1
C1s	285.1	61.9
N1s	399.8	7.0
O1s	531.9	27.9
F1s	688.0	2.0
Fe2p3	708.9	0.6

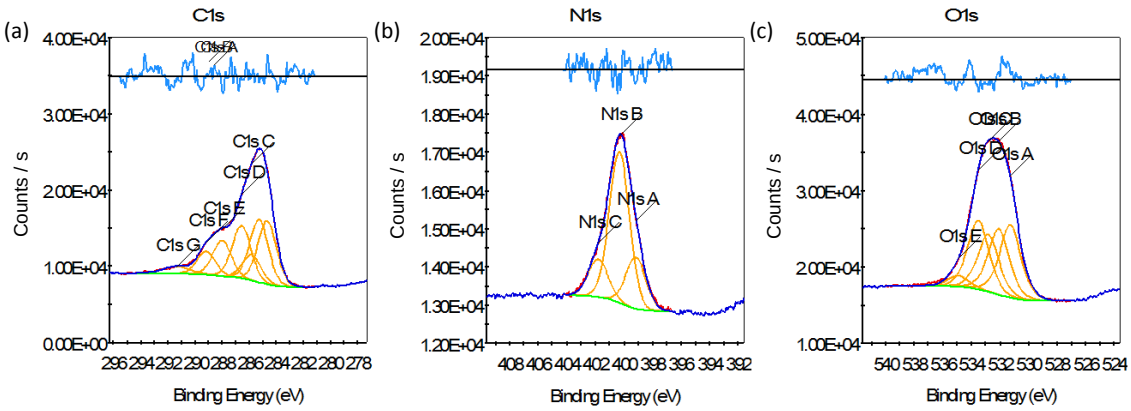

Figure S3: XPS spectra of a eumelanin thin film. C1s (a), N1s (b), and O1s core level (c). The assignment of the individual components used for peak fitting can be found in Tab. S2.

Table S2: Chemical moieties used to fit the XPS spectra of a eumelanin thin film. The composition is normalized to 100 % for each element.

Element	Binding energy	Assignment	Atomic %
C	284.7	C-C aromatic	23.1
	285.3	C-C aromatic	23.0
	285.8	-C-N	9.3
	286.5	-C-OH, -C-N	19.3
	288.0	-C=O	13.0
	289.2	O=C-OH	8.5
	291.4	$\pi - \pi^*$ in C=C	3.9
N	399.2	$-NH_2$	21.4
	400.3	pyrrole	62.9
	401.8	$-NH_3^+$	15.7
O	531.3	O=C	27.5
	532.1	O=C in COOH	24.7
	532.8	HO-C in COOH	21.7
	533.5	HO-C aromatic	26.1

Table S3: The theoretical (for species A-G) and experimental (for *Sigma melanin*) values of the elemental ratios [C]/[N], [O]/[N], the portion of C bound in carboxyl groups, and the portion of N in pyrrole rings.

		[C]/[N]	[O]/[N]	[C in COOH]/[C_{total}]	[N cyclized]/[N_{total}]
A	Tyrosine	9	3	0.11	0
B	L-dopa	9	4	0.11	0
C	DHI	8	2	0	1
D	DHICA	9	4	0.11	1
E	Pyrrole-2,3-dicarboxylic acid	6	4	0.33	1
F	Pyrrole-2,3,5-tricarboxylic acid	7	6	0.43	1
G	Pyrrole-2,3,5-tricarboxylic acid linked	7	2	0.14	1
	Sigma melanin	8.88	4	0.085	0.63

Electrochemical impedance spectroscopy

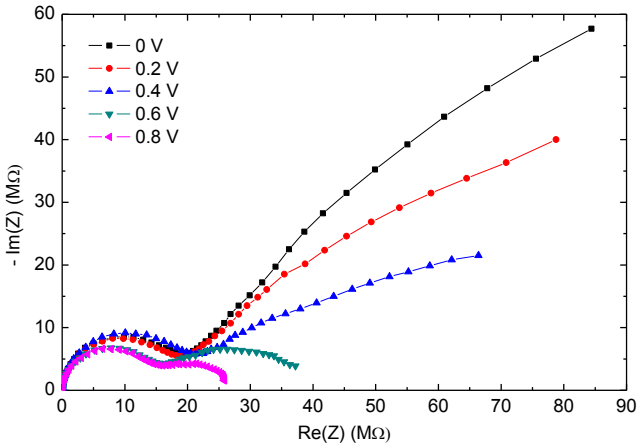

Figure S4: Nyquist plots of the EIS measurement on a eumelanin film at 90% RH, applying a bias between 0 and 0.8 V ($L = 10$ μm, $W = 4$ mm, $A = 0.8$ mm^2, $d = 50$ nm). The frequency range is $10^{-2} - 10^6$ Hz. The electrode geometry used in this measurement is characterized by a larger electrode area but a smaller electrode width compared to the interdigitated electrode design used in most measurements ($W = 24.5$ mm, $A = 8$ mm^2), including the EIS results reported in Fig. 2 of the main text. Compare also with Fig. S8.

Current-voltage measurements

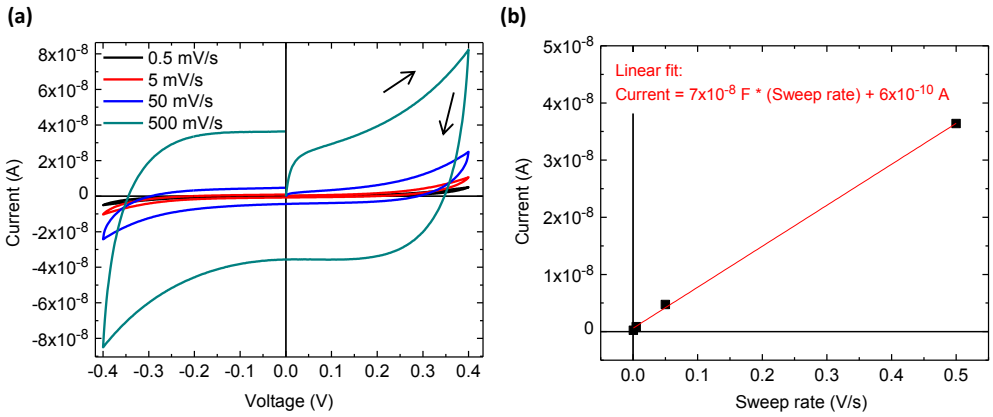

Figure S5: (a) Sweep rate-dependent current-voltage characteristics of a eumelanin film at 90% RH for [-0.4 V, 0.4 V], measured with coplanar Pt electrodes ($L = 10$ μm, $W = 24.5$ mm, $d = 50$ nm). (b) $I(0\text{ V})$ (taken at the end of the cycle) vs sweep rate. The red line is a linear fit. The slope of the fit corresponds is an estimate of the capacitance C of the sample. C divided by the in-plane electrode area (0.8 mm^2) yields 9 μF cm^{-2}.

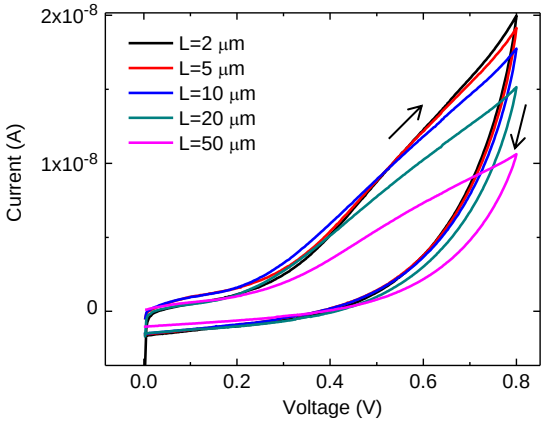

Figure S6: Current-voltage characteristics of eumelanin films at 90% RH for different electrode spacings L (W = 1.5 mm, d = 30 nm). The sweep rate is 5 mV s^{-1}. I(0.8 V) increases when L decreases from 50 μm to 10 μm, indicating that the current is partly limited by (mass or charge) transport in the bulk. I(0.8 V) saturates at L = 2 μm to 5 μm. This suggests that the current is limited by charge transfer at the electrodes for relatively low values of L.

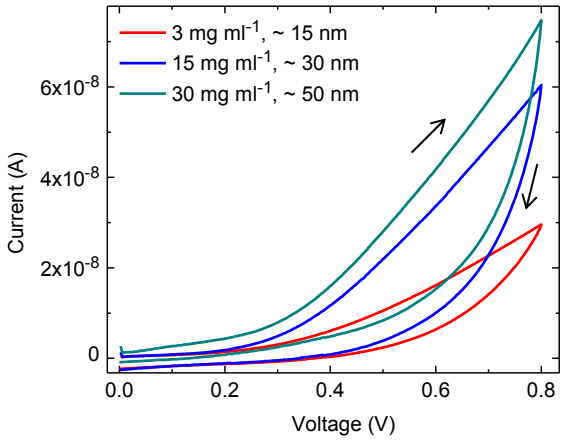

Figure S7: Current-voltage characteristics (sweep rate 5 mV s^{-1}) of eumelanin films at 90% RH (L = 10 μm, W = 24.5 mm). The legend indicates the concentration of the eumelanin suspension and the approximate film thickness obtained by spin-coating. I(0.8 V) increases with the film thickness, indicating the partial limitation of the current by transport in the bulk.

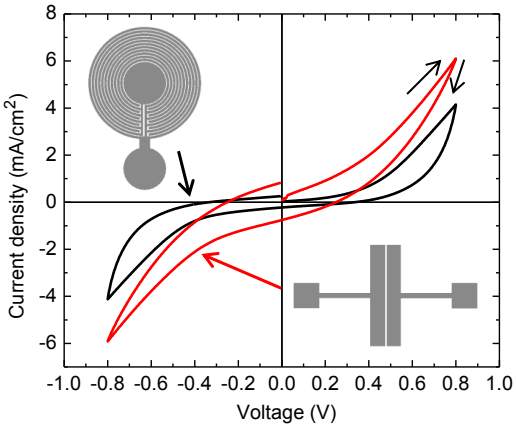

Figure S8: Current density-voltage characteristics (sweep rate 5 mV s^{-1}) of eumelanin films ($d = 50$ nm) at 90% RH using two different electrode geometries shown in the insets (both $L = 10$ μm). The electrode width and in-plane area is 4 mm and 8 mm^2 for the geometry with straight electrodes (red curve) and 24.5 mm and 0.8 mm^2 for the circular interdigitated design (black curve). The dependence of the current density, as evaluated taking into account only the film cross section ($W \cdot d$), on the in-plane area A suggests the contribution of electrochemical reactions to the current.

Cyclic voltammetry

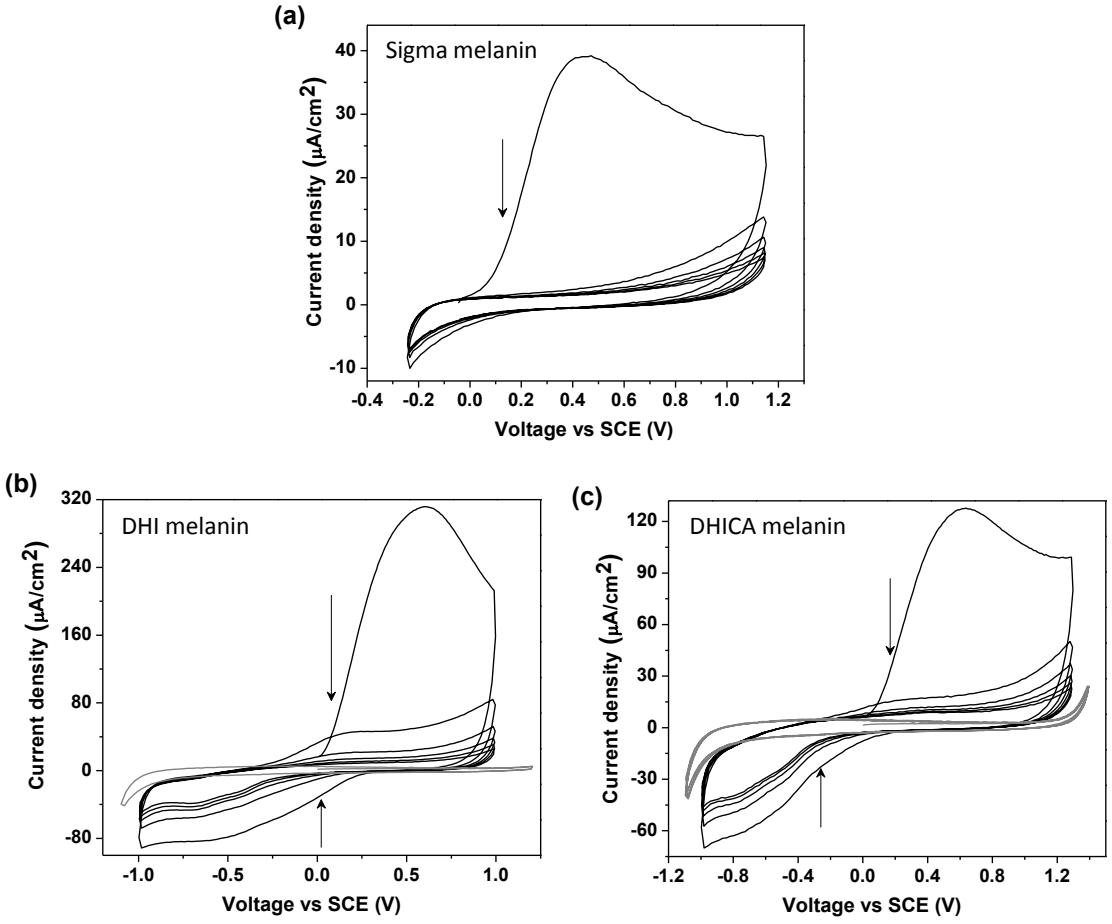

Figure S9: Cyclic voltammetry of *Sigma melanin* (a), *DHI melanin* (b), and *DHICA melanin* films (c) on ITO substrates as working electrode, platinum foil and saturated calomel electrode as the counter and the reference electrodes, respectively. Nitrogen purged PBS buffer (0.01 M) of pH 7.4 is used as the electrolyte and a 50 mV s^{-1} scan rate is maintained. The voltage is cycled from 0 to positive V and then to negative. The cyclic voltammogram of ITO without melanin in PBS is represented in gray. Black arrows indicates the decrease in current density as a function of the number of cycles.

Thermogravimetric analysis

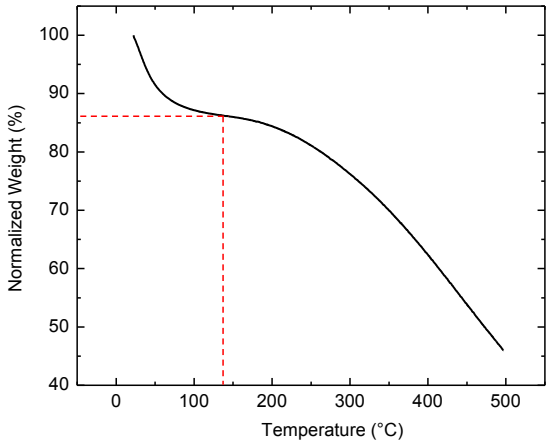

Figure S10: Thermogravimetric analysis of a powder sample of eumelanin having been hydrated at 90% RH during one day. The weight loss of about 14% up to 140 °C is attributed to water evaporation. The sample had to be exposed to ambient air for few minutes during sample transfer. Therefore, the water content might be slightly underestimated.

References

[1] A. Napolitano, A. Pezzella, G. Prota, R. Seraglia, and P. Traldi, *Rapid Commun. Mass Spectrom.*, vol. 10, no. 4, pp. 468472, 1996.

D - List of publications at École Polytechnique de Montréal

Journal articles

J. Wünsche, Y. Deng, P. Kumar, E. Di Mauro, J. Sayago, F. Cicoira, M. Rolandi, F. Soavi, A. Pezzella, and C. Santato, "Protonic and electronic transport in hydrated thin films of the pigment eumelanin", *submitted*.

J. Wünsche, L. Cardenas, F. Rosei, F. Cicoira, R. Gauvin, C. F. O. Graeff, S. Poulin, A. Pezzella, and C. Santato, "In Situ Formation of Dendrites in Eumelanin Thin Films between Gold Electrodes," *Advanced Functional Materials*, 23, 5591, 2013. (Cover)

J. Wünsche, F. Cicoira, C. F. O. Graeff, and C. Santato, "Eumelanin thin films: solution-processing, growth, and charge transport properties," *Journal of Materials Chemistry B*, 1, 3836, 2013.

J. Wünsche, G. Tarabella, S. Bertolazzi, M. Bocoum, N. Coppedè, L. Barba, G. Arrighetti, L. Lutterotti, S. Iannotta, F. Cicoira, and C. Santato, "The correlation between gate dielectric, film growth, and charge transport in organic thin film transistors: the case of vacuum-sublimed tetracene thin films," *Journal of Materials Chemistry C*, 1, 967, 2013.

S. Bertolazzi, J. Wünsche, F. Cicoira, and C. Santato, "Tetracene thin film transistors with polymer gate dielectrics," *Applied Physics Letters*, 99, 013301, 2011.

Book chapters

A. Pezzella and J. Wünsche, "Eumelanin: an old natural pigment – a new material for organic electronics. Chemical, physical, and structural properties in relation to potential applications.," in *Organic Electronics: Emerging Concepts and Technologies*, Eds. F. Cicoira and C. Santato, Wiley-VCH, 2013.

Proceedings

J. Wünsche, F. Rosei, C. F. O. Graeff, and C. Santato, "Growth and morphology of eumelanin thin films-A future bioelectronic material?," *ECS Transactions*, 35, 7, 75, 2011.

Conference contributions

J. Wünsche*, Y. Deng, F. Cicoira, M. Rolandi, and C. Santato, "Mixed ionic-electronic conduction in eumelanin thin films and their interaction with metal electrodes", MRS Fall Meeting 2013, Boston, USA. (oral presentation)

J. Wünsche*, Y. Deng, I. A. Velasco Davalos, A. Pezzella, A. Rüdiger, F. Cicoira, M. Rolandi, and C. Santato, "Mixed ionic-electronic conduction and resistive change in eumelanin thin films", ECME 2013, London. (oral presentation)

J. Wünsche*, L. Cardenas, F. Rosei, C. Santato, "Behavior of hydrated eumelanin films under electrical Bias", EMRS Spring Meeting 2012, Strasbourg, France. (oral presentation)

J. Wünsche*, P. Léger, G. Taillon, H. Guerboukha, M. Simard, F. Rosei, C. Santato, "Structural and electrical properties of eumelanin thin films", Plastic Electronics 2011, Dresden. (poster)

J. Wünsche*, F. Rosei, C. F. O. Graeff, and C. Santato, "Growth and morphology of eumelanin thin films", MRS Spring Meeting 2011, San Francisco, USA. (oral presentation)

J. Wünsche*, F. Rosei, C. F. O. Graeff, and C. Santato, "Growth and morphology of eumelanin thin films", ECS Meeting 2011, Montreal, Quebec, Canada. (oral presentation)

S. Bertolazzi, J. Wünsche*, and C. Santato, "Tetracene thin films on organic dielectrics: growth, structure, and functional properties", MRS Fall Meeting 2010, Boston, USA. (poster)

S. Bertolazzi, C. Brosseau, F. Cicoira, J. Wünsche*, C. Santato. Couches minces de tétracène sur des substrats diélectriques organiques: croissance, morphologie et propriétés fonctionnelles. 78e Congrès de l'Association francophone pour le savoir (Acfas) 2010, Montreal, Quebec, Canada. (oral presentation)